

Vanadium-Based Nanomaterials: A Promising Family for Emerging Metal-Ion Batteries

Xiaoming Xu, Fangyu Xiong, Jiashen Meng, Xuanpeng Wang, Chaojiang Niu, Qinyou An,* and Liqiang Mai*

The emerging electrochemical energy storage systems beyond Li-ion batteries, including Na/K/Mg/Ca/Zn/Al-ion batteries, attract extensive interest as the development of Li-ion batteries is seriously hindered by the scarce lithium resources. During the past years, large amounts of studies have focused on the investigation of various electrode materials toward emerging metal-ion batteries to realize high energy density, high power density, and a long cycle life. In particular, vanadium-based nanomaterials have received great attention. Vanadium-based compounds have a big family with different structures, chemical compositions, and electrochemical properties, which provide huge possibilities for the development of emerging electrochemical energy storage. In this review, a comprehensive overview of the recent progresses of promising vanadium-based nanomaterials for emerging metal-ion batteries is presented. The vanadium-based materials are classified into four groups: vanadium oxides, vanadates, vanadium phosphates, and oxygen-free vanadium-based compounds. The structures, electrochemical properties, and modification strategies are discussed. The structure–performance relationships and charge storage mechanisms are focused on. Finally, the perspectives about future directions of vanadium-based nanomaterials for emerging energy storage devices are proposed. This review will provide comprehensive knowledge of vanadium-based nanomaterials and shed light on their potential applications in emerging energy storage.

to meet the sustainable development. Increasing the electricity generation ratio by renewable energy and replacing the fuel vehicles by electric vehicles are general trends in the future.^[1,2] Energy storage systems, especially electrochemical energy storage (EES) devices, including lithium-ion batteries (LIBs), emerging metal-ion batteries and supercapacitors, play crucial roles on the realization of above two targets.^[3–10] On the one hand, the electric vehicles powered by LIBs have realized commercialization, but the endurance mileage and charge rate are still not satisfactory compared with fuel vehicles. Power batteries with higher energy density and power density are highly desired.^[11–13] On the other hand, since the features of discontinuity and irregularity of renewable energy, a large-scale energy storage system is necessary for the efficient storage and utilization of the generated electricity.^[3,4] Considering the limited lithium resource and increased cost, LIBs are not a good choice for large-scale energy storage system.^[14,15] Replacing Li⁺ by more abundant charge transfer ions, such as Na⁺,

Mg²⁺, and Zn²⁺, is considered as an effective approach to resolve the above limitations, which has inspired a booming research wave of emerging battery technology beyond LIBs in recent years, including sodium-ion batteries (SIBs), potassium-ion batteries (PIBs), magnesium-ion batteries (MIBs), calcium-ion batteries (CIBs), zinc-ion batteries (ZIBs), and aluminum-ion batteries (AIBs).^[6,10,14–30]

Scientifically, electrode materials are the key components of a battery; the voltage gap between cathode and anode, and the amount of charge carriers that can be stored by the electrodes are determinant for the energy density.^[4,31] Besides, the diffusion rate and kinetics of ions in the solid phase of electrodes together with the intrinsic electric conductivity of the electrode materials are highly significant for the power density.^[32,33] Na/K-ion batteries have the similar electrochemical reaction mechanisms with that of LIBs, but their larger ionic radius results in more sluggish diffusion kinetic and severer structure degradation of the electrodes.^[14–17,20] Mg²⁺, Ca²⁺, Zn²⁺, and Al³⁺ are multivalent compared with alkali metal ions, which also suffer from sluggish diffusion in the solid phase due to the strong electrostatic interaction.^[25,27] As a result, conventional

1. Introduction

The greatly increased energy consumption in the past decades has pushed the transformation of the world energy landscape

Dr. X. Xu, F. Xiong, J. Meng, Dr. C. Niu, Dr. Q. An, Prof. L. Mai
State Key Laboratory of Advanced Technology for Materials Synthesis
and Processing

Wuhan University of Technology
Wuhan 430070, China


E-mail: anqinyou86@whut.edu.cn; mlq518@whut.edu.cn

J. Meng

Department of Materials Science and Engineering
Massachusetts Institute of Technology
77 Massachusetts Avenue, Cambridge, MA 02139-4307, USA

Dr. X. Wang

School of Science
Wuhan University of Technology
Wuhan 430070, China

 The ORCID identification number(s) for the author(s) of this article can be found under <https://doi.org/10.1002/adfm.201904398>.

DOI: 10.1002/adfm.201904398

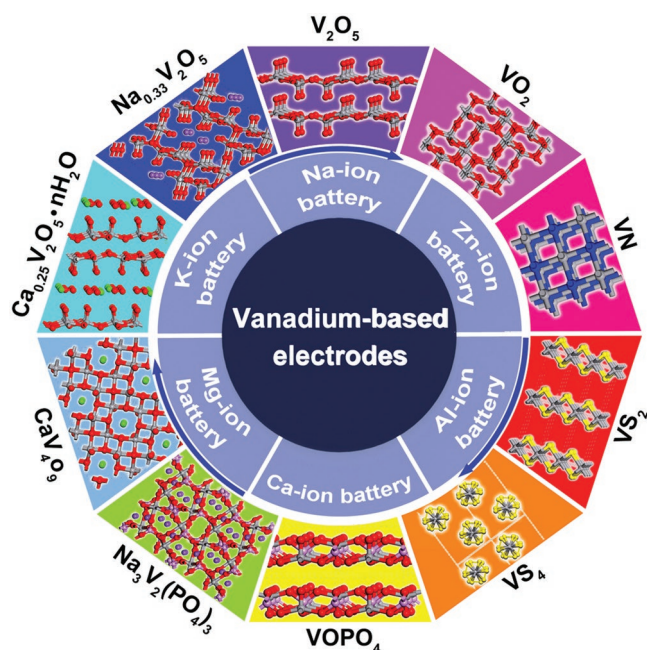


Figure 1. Crystal structures of typical vanadium-based electrodes. The gray balls represent V atoms; red balls represent O atoms; purple balls represent alkali metal ions; green balls represent Ca ions; pink balls represent P atoms; yellow balls represent S atoms and blue balls represent N atoms.

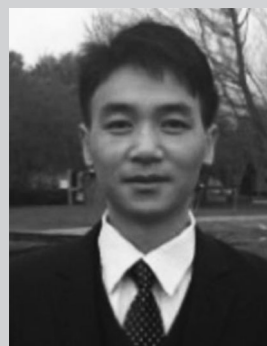
Li-storage electrodes are basically not applicable for these new battery systems. Exploring suitable electrode materials is a key task for the development and application of the emerging battery systems.

In the past years, a large number of new electrode materials with different crystal structures, chemical compositions, and microscopic morphologies have been reported. Nanostructured materials have the unique advantages in energy storage, such as shorter ion diffusion distance, larger surface area and better stress release.^[34–40] Especially, vanadium-based nanomaterials have attracted enormous interests for the emerging EES, even though their practical application in LIBs was unfavorable after studying for more than 40 years.^[41,42] Vanadium has rich valence states varying from +2 to +5 when used as battery electrodes, which means that multielectrons transfer can be realized and a high capacity can be achieved. Besides, since the rich valence states of vanadium, vanadium-based family has a large number of members with different compositions, crystal structures, and electrochemical properties.^[43] **Figure 1** shows the crystal structures of typical vanadium-based electrodes. As the variations of chemical composition and valence state of vanadium, the crystal phases show diverse structures, including layered structure, quasilayered structure, 3D tunnel structure, chain-like structure and rock salt structure, which result in the versatile properties of vanadium-based compounds. The diversity in structure and properties of such a big family provides huge possibilities and choices for the investigation of electrode materials for emerging metal-ion batteries.

Whittingham group has performed a lot of pioneering works on vanadium-based materials for LIBs, and has also made important reviews before 2010.^[43–45] In recent years, we



Xiaoming Xu received his B.S. and Ph.D. degree in material science and engineering from Wuhan University of Technology (WUT) in 2014 and 2019, respectively. His current research focuses on vanadium-based nanomaterials for emerging energy storage and in situ/ex situ characterization of electrochemical reaction.



Qinyou An is Associate Professor of materials science and engineering at Wuhan University of Technology (WUT). He received his Ph.D. degree from WUT in 2014. He carried out his postdoctoral research in the laboratory of Prof. Yan Yao at the University of Houston in 2014–2015. Currently, his research interest includes energy storage materials and devices.



Liqiang Mai is Chair Professor of materials science and engineering at Wuhan University of Technology (WUT). He is Changjiang Scholar Professor and Distinguished Young Scholar of the National Science Fund of China. He received his Ph.D. degree from WUT in 2004 and undertook postdoctoral research with Prof. Zhonglin

Wang at Georgia Institute of Technology in 2006–2007. He worked as advanced research scholar in the laboratory of Prof. Charles M. Lieber at Harvard University in 2008–2011 and Prof. Peidong Yang's group at University of California, Berkeley, in 2017. His current research interests focus on nanomaterials and devices for energy storage.

also note that several reviews that focused on the Li⁺ storage properties of vanadium-based nanomaterials or specific one vanadium-based compound for energy related applications have been published.^[46–57] However, a review article which comprehensively summarizes the vanadium-based nanomaterials family, and focuses on the special merits of their applications for emerging metal-ion batteries is still lacking. Considering that enormous and exciting new results about vanadium-based nanomaterials for metal-ion batteries beyond lithium have been

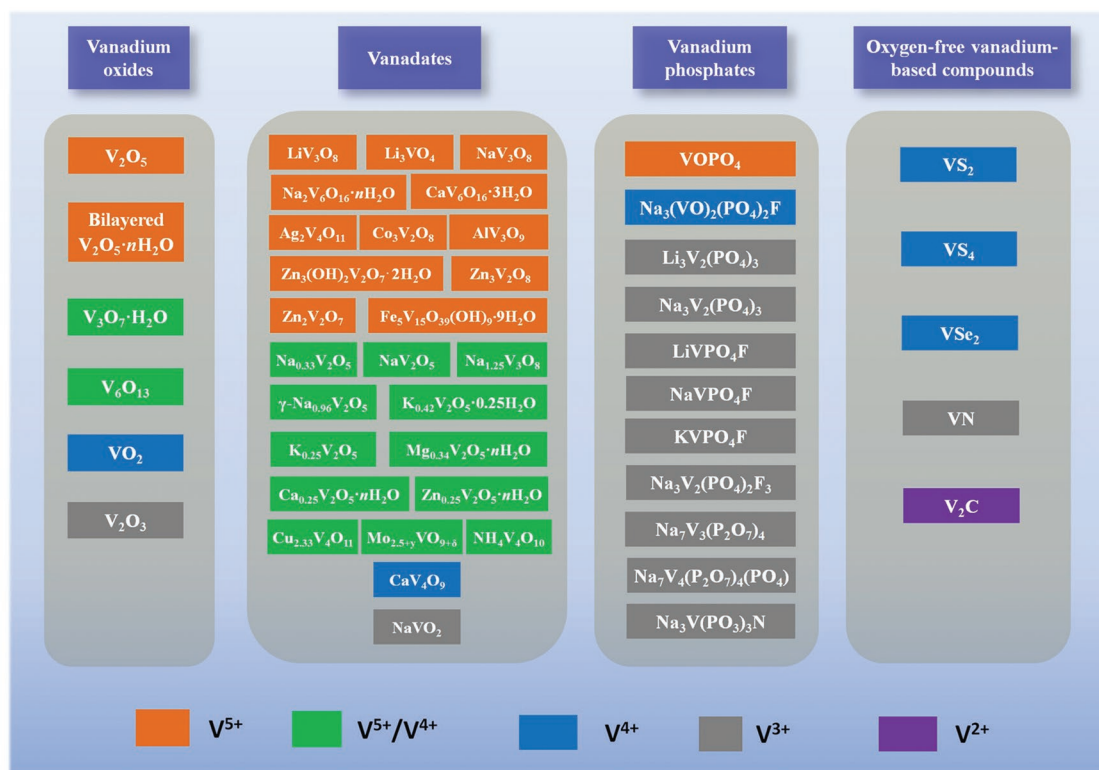


Figure 2. Classification of vanadium-based electrode materials.

achieved in recent years, a review about this topic and scope is timely and important at present.

In this work, we aim to give a comprehensive overview about vanadium-based nanomaterials family with emphasis on the important advances obtained recently about their applications in emerging metal-ion batteries, which we believe would provide essential knowledge for the further development of both vanadium-based nanomaterials and next-generation energy storage systems. This review is organized as follows: after a brief introduction of emerging EES and vanadium-based nanomaterials in Section 1, a detailed classification of vanadium-based electrodes is presented in Section 2. After that, based on the classification of vanadium-based electrodes, the progresses of vanadium oxides, vanadates, vanadium phosphates and other oxygen-free vanadium-based nanomaterials for emerging metal-ion batteries are discussed and summarized in Sections 3–6, respectively. Finally, a summary and an outlook are provided in Section 7 about the future development of vanadium-based nanomaterials for emerging EES.

2. Classification of Vanadium-Based Electrode Materials

Owing to its rich valence states, vanadium can composite with many other anions and cations to form varieties of vanadium-based compounds, such as vanadium oxides, vanadium carbides, vanadium nitrides, vanadium sulfides, vanadium phosphates and metal vanadates, thus resulting in a big family of vanadium-based materials. Among them, vanadium oxides,

vanadium phosphates and metal vanadates have been paid great attentions for electrochemical energy storage in the past decades, while the investigations about vanadium carbides, nitrides and sulfides were mainly centered on recent years. Considering the big family with a large number of members of vanadium-based electrode materials, an appropriate classification is necessary. In this review, based on the features in structure and electrochemical properties, we classified the vanadium-based electrode materials into four groups: vanadium oxides, vanadates, vanadium phosphates, and oxygen-free vanadium-based compounds (Figure 2).

Vanadium oxides are the most common phases among vanadium-based compounds. With the variation of the valence states of vanadium, vanadium oxides possess several variants, mainly including orthorhombic V_2O_5 , bilayered $V_2O_5 \cdot nH_2O$, VO_2 , $V_3O_7 \cdot H_2O$, V_6O_{13} , and V_2O_3 (Figure 2). Among them, orthorhombic V_2O_5 and bilayered $V_2O_5 \cdot nH_2O$ possess typical layered structures with open ion diffusion channels between layers. Vanadium oxides have been studied for decades in LIBs, but suffer from low voltage and Li-poor properties. However, the two drawbacks are basically disappeared when used in MIBs, AIBs and ZIBs. Therefore, the research of vanadium oxides in multivalent metal-ion batteries has attracted significant interests recently.

The facile distortion of V–O polyhedrons and the rich valence state variation of vanadium lead to the great adaptation ability of V–O structure to composite with other cations, and thus generate plenty of derivatives. These derivatives with a variety of A–V–O structures (A represents metal ions or NH_4^+) can be called vanadates. According to the previous reports, more than 20 kinds of metal ions can be incorporated into vanadium oxides to generate

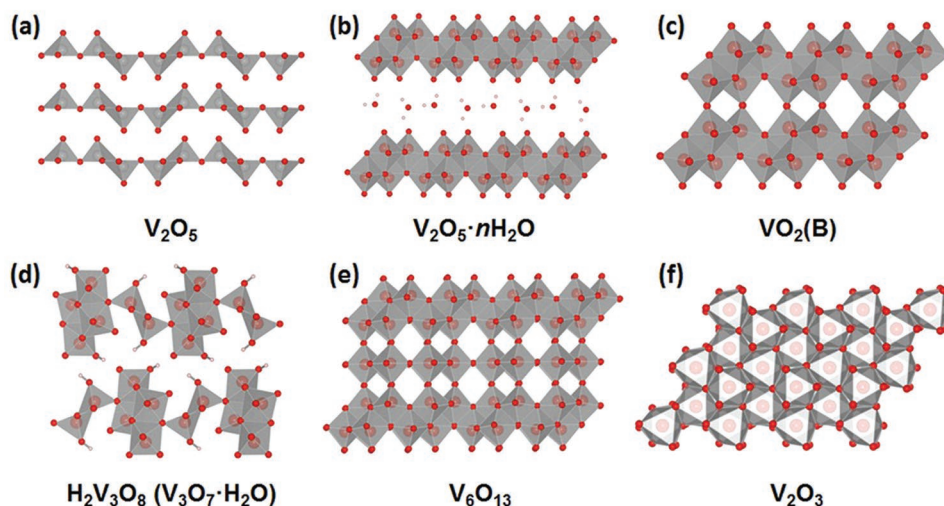


Figure 3. The crystal structures of six typical vanadium oxides: a) Orthorhombic V_2O_5 , b) $V_2O_5 \cdot nH_2O$, c) $VO_2(B)$, d) $H_2V_3O_8 (V_3O_7 \cdot H_2O)$, e) V_6O_{13} , and f) V_2O_3 .

a large number of vanadates (Figure 2) with different compositions, structure and properties. In general, the introduced cations will produce certain benefits and result in a better electrochemical performance. For example, the reported alkali metal vanadates (such as $Na_{0.33}V_2O_5$ and $K_{0.25}V_2O_5$) generally show better cycling stability than V_2O_5 when used as lithium battery cathodes, due to the pillar effect of introduced alkali metal ions.^[58–60] With different metal-ions incorporation, the composited vanadates display a diversity of crystal structures with different electrochemical properties, which provides large amounts of choices for the investigation of electrodes for emerging metal-ion batteries.

Vanadium phosphates have distinct crystal structures and electrochemical properties compared with other vanadium-based electrodes, due to the existence of $[PO_4]$ tetrahedrons in the structures. Most of the vanadium phosphates possess 3D open framework structure (such as $Li_3V_2(PO_4)_3$ and $Na_3V_2(PO_4)_3$) constructed by $[VO_6]$ octahedrons and $[PO_4]$ tetrahedrons through corner-sharing connection,^[49,61,62] while a few of them are layered structure (such as $\alpha_1\text{-VOPO}_4$).^[63–66] Vanadium phosphates generally possess higher redox potential compared with the vanadium oxides or vanadates, attributing to the strong inductive effect from $[PO_4]$ tetrahedrons.^[13,67,68] But like other phosphate electrodes, vanadium phosphates generally suffer from low electric conductivity, due to the $[VO_6]$ octahedrons are isolated from each other and separated by the $[PO_4]$ tetrahedrons.^[13] Nanostructure design and conductive coating are the main optimization strategies.

Apart from the above-mentioned vanadium-based electrodes, increasing interests in recent years have also been paid on vanadium carbides (such as V_2C),^[69–71] vanadium nitrides (such as V_2N),^[72–75] and vanadium sulfides (such as VS_2),^[76–78] etc. These oxygen-free vanadium-based compounds have special characteristics in both structures and properties compared with vanadium oxides, which make them highly attractive for electrochemical energy storage.^[79] Because these compounds have similar features and properties, and the published works are relatively less, the progress about the oxygen-free vanadium-based compounds for emerging energy storage will be integrated and discussed in one chapter (Section 6).

3. Vanadium Oxides

Vanadium oxides mainly include orthorhombic V_2O_5 , bilayered $V_2O_5 \cdot nH_2O$, VO_2 , $V_3O_7 \cdot H_2O$, V_6O_{13} , and V_2O_3 (Figure 3), which have been studied in LIBs for more than 40 years. In recent years, the investigations about vanadium oxides for emerging energy storage devices, including SIBs, MIBs, ZIBs, and AIBs, have also attracted much attention. Table 1 displays the typical vanadium oxides and the application examples for emerging metal-ion batteries. Note that in the past years, several reviews about vanadium oxides for

Table 1. The electrochemical properties of the typical vanadium oxides for emerging metal-ion batteries.

Materials	Applications	Average discharge voltage [V]	Highest reversible capacity [mAh g ⁻¹]	Refs.
Orthorhombic V_2O_5	SIB cathode	≈1.5	≈160	[82]
	MIB cathode	≈1.3	≈260	[83]
	AIB cathode	≈0.5	≈305	[84]
	ZIB cathode	≈0.7	≈470	[85]
Bilayered V_2O_5	SIB cathode	≈2.0	≈305	[86]
	MIB cathode	≈2.1	≈600	[87]
	ZIB cathode	≈0.7	≈380	[88]
$VO_2(B)$	SIB cathode	≈2.3	≈325	[89]
	MIB cathode	≈2.0	≈390	[90]
	AIB cathode	≈0.2	≈160	[91]
	ZIB cathode	≈0.8	≈355	[92]
$H_2V_3O_8$	SIB cathode	≈2.9	≈160	[93]
	MIB cathode	≈1.8	≈300	[94]
	ZIB cathode	≈0.6	≈450	[95]
V_6O_{13}	SIB cathode	≈2.1	≈225	[96]
V_2O_3	SIB anode	≈0.6	612	[97]

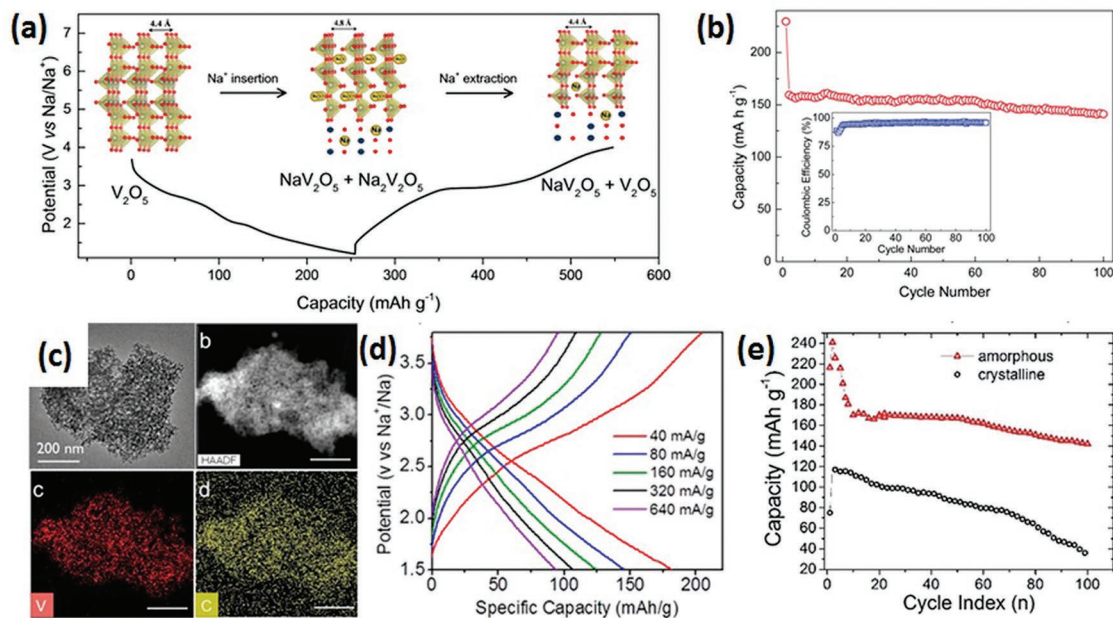


Figure 4. a) The schematic illustration for sodium storage mechanism of nanosized orthorhombic V_2O_5/C composites and corresponding charge/discharge curves. Reproduced with permission.^[100] Copyright 2016, American Chemical Society. b) Cycling performance of hierarchical orthorhombic V_2O_5 hollow nanospheres as cathode material for SIBs at 20 mA g^{-1} . Reproduced with permission.^[82] Copyright 2014, Royal Society of Chemistry. c) The TEM image and the corresponding energy dispersive X-ray spectrometry mappings of 55- V_2O_5 -RFC (scale bar = 200 nm). d) The charge/discharge curves of 55- V_2O_5 -RFC as a cathode material for SIBs at different current densities. Reproduced with permission.^[101] Copyright 2014, American Chemical Society. e) The comparison of sodium storage performance between orthorhombic and amorphous V_2O_5 . Reproduced with permission.^[102] Copyright 2014, Royal Society of Chemistry.

LIBs have been reported.^[43,53,54,80,81] However, the comprehensive review about their application for beyond LIBs is absent although a lot of works about vanadium oxides for emerging energy storage have been reported. In this section, we discuss the recent progresses, existed problems and possible development directions of vanadium oxides for beyond LIBs in detail.

3.1. Orthorhombic V_2O_5

Orthorhombic V_2O_5 possesses typical layered crystal structure (Figure 3a).^[82] The distorted VO_5 square pyramids are connected by sharing edges and corners with periodic up–up–down–down sequence to form the 2D structure, and the layers are stacked along c -axis with weak van der Waals interaction. The intrinsic interlayer spacing of about 4.37 Å endows α - V_2O_5 as a possible intercalation host for different metal ions. Therefore, V_2O_5 has attracted much interest in the energy storage field due to its unique structural characteristics. Previous review papers have discussed the lithium storage of V_2O_5 .^[43,46,80,81,98,99] Here we will focus on the recent advances of V_2O_5 for beyond LIBs.

3.1.1. V_2O_5 for SIBs

The reaction mechanism of V_2O_5 as a cathode for SIBs is different from its lithium storage mechanism, owing to the differences between Li^+ and Na^+ . Ali et al.^[100] systematically

investigated the sodium-ion intercalation mechanism of V_2O_5 in the potential windows of 1.2–4.0 V (vs Na^+/Na) via ex situ X-ray diffraction (XRD), transmission electron microscopy (TEM) and near edge X-ray absorption fine structure spectroscopy. After the intercalation of Na^+ ions, V_2O_5 transforms to a mixture with NaV_2O_5 as the major phase and $Na_2V_2O_5$ as the minor phase. Both the crystalline and amorphous $Na_2V_2O_5$ existed in the discharged mixture (Figure 4a). During the charge process, the NaV_2O_5 and $Na_2V_2O_5$ transform back to orthorhombic V_2O_5 with trace NaV_2O_5 .

In order to achieve high performance, some V_2O_5 nanostructures have been fabricated as cathodes for SIBs. The sodium storage performance of hollow hierarchical V_2O_5 nanospheres has been investigated.^[82] As an SIB cathode, a high initial discharge capacity of $\approx 230 \text{ mAh g}^{-1}$ at 20 mA g^{-1} in 1.0–4.2 V (vs Na^+/Na) was displayed, with two plateaus located at ≈ 2.0 and 1.4 V, respectively. The discharge capacity significantly decreases to $\approx 159 \text{ mAh g}^{-1}$ in the second cycle and decays to 141 mAh g^{-1} at the 100th cycle (Figure 4b). Note that the achieved reversible capacity of hollow V_2O_5 nanospheres is much lower than its theoretical capacity for lithium storage. Moreover, the plateau located at low potential ($\approx 1.4 \text{ V}$) is the main contributor for the reversible capacity, which means the much lower energy density of V_2O_5 for sodium storage than that for lithium storage. To further enhance the sodium storage performance, V_2O_5 nanoparticles with sizes of 5–7 nm encapsulated in nanoporous carbon (was referred to RFC) were obtained by Raju et al. (Figure 4c).^[101] The optimized sample (55- V_2O_5 -RFC) displayed a high reversible capacity of 170 mAh g^{-1} at 40 mA g^{-1} in 1.5–3.8 V (vs Na^+/Na). The

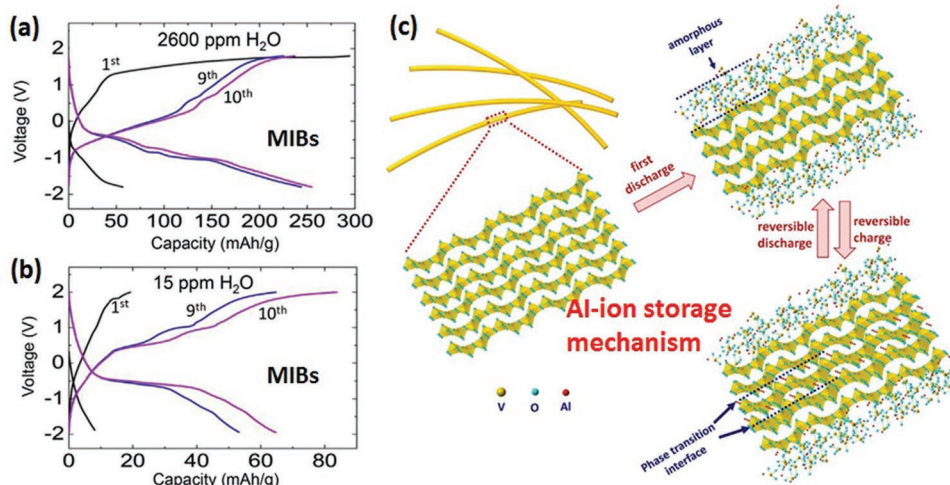


Figure 5. The charge/discharge curves of V_2O_5 in 1 M $Mg(TFSI)_2$ /diglyme with a) 2600 ppm and b) 15 ppm H_2O at 20 mA cm^{-2} . Reproduced with permission.^[83] Copyright 2016, Elsevier. c) Schematic illustration of Al^{3+} insertion/extraction in crystallized V_2O_5 nanowire. Reproduced with permission.^[112] Copyright 2017, Elsevier.

capacity of V_2O_5 nanoparticles was estimated to be 276 mAh g^{-1} after deducting the mass and capacity contribution of RFC. In addition, 55- V_2O_5 -RFC delivers an enhanced rate performance (over 90 mAh g^{-1} at 640 mA g^{-1}) (Figure 4d) and cycling stability (140 mAh g^{-1} after 70 cycles). But on the whole, the performance of orthorhombic V_2O_5 for sodium storage is still far from the requirement for practical application regarding to the cycling, rate and voltage.

Efforts have also been made to improve the sodium storage performance of V_2O_5 via crystal structure modification. Renard et al.^[103] evaluated the electrochemical performance of γ' - V_2O_5 in SIBs. In the potential range of 1.75–4.0 V (vs Na^+/Na), the γ' - V_2O_5 can reach a reversible capacity of about 147 mAh g^{-1} at elevated temperature (50 °C) with a flat potential plateau at ≈ 3.3 V, which is different from that of orthorhombic V_2O_5 . However, γ' - V_2O_5 displays decreased capacity at room temperature with poor rate performance. Amorphization is another effective way to improve the performance of V_2O_5 .^[102,104] Cao group compared the sodium storage performance of amorphous V_2O_5 nanoparticles and V_2O_5 nanocrystals.^[102] It was found that the amorphous V_2O_5 exhibits higher reversible capacity (≈ 241 mAh g^{-1}) compared to ≈ 120 mAh g^{-1} and better cycling performance (as shown in Figure 4e) than that of crystalline V_2O_5 . The amorphous structure with more open framework and isotropic structure are favorable to the diffusion of Na^+ ions, which is responsible for the improved capacity and enhanced cycling stability.

3.1.2. V_2O_5 for MIBs

For LIBs, V_2O_5 achieves high capacity via the multilithium insertion. However, the insertion of multilithium ions leads to serious structure degradation, resulting in poor cycling stability. It is interesting that multielectron reaction can be realized by inserting single multivalent metal ions. Moreover, multivalent metal anodes such as Mg, Zn, and Al have attracted considerable attentions due to their high volumetric capacity (3832, 5851, and

8045 mAh mL^{-1} for Mg, Zn, and Al, respectively) without safety issues. Thus, the development of multivalent secondary batteries has been considered as a promising approach to achieve high energy density for electric vehicles or large-scale energy storage.

The investigation of electrochemical intercalation of magnesium-ion into orthorhombic V_2O_5 can retrospect to 1987.^[105] However, the subsequent progress of V_2O_5 as a cathode material for MIBs is sluggish because the development of MIBs is limited by a dearth of suitable electrolytes, until the full MIBs prototype with long-term cycle life was realized by Aurbach et al. in 2000.^[106] After that, the investigation of V_2O_5 as cathode materials for MIBs began to attract more and more attention, especially as the research fever of post-LIBs rising in recent years.^[83,107–110]

Aurbach and co-workers investigated the electrochemical performance of V_2O_5 thin film as cathode materials for MIBs.^[109] With 0.5 M $Mg(ClO_4)_2$ in acetonitrile as electrolyte and activated carbon cloth (ACC) as quasireference electrodes, the reversible intercalation/deintercalation of Mg^{2+} into V_2O_5 thin film was realized. An initial capacity of 180 mAh g^{-1} was obtained and 150 mAh g^{-1} was retained after 35 cycles. Moreover, the reversible change between V_2O_5 and $Mg_{0.5}V_2O_5$ phase was monitored during the Mg^{2+} intercalation/deintercalation process.

The strong electrostatic force between Mg^{2+} ion and V_2O_5 is one of the major challenges for V_2O_5 as cathode materials for MIBs. Cointercalation of water is an efficient approach to overcome this problem by charge screening. Thus, the water content in electrolyte will greatly influence the Mg^{2+} storage performance of V_2O_5 . For example, when the water content is infinite, that is in aqueous electrolyte (such as aqueous $MgCl_2$ solution), a high magnesium storage capacity of 427 mAh g^{-1} was demonstrated for V_2O_5 .^[111] Sa et al.^[83] investigated the magnesium storage performance of V_2O_5 in the 1 M magnesium bis(trifluoromethane sulfonyl)imide ($Mg(TFSI)_2$)/diglyme electrolyte with different water content. With 2600 ppm water in electrolyte, the V_2O_5 cathode achieved a high capacity of ≈ 260 mAh g^{-1} (Figure 5a). However, the capacity only reached ≈ 60 mAh g^{-1} in the dry electrolyte (with 15 ppm water)

(Figure 5b). But no obvious electrochemical evidence for reversible Mg plating/stripping was observed in 1 M Mg(TFSI)₂/diglyme electrolyte with 2600 ppm water, which limits the use of Mg metal anode. Thus, searching for suitable electrolyte is still a key point for the development of V₂O₅ as MIB cathode. Du et al.^[110] reported the Mg²⁺ storage performance of V₂O₅ with graphene oxide (GO) decoration in 0.25 M Mg(AlCl₂EtBu)₂/tetrahydrofuran electrolyte. The V₂O₅/GO composites delivered an initial capacity of 178 mAh g⁻¹, and retained 140 mAh g⁻¹ after 20 cycles. This study demonstrates that V₂O₅ also can achieve high reversible capacity in the dry electrolyte, which is of great significance in the development of high-performance full MIBs based on Mg metal anode and V₂O₅ cathode.

3.1.3. V₂O₅ for AIBs

The first stable AIB based on V₂O₅ with extended cycle life was reported by Jayaprakash et al.^[84] in 2011. In this AIB, V₂O₅ nanowires were used as the cathode material with ionic liquid as electrolyte and aluminum metal as anode. The V₂O₅ nanowires exhibit high discharge capacities of 305 mAh g⁻¹ in the 1st cycle and 273 mAh g⁻¹ in the 20th cycle at 125 mA g⁻¹ with a discharge plateau at about 0.55 V. However, the cathode reaction in this system is controversial. Reed and Menke^[113] reported that the V₂O₅ nanowires were electrochemically inactive in the above AIB system, and the capacity was attributed to the reactions with the iron and chromium metal in the stainless steel current collector. While Gu et al.^[112] demonstrated the reversible insertion/extraction of aluminum-ion into V₂O₅ nanowires. The surface amorphization of V₂O₅ nanowires arises during the intercalation of Al³⁺ ions (Figure 5c). However, V₂O₅ nanowires with Ni current collector display a lower discharge capacity (53.4 mAh g⁻¹ in 2nd cycle at 10 mA g⁻¹) compared to V₂O₅ nanowires with stainless steel current collector. Therefore, it can be concluded that both the reactions with stainless steel current collector and reversible insertion/extraction of aluminum-ion into V₂O₅ nanowires exist.

To further excavate the capacity for reversible aluminum-ion storage, the amorphous V₂O₅/C composite was synthesized as a cathode for aluminum batteries.^[114] The aluminum-ion storage performance was measured in glass cells with Mo plate as the current collector. At a current density of 11 mA g⁻¹, amorphous V₂O₅/C composite exhibits a high discharge capacity of over 200 mAh g⁻¹ in the first cycle and about 70 mAh g⁻¹ in the 30th cycle. The reversible insertion/extraction of Al³⁺ into V₂O₅ has been demonstrated. However, extensive efforts are still needed to improve the cycling performance.

3.1.4. V₂O₅ for ZIBs

Aqueous rechargeable ZIBs have become one of the research hotspots in energy storage fields in recent years. As a typical layered cathode material, V₂O₅ was recently investigated as a potential cathode for ZIBs. Hu et al.^[115] reported a Zn/V₂O₅ aqueous hybrid-ion battery using a mixed Zn(CF₃SO₃)₂-LiTFSI electrolyte. It was demonstrated that both Li⁺ and Zn²⁺ can be intercalated into V₂O₅ structure, but the Li⁺ intercalation/

deintercalation is dominant. Such a hybrid-ion battery realized a high discharge capacity of 238 mAh g⁻¹ and long cycle life of 2000 cycles with retention of 80%. Afterward, Zhang et al.^[85] reported a ZIB based on Zn/V₂O₅ with aqueous Zn(CF₃SO₃)₂ electrolyte. Remarkably, a high reversible capacity of 470 mAh g⁻¹ and long-term cycling stability over 4000 cycles were achieved. The reversible structure transformation between layered V₂O₅ and layered Zn_xV₂O₅ · nH₂O was demonstrated during the discharge and charge process. A distinct morphology changes from solid bulk initially to porous nanosheets upon cycling was observed, which was believed to benefit to the mass diffusion of ions and enable a high utilization of the active materials.

3.2. Bilayered V₂O₅

Bilayered V₂O₅ mainly refers to V₂O₅ · xH₂O, including V₂O₅ xerogels and aerogels.^[50] Different from orthorhombic V₂O₅, the layer structure of bilayered V₂O₅ is consisted of two [VO₆] octahedron layers (Figure 3b).^[116] In general, the crystal water (or residual micromolecule organics) would exist in the interlayer of bilayered V₂O₅, resulting in a large interlayer spacing (>10 Å). Thus, the intercalation of various metal ions, such as Li⁺, Na⁺, K⁺, Mg²⁺, Ca²⁺, Zn²⁺, and Al³⁺, into bilayered V₂O₅ can be realized easily,^[117,118] indicating that bilayered V₂O₅ is a promising electrode material for various metal-ion batteries. In this section, we focus on the progresses of bilayered V₂O₅ in SIBs, MIBs, and ZIBs.

3.2.1. Bilayered V₂O₅ for SIBs

Compared to the orthorhombic V₂O₅, the bilayered V₂O₅ is more suitable as an SIB cathode due to the larger interlayer spacing.^[86,119,120] The Na⁺ storage capacity exceeding 300 mAh g⁻¹ has been achieved, which is almost the highest capacity among the reported SIB cathode materials.^[86,121] Tepavcevic et al.^[122] investigated the Na⁺ ions intercalation/deintercalation mechanism of bilayered V₂O₅ via small and wide-angle X-ray scattering measurements. In the first discharge process, the intercalation of Na⁺ ions into bilayered V₂O₅ results in the expansion of layer spacing. However, after the deintercalation of Na⁺ ions in the first charge process, the stacking order of layer structure in bilayered V₂O₅ is removed and the [VO₆] octahedron layers are still remained.

The V₂O₅ · xH₂O xerogel synthesized via a freeze-drying method has been studied as a cathode material for SIB.^[86] At 100 mA g⁻¹, an initial capacity of 308 mAh g⁻¹ in 1.0–4.0 V (vs Na⁺/Na) was displayed, which is much higher than that of the orthorhombic V₂O₅ (170 mAh g⁻¹) (Figure 6a,b). However, fast capacity fading was observed. Based on ex situ XRD measurements, the accumulation of the interlayer shrinkage and collapse during cycling is one of the primary reasons for the fast capacity decay. Thus, maintaining the layer structure with stable interlayer spacing is an efficient way to improve the cycling stability of V₂O₅ · xH₂O as cathode materials for SIBs. In this case, Wei et al.^[119] obtained a lattice breathing inhibited bilayered V₂O₅ nanobelts with stabilized large interlayer

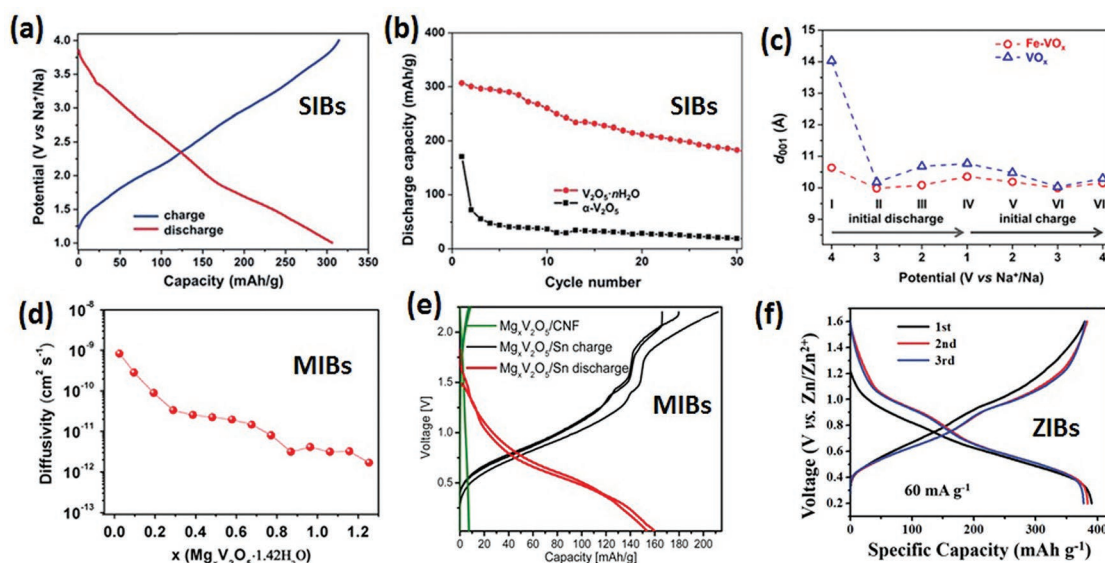


Figure 6. a) The charge/discharge curves of $V_2O_5 \cdot xH_2O$ as cathode materials for SIBs at 100 mA g^{-1} . b) The cycling performance comparison of $V_2O_5 \cdot xH_2O$ and orthorhombic V_2O_5 as cathode materials for SIBs. Reproduced with permission.^[86] Copyright 2015, Royal Society of Chemistry. c) The d_{001} value variation of $Fe-VO_x$ and VO_x as SIBs cathode materials in the initial discharge/charge cycle. Reproduced with permission.^[119] Copyright 2015, American Chemical Society. d) The Mg-ion diffusivity of $V_2O_5 \cdot xH_2O$ nanowire/graphene composites versus discharge state. Reproduced with permission.^[123] Copyright 2015, Elsevier. e) The charge/discharge curves of full magnesium-ion batteries based on Mg-enriched bilayered V_2O_5 cathode and nanocrystalline Sn anode at 20 mA g^{-1} . Reproduced with permission.^[124] Copyright 2015, American Chemical Society. f) The charge/discharge curves of bilayered V_2O_5 /graphene as a cathode material for ZIBs. Reproduced with permission.^[125] Copyright 2018, Wiley-VCH.

spacing via iron-ion preintercalation strategy. The interlayer spacing of as-synthesized iron-ion preintercalated $V_2O_5 \cdot xH_2O$ nanobelts ($Fe-VO_x$) is 10.6 \AA , which is smaller than that of pure $V_2O_5 \cdot xH_2O$ nanobelts (VO_x). However, the $Fe-VO_x$ cathode displays an enhanced cycling stability with the capacity retention of 80.0% after 200 cycles at 100 mA g^{-1} . Ex situ XRD results indicate that the total shrinkage of the interlayer spacing of VO_x reaches 3.74 \AA , while that of $Fe-VO_x$ is only 0.49 \AA (Figure 6c). The interlayer spacing of $Fe-VO_x$ stabilizes at 10.14 \AA after the first cycle, while that of VO_x reduces greatly in the initial several cycles and then stabilizes at 9.93 \AA . The larger stabilized interlayer spacing of $Fe-VO_x$ is responsible for the enhanced capacity, rate performance and cycling stability.

3.2.2. Bilayered V_2O_5 for Multivalent-Ion Batteries

The intercalation/deintercalation of multivalent cations in bilayered V_2O_5 has been reported firstly by Liu et al. in 1998.^[117] Imamura et al.^[87] investigated the Mg^{2+} ions storage performance of bilayered V_2O_5 /carbon composites, and a high capacity of 600 mAh g^{-1} with an average operating potential of about 2.5 V was obtained. However, the other reported Mg^{2+} ions storage capacities of bilayered V_2O_5 are generally lower than 350 mAh g^{-1} .^[123,126] Even so, the energy density of bilayered V_2O_5 is still higher than those of the most reported cathode materials for MIBs. In the investigation of V_2O_5 as cathode materials for MIBs, the water in electrolyte enhances the capacity due to the charge shielding effect. Similarly, the crystal water in bilayered V_2O_5 can effectively screen the divalent charge by coordinating to Mg^{2+} ions as the solvation shell. The high capacity and the charge shielding effect make bilayered V_2O_5 a promising cathode material for MIBs.

The poor cycling stability is one of the problems affecting the application of $V_2O_5 \cdot xH_2O$ in MIBs. An et al.^[123] reported graphene decorated $V_2O_5 \cdot xH_2O$ nanowires (VOG-1) which exhibited excellent cycling stability for Mg^{2+} ions storage. The electrochemical performance of VOG-1 was tested with $Mg(TFSI)_2$ /acetonitrile as the electrolyte and ACC as quasireference electrode. A capacity as high as 330 mAh g^{-1} was achieved in the galvanostatic intermittent titration technique (GITT) measurement in $1.6\text{--}3.4 \text{ V}$. Besides, the calculated average Mg^{2+} diffusion coefficient of VOG-1 during the intercalation process is about $3 \times 10^{-11} \text{ cm}^2 \text{ s}^{-1}$ (Figure 6d), which is higher than those of Chevrel Mo_6S_8 ($2\text{--}6 \times 10^{-12} \text{ cm}^2 \text{ s}^{-1}$). When cycled at 1000 mA g^{-1} , the capacity retention of 81% was obtained after 200 cycles. The enhanced Mg^{2+} storage performance of VOG-1 is ascribed to the charge shielding effect from crystal water, the fast electronic conduction pathway from graphene, and short Mg^{2+} ions diffusion channel from nanowires.

For practical application, the development of full MIBs is necessary. However, Mg metal anode is incompatible with the most present electrolytes which suitable for bilayered V_2O_5 , such as $Mg(TFSI)_2$ -based and $Mg(ClO_4)_2$ -based electrolytes. The $Mg(TFSI)_2$ -based electrolytes do not enable reversible Mg deposition/dissolution and the $Mg(ClO_4)_2$ -based electrolytes will result in the formation of passivation layers on the surface of Mg metal anode which block the Mg^{2+} ions conduction.^[123,126] The full MIBs based on the magnesiated bilayered V_2O_5 as cathode, $Mg(ClO_4)_2$ /acetonitrile as electrolyte and Sn as anode have been designed (Figure 6e) by Tepakcevic et al.^[124] This full MIB displays a capacity over 100 mAh g^{-1} (based on the mass of bilayered V_2O_5) after 50 cycles. Using other anodes which are compatible with $Mg(TFSI)_2$ -based or $Mg(ClO_4)_2$ -based electrolytes to replace Mg metal anode can realize the full MIBs based

on bilayered V_2O_5 , but it will give up the advantages of Mg anode, such as high energy density and rich resource. Thus, electrolyte exploitation, which is compatible with both bilayered V_2O_5 cathode and Mg metal anode, is significant for the development of bilayered V_2O_5 -based full MIBs.

Recently, some investigations about bilayered V_2O_5 as cathode materials for ZIBs have been reported. Senguttuvan et al.^[127] investigated the electrochemical performance of bilayered V_2O_5 cathode with 0.5 M Zn(TFSI)₂/acetonitrile electrolyte and zinc metal anode. When cycled at 0.1 C (1 C = 144 mA g⁻¹), a stabilized capacity of 170 mAh g⁻¹ with average potential of 0.85 V was realized, and no obvious decay was observed for 120 cycles. The energy density of the Zn/bilayered V_2O_5 full battery based on the total mass of two electrodes is about 114 Wh kg⁻¹, which is lower than that of the present state-of-the-art LIBs. However, the achieved power density (1500 W kg⁻¹) is comparable to or even better than standard LIBs. Yan et al.^[88] investigated the zinc storage performance of bilayered V_2O_5 in aqueous electrolyte. The prepared $V_2O_5 \cdot xH_2O$ /graphene cathode can achieve a high capacity of 381 mAh g⁻¹ at 60 mA g⁻¹ (Figure 6f). Moreover, it also delivers superior cycling stability (capacity retention of 71% after 900 cycles) and rate performance (248 mAh g⁻¹ at 30 A g⁻¹). The excellent electrochemical performance of $V_2O_5 \cdot xH_2O$ /graphene is beneficial from the structural water, which decreases the effective charge of Zn²⁺ by solvation, facilitating the ion diffusion. Yang et al.^[128] recently proposed a Li⁺ preintercalation strategy to enhance the Zn²⁺ storage performance of bilayered $V_2O_5 \cdot xH_2O$. Different from the above-mentioned Fe-ion preintercalation which results in a shrinkage of the layer spacing, the Li⁺ intercalation was found to expand the layer spacing of $V_2O_5 \cdot xH_2O$ from 12.0 to 13.77 Å, resulting in a faster Zn²⁺ diffusion. The obtained Li_xV₂O₅ · nH₂O displayed a high discharge capacity of ≈470 mAh g⁻¹ at 0.5 A g⁻¹ and 192 mAh g⁻¹ after 1000 cycles at 10 A g⁻¹.

In summary, as typical layered cathode materials, orthorhombic V_2O_5 and bilayered V_2O_5 have received great attentions beyond LIBs. The layered structure, multielectrons transfer, and suitable voltage make them highly promising cathodes for emerging metal-ion batteries. Note that the main drawbacks of V_2O_5 as cathode in LIBs (Li-poor property and low voltage) are basically nonexistent in MIBs, AIBs, and ZIBs. Therefore, the research of V_2O_5 -based multivalent metal-ion batteries is a very important direction in the future. Further improving the capacity, rate capability and cycling performance is highly desired. The optimization strategies of V_2O_5 in LIBs, such as enlarging interlayer spacing, doping, and fabricating conductive nanocomposite, may be also useful in multivalent metal-ion batteries. Among them, controllably adjusting the interlayer spacing to optimize the ion diffusion by certain strategies, such as metal-ion preintercalation,^[58,129,130] organic molecules preintercalation^[131,132] and water content regulation,^[123] is expected to be the most effective way to improve the performance.

3.3. VO₂(B)

VO₂ has more than ten phases,^[133] and the structure determines the properties. For the application in metal-ion batteries, the metastable VO₂(B) exhibits the best electrochemical

performance among the various VO₂ phases and has attracted much attention from researchers. The VO₂(B) possesses the layered structure consisted of [VO₆] octahedron bilayers, which can be described as the collapsed bilayered V_2O_5 structure after removing the crystal water and interlayer spacing (Figure 3c). The [VO₆] octahedron bilayers of VO₂(B) are connected by sharing corners, and the 1D channel between layers provides the diffusion pathway for the metal ion.^[43,46,134]

3.3.1. VO₂(B) for SIBs

The application of VO₂(B) as an SIB cathode was investigated by Wang et al.^[135] A reversible capacity of about 200 mAh g⁻¹ was achieved at 50 mA g⁻¹ between 1.5 and 4.0 V (Figure 7a). However, the VO₂(B) nanosheets cathode delivers a poor cycling stability. The Na⁺ storage mechanism of VO₂(B) was investigated. In the first discharge process, the VO₂(B) transforms to NaVO₂ with the intercalation of one Na⁺ ion per formula (Figure 7b), corresponding to a theoretical capacity of 323 mAh g⁻¹. Then, the transformation of NaVO₂ to Na_xVO₂ (x ≈ 0.3) occurs in the subsequent charge process with the incomplete Na⁺ ions deintercalation. In the subsequent cycling process, the reaction is the reversible transformation between NaVO₂ and Na_xVO₂ (x ≈ 0.3).

In order to enhance the electrochemical performance of VO₂(B), Fan group designed and fabricated the graphene foam (GF) supported graphene quantum dots (GQDs) coated VO₂(B) nanobelt arrays (GVG) (Figure 7c).^[136] The GQDs layers can restrain the agglomeration and dissolution of VO₂(B) nanobelts during cycling, which together with the increased electron/ion transport properties, results in the excellent Na⁺ storage performance. Even at a high rate of 120 C, the capacity of GVG cathode still remains at 93 mAh g⁻¹. In addition, an outstanding cycling performance with capacity retention of 88% after 1500 cycles at 60 C was realized.

Besides, the Na⁺ storage performance of VO₂(B)-based flexible cathode has been investigated. Tong's group fabricated carbon cloth supported VO₂(B) nanowires (C-VO), and the carbon quantum dots (CQDs) was introduced to further improve the electrochemical performance.^[89] In the CQDs decorated C-VO (C-VOCQD), the carbon cloth was covered by CQDs decorated VO₂(B) nanowires layer with thickness of ≈800 nm (Figure 7d). As a binder-free and flexible cathode material for SIBs, C-VOCQD displays a high initial discharge capacity of 328 mAh g⁻¹ at 0.3 C and 133 mAh g⁻¹ at 60 C in 1.5–3.5 V (Figure 7e). Energy density of 334 Wh kg⁻¹ (based on total mass of whole electrode) and power density of over 40 kW kg⁻¹ can be achieved. The unique structure of C-VOCQD is responsible for the high capacity and enhanced rate performance. The CQDs not only enhances the electronic transport, but also prevents the VO₂(B) nanowires from self-agglomeration.

3.3.2. VO₂(B) for Multivalent-Ion Batteries

Except SIBs, VO₂ has also been investigated as a cathode for multivalent-ion batteries, including MIBs, AIBs and ZIBs. In a three-electrode system with Mg(ClO₄)₂/acetonitrile electrolyte, VO₂(B) nanorods cathode displayed a high Mg²⁺ storage

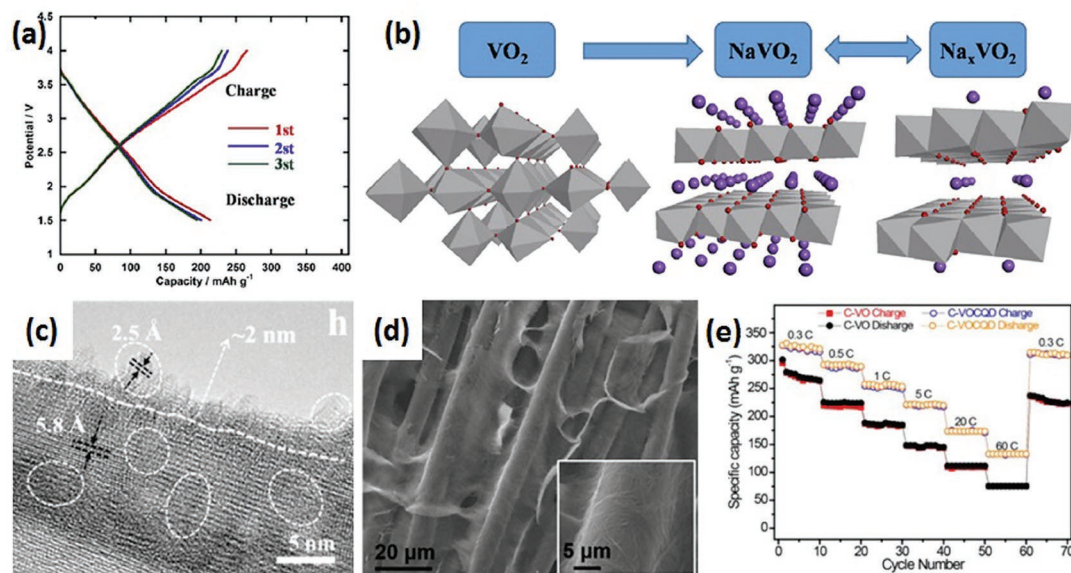


Figure 7. a) The charge/discharge curves of VO₂(B) nanosheets as cathode materials for SIBs at 50 mA g⁻¹. b) The schematic illustration for sodium storage mechanism of VO₂(B). Reproduced with permission.^[135] Copyright 2014, Elsevier. c) The TEM image of GQD-coated VO₂(B) nanobelts. Reproduced with permission.^[136] Copyright 2015, American Chemical Society. d) The SEM images of C-VOCQD. e) The rate performance of C-VOCQD and C-VO. Reproduced with permission.^[89] Copyright 2016, American Chemical Society.

capacity of 391 mAh g⁻¹ with an average voltage about 2.0 V (vs Mg²⁺/Mg).^[90] After 60 cycles, the discharge capacity remained at about 200 mAh g⁻¹. In addition, VO₂ has been utilized as cathode material for emerging Li⁺/Mg²⁺ hybrid battery and achieves a high energy density of 427 Wh kg⁻¹.^[137] Wang et al.^[91] reported a coin cell AIB based on VO₂ as a cathode, aluminum foil as an anode and stainless steel as a current collector. At the current density of 50 mA g⁻¹, an initial discharge capacity of 165 mAh g⁻¹ was obtained, which retained 116 mAh g⁻¹ after 100 cycles. However, the reactions with stainless steel may also occur during the charge/discharge, thus the practical discharge capacity of VO₂ is inconclusive.

Recently, Ding et al.^[92] reported a Zn/VO₂ aqueous battery and obtained a high reversible capacity of 357 mAh g⁻¹ at 0.25 C and 171 mAh g⁻¹ at 300 C. Based on the kinetics analyses and in situ XRD characterizations, it was demonstrated that VO₂ shows abundant tunnel transport pathways with slight structural change upon Zn²⁺ intercalation, which triggers the intercalation pseudocapacitance behavior of VO₂ for Zn²⁺ storage and thus results in the observed excellent rate capability. Soon after that, Chen et al.^[138] also reported the superior cycling and rate performance of Zn/VO₂ batteries. Besides, the reversible single-phase reaction with a more detailed lattice parameters variation during Zn²⁺ insertion/extraction was revealed. These results are consistent well with that reported by Ding et al., indicating that VO₂ shows great potential for high-capacity, high-rate and long-life ZIBs.

3.4. V₃O₇·H₂O (H₂V₃O₈)

V₃O₇·H₂O (H₂V₃O₈) is a mixed-valence state vanadium oxide with V⁵⁺/V⁴⁺ ratio of 2:1. H₂V₃O₈ is also a layered structure compound, in which V₃O₈ layers are stacked along *a*-axis with the interaction of hydrogen bonds (Figure 3d).^[139] The V₃O₈ layer

is composed of [VO₆] octahedrons and [VO₅] square pyramids which are connected by sharing edges and corners. Compared to orthorhombic V₂O₅, H₂V₃O₈ displays a larger interlayer spacing with hydrogen ion in the interlayer and higher electronic conductivity due to the mixed-valence state. Besides, H₂V₃O₈ usually possesses 1D nanostructure, which facilitates the ionic/electronic transport. The above-mentioned properties make H₂V₃O₈ attractive for LIBs and post-LIBs application.

Wang et al.^[93] investigated the Na⁺ storage performance of flexible and additive-free H₂V₃O₈ nanowire film. At the low current density of 10 mA g⁻¹, the capacity can reach 168 mAh g⁻¹ in the potential window of 1.5–4.0 V. The Na⁺ storage mechanism was studied via ex situ XRD measurement, and the slight structural breathing effect was observed. Tang et al.^[94] reported the Mg²⁺ storage behavior of H₂V₃O₈ nanowires with Mg(ClO₄)₂/acetonitrile electrolyte in a three-electrode system. The H₂V₃O₈ nanowires realized a high capacity of about 304 mAh g⁻¹ with a slope plateau at about 2.0 V and maintained a capacity of 261 mAh g⁻¹ after 20 cycles. Unfortunately, H₂V₃O₈ nanowires are almost inactive in the electrolyte with good Mg metal anode compatibility. The zinc storage performance of H₂V₃O₈ nanowires was investigated by He et al.^[95] and Pang et al.^[140] with Zn(CF₃SO₃)₂ aqueous electrolyte. A high capacity of about 400 mAh g⁻¹ was achieved with two slope plateaus at about 0.8 and 0.5 V, respectively. Stable cycling over 1000 cycles was obtained at high rates. These results demonstrate that H₂V₃O₈ is a versatile and promising high-capacity cathode, especially for MIBs and ZIBs.

3.5. V₆O₁₃

The V₆O₁₃ consists of alternating single and double [VO₆] octahedron layers with mixed-valence vanadium of V⁵⁺/V⁴⁺ (Figure 3e). According to the valence bond sum calculations,

only partial V sites in the double layer display V^{5+} property while the other V sites are occupied by V^{4+} .^[43,141] In the layers, the $[VO_6]$ octahedrons are connected by sharing corners and edge, and the adjacent layers are only connected by sharing corners. Theoretically, with the reduction of all vanadium-ions to V^{3+} , V_6O_{13} can achieve high capacity of 417 mAh g^{-1} . Moreover, V_6O_{13} exhibits a metallic property at room temperature.

The previous investigations on V_6O_{13} mainly focused on its Li storage properties. The reports about V_6O_{13} for emerging energy storage are rare. In 1989, Munshi^[142] reported the electrochemical performance of V_6O_{13} as cathode materials for sodium polymer electrolyte cells. Afterward, only few related studies were reported.^[96,143] Recently, Fei et al.^[96] reported the Na^+ storage performance of V_6O_{13} microflowers. At a low current density of 20 mA g^{-1} , a high capacity of $\approx 226 \text{ mAh g}^{-1}$ can be obtained in the potential range of 1.5–3.5 V (vs Na^+/Na). After 30 cycles at 160 mA g^{-1} , the V_6O_{13} microflowers retained a capacity of $\approx 118 \text{ mAh g}^{-1}$, corresponding to 73.5% of the capacity in the second cycle.

3.6. V_2O_3

The crystal structure of V_2O_3 is rhombohedral corundum-type structure at ambient temperature, in which the vanadium

atoms form 3D V–V chains, and the oxygen atoms around the vanadium sites form distorted octahedron (Figure 3f). Because of the low valence state of vanadium (+3), the surface of V_2O_3 will generally be oxidized into high valence state (V^{4+} or V^{5+}) when exposed to air.^[144,145] Therefore, a carbon coating may be necessary to improve its phase stability in air.

Different from the vanadium oxides discussed above, V_2O_3 displays a low capacity in the potential over 2 V (vs Li^+/Li) with no obvious plateau in charge/discharge curves, and has been considered unusable as a cathode for LIBs by Tranchant et al. in 1980.^[146] However, Li et al.^[147] reported that V_2O_3 possesses a high theoretical Li^+ storage capacity of 1070 mAh g^{-1} when used as an anode material for LIBs in 2004. Moreover, the corundum-type V_2O_3 delivers metallic character. Therefore, V_2O_3 attracted research interests as an anode afterward.

Considering the high capacity of V_2O_3 for Li storage, recently the electrochemical performance of V_2O_3 as anode materials for SIBs has been investigated.^[53,97,148,149] Xia et al.^[97] reported the GF supported CNTs decorated V_2O_3 nanoflake arrays (GF+ V_2O_3 /CNTs) for Na^+ storage. A high reversible capacity of $\approx 612 \text{ mAh g}^{-1}$ at 100 mA g^{-1} in the potential window of 0.01–3.0 V (Figure 8a) was obtained. Even at $10\,000 \text{ mA g}^{-1}$, the reversible capacity still remains at 207 mAh g^{-1} (Figure 8b). Moreover, the GF+ V_2O_3 /CNTs anode exhibits superior cycling stability with capacity retention of

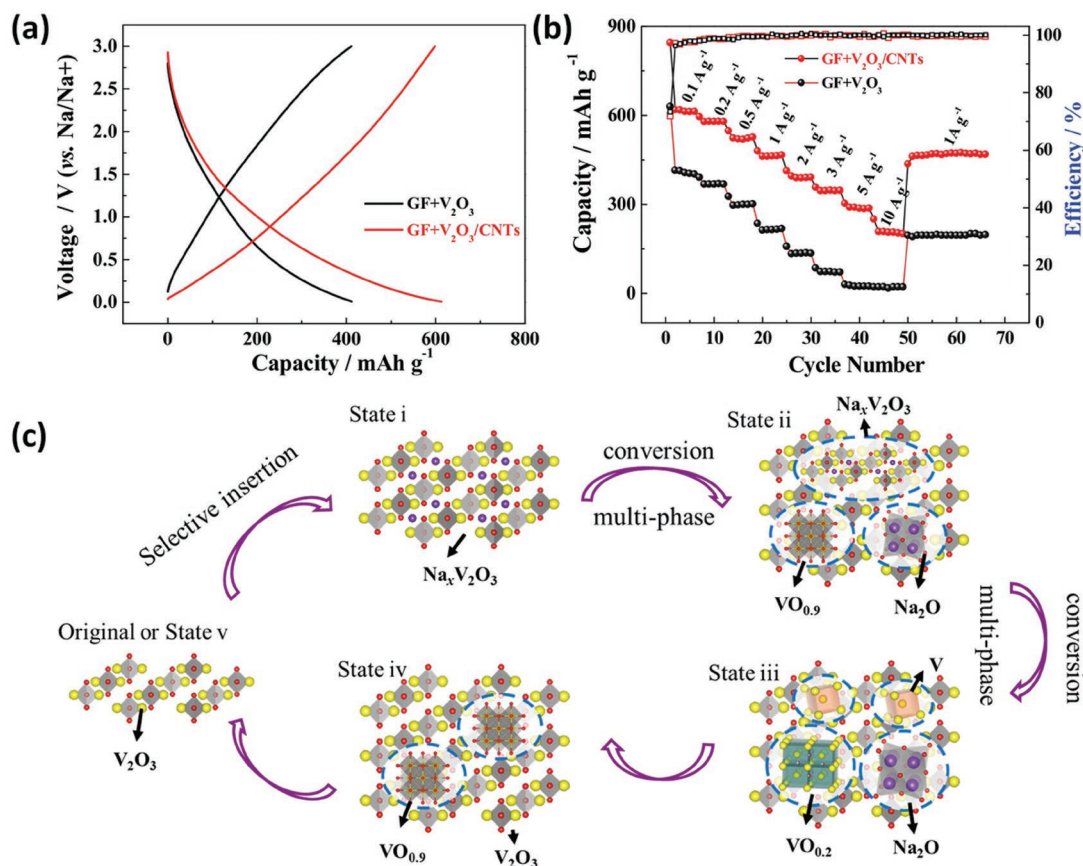


Figure 8. a) The charge/discharge curves at 100 mA g^{-1} and b) rate performance of GF+ V_2O_3 /CNTs and GF+ V_2O_3 as anode materials for SIBs. Reproduced with permission.^[97] Copyright 2016, Wiley-VCH. c) The schematic for sodium storage mechanism of V_2O_3 . Reproduced with permission.^[149] Copyright 2018, Wiley-VCH.

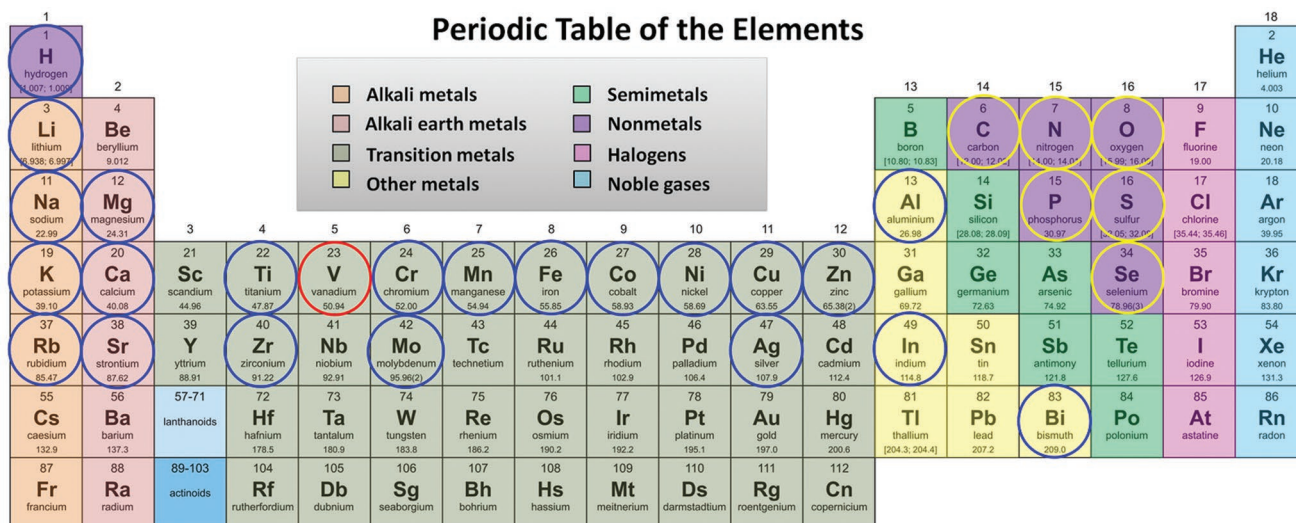


Figure 9. The periodic table showing the different elements. The element marked with a red circle represents the vanadium; the elements marked with blue circles represent cations which can composite with vanadium oxides; the elements marked with yellow circles represent anions which can composite with vanadium.

70% after 10 000 cycles at 10 000 mA g⁻¹. The enhanced Na⁺ storage performance of GF+V₂O₃/CNTs was attributed to the decoration of CNTs and GF substrate, which hinders the self-aggregation of V₂O₃ nanoflakes and provides fast electronic conduction network. Tan et al.^[149] recently designed a multidimensional synergistic nanoarchitecture which consists of 0D V₂O₃ nanoparticles embedded in 1D amorphous carbon nanotubes that are then coassembled within a 3D reduced graphene oxide (rGO) network (denoted as V₂O₃@C-NTs@rGO). In such a nanoarchitecture, each unit with different dimensions was believed to exert their own advantages and overcome the deficiencies of the other units, thus resulting in unique synergistic effects. Benefiting from that, the V₂O₃@C-NTs@rGO nanoarchitecture exhibited an ultralong cycling stability with capacity retention of 72.3% even after 15 000 cycles when used as SIB anode. Besides, the detailed sodium storage mechanism was carefully investigated based on in situ and ex situ TEM characterizations. An incomplete conversion reaction was demonstrated with the generation of VO_{0.2}, metal V and Na₂O when discharged to 0.01 V, which returned to VO_{0.9} and V₂O₃ when charge to 3.0 V (Figure 8c).

In this section, we have summarized and discussed the electrochemical properties, reaction mechanisms and optimization strategies of typical vanadium oxides beyond LIBs. The research attentions about vanadium oxides in recent years are mainly focused on the emerging metal-ion batteries, especially multivalent metal-ion batteries with corresponding metal anodes. Owing to the multielectrons transfer properties and suitable voltage, we have witnessed great progresses of vanadium oxides in aqueous ZIBs very recently with high capacity, excellent cycling and rate performance. Besides, vanadium oxides such as V₂O₅ and bilayered V₂O₅ · xH₂O are also promising cathodes for MIBs. However, the research of emerging multivalent metal-ion batteries is still nascent. With the further development of advanced electrolytes and deeper insights into the energy storage mechanism, the vanadium oxides based

multivalent metal-ion batteries are promising to become one of the next-generation new battery technologies.

4. Vanadates

Vanadates are another important group of vanadium-based materials. This category can be regarded as the derivatives of vanadium oxides composited with other ions or clusters. Until now, a large number of vanadates have been reported, and most of which have been studied for Li⁺ storage. Recently, considerable new vanadate phases were identified to display promising electrochemical properties for metal-ion batteries beyond Li, such as CaV₄O₉ for Na⁺ storage,^[150] Mg_{0.3}V₂O₅ · 1.1H₂O for Mg²⁺ storage,^[151] and Zn_{0.25}V₂O₅ · nH₂O for Zn²⁺ storage.^[22] The big family of vanadates with large amounts of members is as a result of the rich chemical valence state of vanadium and facile distortion of V–O polyhedra. Based on the existing reports about vanadate electrodes, the ions or clusters that can composite with vanadium oxides include alkali metal ions (Li⁺, Na⁺, K⁺, and Rb⁺), alkali earth metal ions (Mg²⁺, Ca²⁺, and Sr²⁺), transition metal ions (Ag⁺, Co²⁺, Cu²⁺, Zn²⁺, etc.) and others (NH₄⁺, Al³⁺, In³⁺, Bi³⁺, etc.) (Figure 9). Based on that, here we classified the vanadates into alkali metal vanadates, alkali earth metal vanadates, transition metal vanadates and other vanadates. With different components introduction, the resulting vanadates display various electrochemical properties, which make vanadates have a wide application in energy storage. Table 2 presents the typical reported vanadates and their applications and electrochemical properties for emerging metal-ion batteries.

Three aspects, namely the different kinds of metal ions, the different A/V (A corresponds to the introduced metal ions) ratios, and the variation of the vanadium valance, determine the structural features and electrochemical properties of the final vanadates. Figure 10 displays the crystal structures of the typical vanadates which have been reported for emerging metal-ion batteries,

Table 2. The typical vanadates and their electrochemical properties for emerging metal-ion batteries.

Materials	Applications	Morphology	Average discharge voltage [V]	Highest capacity [mAh g ⁻¹]	Cycling stability	Refs.
LiV ₃ O ₈	ZIB cathode	Bulk	≈0.82 (vs Zn ²⁺ /Zn)	≈280	Retained 75% after 65 cycles at 133 mA g ⁻¹	[152]
Na _{1.25} V ₃ O ₈	SIB cathode	Zigzag nanowires	≈2.3 (vs Na ⁺ /Na)	≈172	Retained 87% after 1000 cycles at 1000 mA g ⁻¹	[153]
Na ₂ V ₆ O ₁₆ ·3H ₂ O	ZIB cathode	Nanowires	≈0.8 (vs Zn ²⁺ /Zn)	≈350	Retained 90% after 6000 cycles at 5000 mA g ⁻¹	[154]
Na _{0.33} V ₂ O ₅	ZIB cathode	Nanowires	≈0.7 (vs Zn ²⁺ /Zn)	≈350	Retained 93% after 1000 cycles at 1000 mA g ⁻¹	[155]
γ-Na _{0.96} V ₂ O ₅	SIB cathode	Coral-like nanorod agglomerates	≈3.4 (vs Na ⁺ /Na)	≈125	Retained 90% after 50 cycles at C/5	[156]
K _{0.42} V ₂ O ₅ ·0.25H ₂ O	PIB cathode	Nanobelts	≈2.8 (vs K ⁺ /K)	268	Retained 74% after 50 cycles at C/15	[157]
NaVO ₂	SIB cathode	Bulk	≈1.8 (vs Na ⁺ /Na)	≈120	Without capacity fading after 15 cycles	[158]
Ca _{0.25} V ₂ O ₅ ·nH ₂ O	ZIB cathode	Nanobelts	≈0.8 (vs Zn ²⁺ /Zn)	≈340	Retained 96% after 3000 cycles at 80 C	[159]
Mg _{0.3} V ₂ O ₅ ·1.1H ₂ O	MIB cathode	Nanowires	≈2.2 (vs Mg ²⁺ /Mg)	164	10 000 cycles without capacity fading at 1000 mA g ⁻¹	[151]
Mg _{0.25} V ₂ O ₅ ·H ₂ O	CIB cathode	parallelogram-shaped plate	≈-0.1 (vs Ag ⁺ /Ag)	≈120	Retained 86.9% after 500 cycles at 100 mA g ⁻¹	[160]
CaV ₄ O ₉	SIB anode	Nanowires	≈1.0 (vs Na ⁺ /Na)	≈350	Retained 79% after 1000 cycles at 1000 mA g ⁻¹	[150]
Mo _{2.5+y} VO _{9+δ}	MIB cathode	Nanorods	≈2.2 (vs Mg ²⁺ /Mg)	397	Retained 59% after 15 cycles at C/70	[161]
Zn _{0.25} V ₂ O ₅ ·nH ₂ O	ZIB cathode	Nanobelts	≈0.75 (vs Zn ²⁺ /Zn)	≈280	Retained 80% after 1000 cycles at 2400 mA g ⁻¹	[22]
Zn ₃ V ₂ O ₇ (OH) ₂ ·2H ₂ O	ZIB cathode	Nanowires	≈0.7 (vs Zn ²⁺ /Zn)	213	Retained 68% after 300 cycles at 200 mA g ⁻¹	[162]
Zn ₂ V ₂ O ₇	ZIB cathode	Nanowires	≈0.7 (vs Zn ²⁺ /Zn)	≈250	Retained 85% after 1000 cycles at 4000 mA g ⁻¹	[163]
NH ₄ V ₄ O ₁₀	CIB cathode	Nanobelts	≈-0.3 (vs Ag ⁺ /Ag)	≈150	Without capacity fading after 100 cycles	[164]

namely, LiV₃O₈, Na_{0.33}V₂O₅, NaVO₂, CaV₄O₉, Ca_{0.25}V₂O₅·H₂O, and Zn₃V₂O₇(OH)₂·2H₂O, respectively. It is known that their structures have distinct differences from one another, and so does the electrochemical properties. In the following we will discuss the details of these materials and other related vanadates and their application in emerging metal-ion batteries.

4.1. Alkali Metal Vanadates

Alkali metal vanadates include lithium vanadates, sodium vanadates and potassium vanadates. Compared with the pristine

vanadium oxides, most of the vanadates displayed more attractive electrochemical properties. The incorporated alkali metal ions are believed to have significant influence on both the structures and electrochemical properties. For example, the large K⁺ ions in K_{0.25}V₂O₅ have been demonstrated to act as pillars to bring a stabilizing effect, which effectively enhances the structural stability and increases the ion diffusion channel size, and then improves both the cycling and rate performance compared to V₂O₅.^[58] Over the past decades, most of the alkali metal vanadates have been studied for Li storage. While in recent years, considerable efforts have been devoted to the applications of alkali metal vanadates in emerging metal-ion batteries.

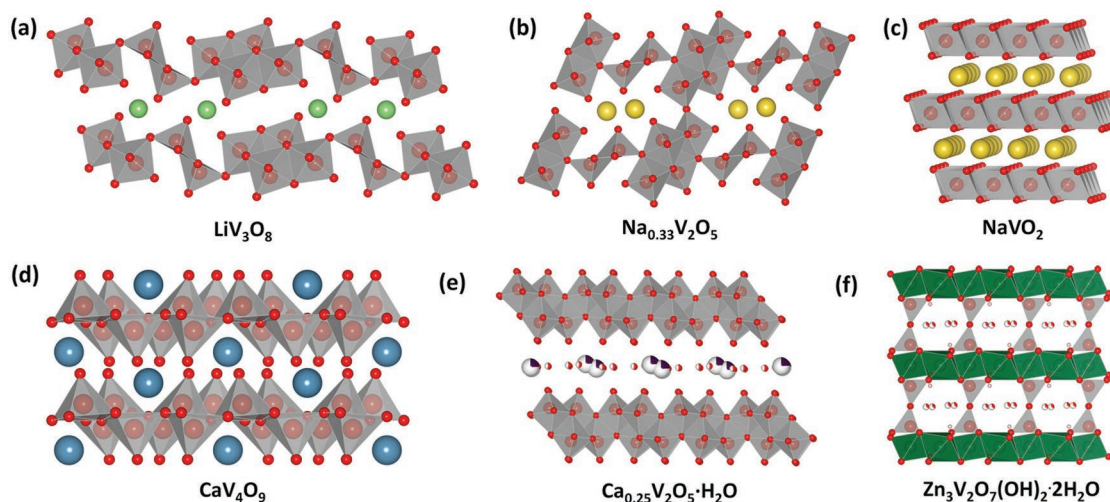


Figure 10. Crystal structures of the typical vanadates for emerging energy storage: a) LiV₃O₈, b) Na_{0.33}V₂O₅, c) NaVO₂, d) CaV₄O₉, e) Ca_{0.25}V₂O₅·H₂O, and f) Zn₃V₂O₇(OH)₂·2H₂O.

4.1.1. LiV_3O_8

LiV_3O_8 is a layered structure with $(\text{V}_3\text{O}_8)^-$ layers stacked along *a* axis (Figure 10a), and Li^+ ions occupy all octahedral sites and partial tetrahedral sites in the interlayers to hold the adjacent layers.^[43] These Li^+ ions in the interlayers were found to be immobile in the structure. In the past years, LiV_3O_8 was mainly studied as a LIB cathode.^[165,166] Recently, Alfaruqi et al.^[152] investigated the Zn^{2+} storage properties of LiV_3O_8 for aqueous ZIBs with 1 M ZnSO_4 (pH 4.0) as electrolyte. High reversible capacities of $\approx 250 \text{ mAh g}^{-1}$ at a current density of 16 mA g^{-1} , and 172 mAh g^{-1} at 133 mA g^{-1} with capacity retention of 75% after 65 cycles were demonstrated. The phase evolution during Zn^{2+} intercalation was studied by in situ XRD and simulation techniques. It was found that Zn^{2+} intercalation firstly results in the formation of a stoichiometric ZnLiV_3O_8 phase, which proceeds to reversible solid-solution $\text{Zn}_\gamma\text{LiV}_3\text{O}_8$ ($\gamma > 1$) phase. Upon Zn^{2+} deintercalation, $\text{Zn}_\gamma\text{LiV}_3\text{O}_8$ transforms back to LiV_3O_8 via a single-phase behavior. Such a Zn^{2+} storage mechanism is different from that for Li^+ storage.

Note that the reported cycling performance of LiV_3O_8 for aqueous ZIBs is inferior compared to that of the above-mentioned V_2O_5 or VO_2 . The reason may be due to the dissolution of vanadium into the ZnSO_4 aqueous electrolyte which is weakly acidic. The dissolution of LiV_3O_8 during charge/discharge in aqueous electrolyte was previously evidenced by the yellow colored electrolyte after cycling.^[167] Actually, the dissolution of vanadium in aqueous electrolyte is a non-negligible issue for most of the vanadium-based electrodes, which requires special attention. Electrolyte optimization is very important for LiV_3O_8 or other vanadium-based materials as aqueous battery electrodes. Generally, a neutral electrolyte is the best choice to inhibit the dissolution.^[168,169] Besides, adding additives such as vanadium sol is an effective way to suppress the dissolution.^[88]

4.1.2. $\text{Na}_{1+x}\text{V}_3\text{O}_8$

$\text{Na}_{1+x}\text{V}_3\text{O}_8$ can be regarded as the derivative of LiV_3O_8 with the replacement of Li by Na. The crystal structure of $\text{Na}_{1+x}\text{V}_3\text{O}_8$ is similar to LiV_3O_8 , with $[\text{V}_3\text{O}_8]^-$ layers stacked along certain direction and Na ions occupied the octahedral sites in the interlayers to form a pillared layered structure.^[153] Like the anchored Li ions in LiV_3O_8 , the Na ions in the layers are also immobile during the electrochemical process. Since the larger size of Na ions than Li ions, $\text{Na}_{1+x}\text{V}_3\text{O}_8$ possess a larger interlayer distance than LiV_3O_8 , which means better ion diffusion kinetics. Besides, sodium is much abundant than lithium, which determines the lower cost of $\text{Na}_{1+x}\text{V}_3\text{O}_8$ than LiV_3O_8 . Due to these superiorities, $\text{Na}_{1+x}\text{V}_3\text{O}_8$ have been paid much attention recent years. Ultrathin $\text{Na}_{1.08}\text{V}_3\text{O}_8$ nanosheets,^[170] NaV_3O_8 nanoflakes,^[171] hydrous $\text{Na}_2\text{V}_6\text{O}_{16} \cdot x\text{H}_2\text{O}$ nanowires,^[172] $\text{Na}_{1.25}\text{V}_3\text{O}_8$,^[173] and $\text{Na}_{1.1}\text{V}_3\text{O}_{7.9}$ nanobelts^[174] have been investigated for Li^+ storage.

Due to the expanded interlayer distance, which means better accommodation of larger Na ions, $\text{Na}_{1+x}\text{V}_3\text{O}_8$ have also attracted considerable attentions for the sodium storage. Annealed NaV_3O_8 nanowires were used as an SIB cathode by Wang and co-workers.^[175] An initial reversible capacity of 145.8 mAh g^{-1} was obtained with average voltage of $\approx 2.5 \text{ V}$. The

capacity retained 91.1% after 50 cycles. Through ex situ XRD analyses, a single-phase reaction mechanism was proposed, which is different from the two-phase reaction of LiV_3O_8 during Li^+ insertion. Zhang group reported the single-crystalline $\text{Na}_{1.1}\text{V}_3\text{O}_{7.9}$ nanobelts for sodium storage.^[176] A high capacity of 173 mAh g^{-1} and good cycling stability over 190 cycles were achieved. Recently, Dong et al. fabricated a novel kind of hierarchical $\text{Na}_{1.25}\text{V}_3\text{O}_8$ nanowires with a zigzag shape (Figure 11a,b), which displayed excellent performance as an SIB cathode.^[153] A high capacity of 172.5 mAh g^{-1} at 100 mA g^{-1} was achieved (Figure 11c), and outstanding cycling and rate capability at 1000 mA g^{-1} with capacity retention of 87.7% after 1000 cycles were demonstrated (Figure 11d). The good sodium storage performance was believed to be resulted from the synergistic effect of the good structural features of $\text{Na}_{1.25}\text{V}_3\text{O}_8$ and the zigzag nanowire morphology.

Note that $\text{Na}_{1+x}\text{V}_3\text{O}_8$ possess several analogues with different sodium and oxygen stoichiometry. The excess Na in the structure and oxygen vacancies may have important impacts on the electrochemical performance. To clarify the role of defects on the electrochemical performance of $\text{Na}_{1+x}\text{V}_3\text{O}_8$, Cao and co-workers^[177] prepared $\text{Na}_{1.25+x}\text{V}_3\text{O}_8$ (with $x < 0$, $=0$, and >0), and compared their sodium storage performance. They demonstrated that oxygen vacancies were generated in the case of Na-deficiency, while Na excess resulted in partial reduction of the transition metal, or formation of a cation disordered structure. The Na-deficiency sample displayed a slightly higher capacity in initial cycles compared to the sample with ideal stoichiometry, but severer capacity fading was observed upon further cycling. It was believed that oxygen vacancies may lead to the loss of domain order and then structural collapse, which accounts for the capacity fading. However, the Na-excess sample exhibited more than 50% higher in capacity than the ideal one, with good rate capability and cycling stability. The authors pointed out that the presence of excess sodium can reduce the number of sp^3 orbitals of oxygen available for bonding with the incoming Na^+ , which will reduce the migration energy of Na^+ and then leads to fast movement of Na^+ from site to site. Besides, the excess of Na may also result in a cation disordered structure, which will benefit to the sodium diffusion and result in the higher capacities.

Aqueous SIB based on $\text{Na}_{1+x}\text{V}_3\text{O}_8$ as anodes have also attracted interests in recent years. The Na^+ insertion properties of $\text{Na}_2\text{V}_6\text{O}_{16} \cdot n\text{H}_2\text{O}$ in aqueous electrolyte system were investigated by Deng et al. They constructed a full aqueous SIB based on bundled $\text{Na}_2\text{V}_6\text{O}_{16} \cdot n\text{H}_2\text{O}$ nanobelts as anode and $\text{Na}_{0.44}\text{MnO}_2$ as cathode. Fast capacity fading in initial cycles was observed. Based on ex situ XRD analyses, the authors attributed the capacity fading to the irreversible structural change of $\text{Na}_2\text{V}_6\text{O}_{16} \cdot n\text{H}_2\text{O}$ upon sodium intercalation.^[178]

Important advances of $\text{Na}_{1+x}\text{V}_3\text{O}_8$ electrodes are their applications for emerging aqueous ZIBs very recently. $\text{Na}_{1.1}\text{V}_3\text{O}_{7.9}$ nanoribbons,^[179] $\text{NaV}_3\text{O}_8 \cdot 1.5\text{H}_2\text{O}$ nanobelts,^[180] $\text{Na}_2\text{V}_6\text{O}_{16} \cdot 1.63\text{H}_2\text{O}$ nanowires^[154] and $\text{Na}_2\text{V}_6\text{O}_{16} \cdot 3\text{H}_2\text{O}$ nanorods^[181] have been demonstrated as exciting high-performance ZIB cathodes with high capacity (over 300 mAh g^{-1}), excellent cycling stability and rate capability. For example, $\text{NaV}_3\text{O}_8 \cdot 1.5\text{H}_2\text{O}$ nanobelts were reported to realize a high reversible capacity of 380 mAh g^{-1} and capacity retention

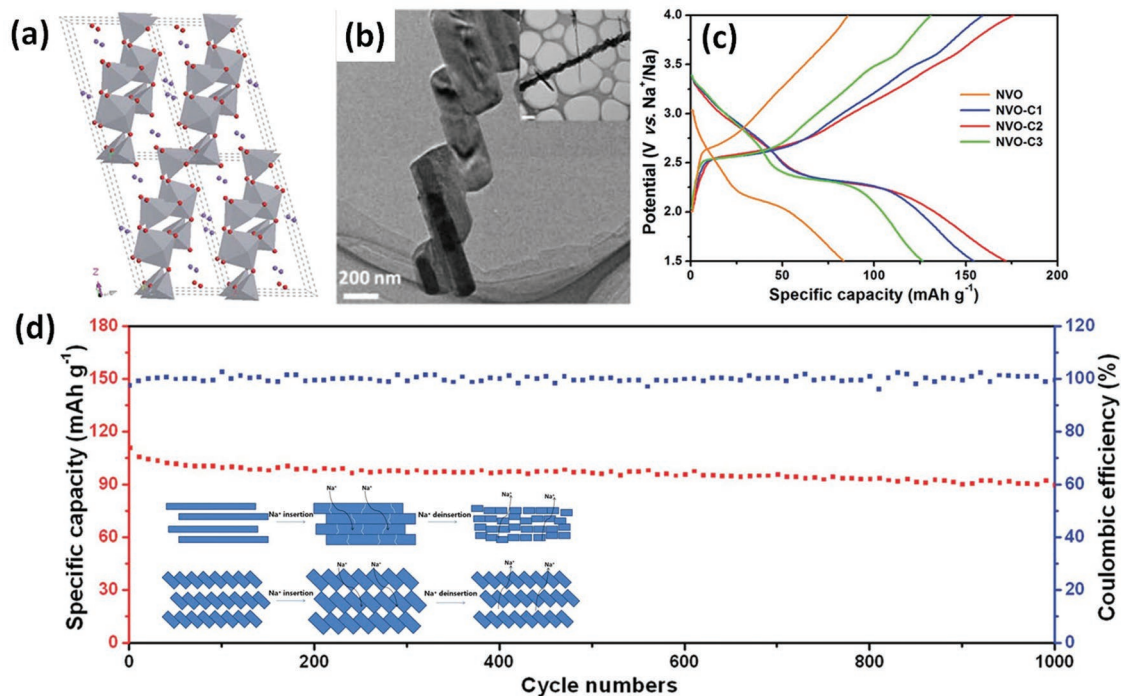


Figure 11. a) Crystal structure of $\text{Na}_{1.25}\text{V}_3\text{O}_8$. b) TEM image of the $\text{Na}_{1.25}\text{V}_3\text{O}_8$ zigzag nanowires, and the inset shows the morphology at a different scale. c) Charge/discharge profiles of $\text{Na}_{1.25}\text{V}_3\text{O}_8$ nanowires with different morphology at 100 mA g^{-1} for sodium storage. d) The long-term cycling performance of $\text{Na}_{1.25}\text{V}_3\text{O}_8$ zigzag nanowires for sodium storage at 1000 mA g^{-1} , and the inset shows the illustration of electrochemical process of simple nanowires and zigzag nanowires. Reproduced with permission.^[153] Copyright 2015, Royal Society of Chemistry.

of 82% after 1000 cycles, while $\text{Na}_2\text{V}_6\text{O}_{16} \cdot 1.63\text{H}_2\text{O}$ nanowires was found to exhibit a capacity retention of 90% over 6000 cycles at 5000 mA g^{-1} . These exciting results suggest that appropriate vanadates as cathodes are one of the good choices for aqueous ZIBs in practical applications.

4.1.3. $\text{A}_x\text{V}_2\text{O}_5$ ($A = \text{Li}, \text{Na}, \text{and K}$)

$\text{A}_x\text{V}_2\text{O}_5$ ($A = \text{Li}, \text{Na}, \text{and K}$) is the other group in alkali metal vanadates. $\text{Na}_{0.33}\text{V}_2\text{O}_5$ is a typical example for this series of compounds. Different from V_2O_5 or LiV_3O_8 , $\text{Na}_{0.33}\text{V}_2\text{O}_5$ is not a typical layered structure but 3D tunnel structure; this kind of structure also can be seen as quasilayered.^[182] As shown in **Figure 12a**, the infinite V–O layers are linked by corner-shared V–O pyramids, which act as “pillars” to connect the adjacent layers and transform the layered structure to 3D tunnel structure. Based on this structure feature, a better structure stability than the typical layered structures during ions insertion/extraction can be expected. The other feature of $\text{Na}_{0.33}\text{V}_2\text{O}_5$ is the mixed valance state of V^{5+} and V^{4+} , which is different from LiV_3O_8 where only V^{5+} exists. The existence of V^{4+} means a better electronic conductivity.^[183] Both the structure and valance state features determine the superior electrochemical properties and versatile applications of $\text{Na}_{0.33}\text{V}_2\text{O}_5$ in energy storage. Based on the reported results, $\text{Na}_{0.33}\text{V}_2\text{O}_5$ has been studied as different roles in various energy storage systems, including as LIB cathode,^[59,184,185] LIB anode,^[186] SIB cathode,^[183,187] supercapacitor electrode,^[188] aqueous LIB anode^[189,190] and aqueous

ZIB cathode.^[155] He et al.^[155] studied the electrochemical properties of $\text{Na}_{0.33}\text{V}_2\text{O}_5$ nanowires as cathode for aqueous ZIBs. At a current density of 0.2 A g^{-1} , the reversible capacity reached to over 250 mAh g^{-1} (Figure 12b). After 1000 cycles at 1.0 A g^{-1} , a capacity retention over 93% was obtained. Based on the single nanowire device and in situ XRD analyses, it is demonstrated that the Na ions in the structure can both increase the electric conductivity and act as pillars to enhance the structure stability.

NaV_2O_5 is another $\text{A}_x\text{V}_2\text{O}_5$ phase with $x = 1$, which has a similar layered structure with the orthorhombic V_2O_5 . The electrochemically formed NaV_2O_5 was found to display a specific capacity of 120 mAh g^{-1} at C/10 for Na intercalation, with a low voltage of $\approx 1.6 \text{ V}$ (vs Na^+/Na).^[191] Recently Emery et al.^[156] synthesized a new $\gamma\text{-Na}_{0.96}\text{V}_2\text{O}_5$ (Figure 12c) as cathode for SIBs. Interestingly, this phase displays a high voltage of 3.4 V (vs Na^+/Na), with initial specific capacity of 125 mAh g^{-1} and capacity retention of $\approx 90\%$ after 50 cycles (Figure 12d). Such a high voltage can compete with other well-known SIB cathode materials such as $\text{NaNi}_{1/3}\text{Mn}_{1/3}\text{Co}_{1/3}\text{O}_2$, which is not common for vanadium oxides or vanadates. However, the origin of the high voltage is still not clear, which needs to be further studied. But this example is encouraging, and it suggests that vanadates family may give more surprise in high-voltage cathodes for SIB and other emerging metal-ion batteries in the future.

Recently, Clites et al.^[157] reported a bilayered $\text{K}_{0.42}\text{V}_2\text{O}_5 \cdot 0.25\text{H}_2\text{O}$ nanobelts for PIBs. This phase exhibits a large layer spacing of 9.65 \AA (Figure 12e), which facilitates the diffusion of large-sized K^+ ions. High reversible capacity of 268 mAh g^{-1} (Figure 12f) and 226 mAh g^{-1} were obtained at

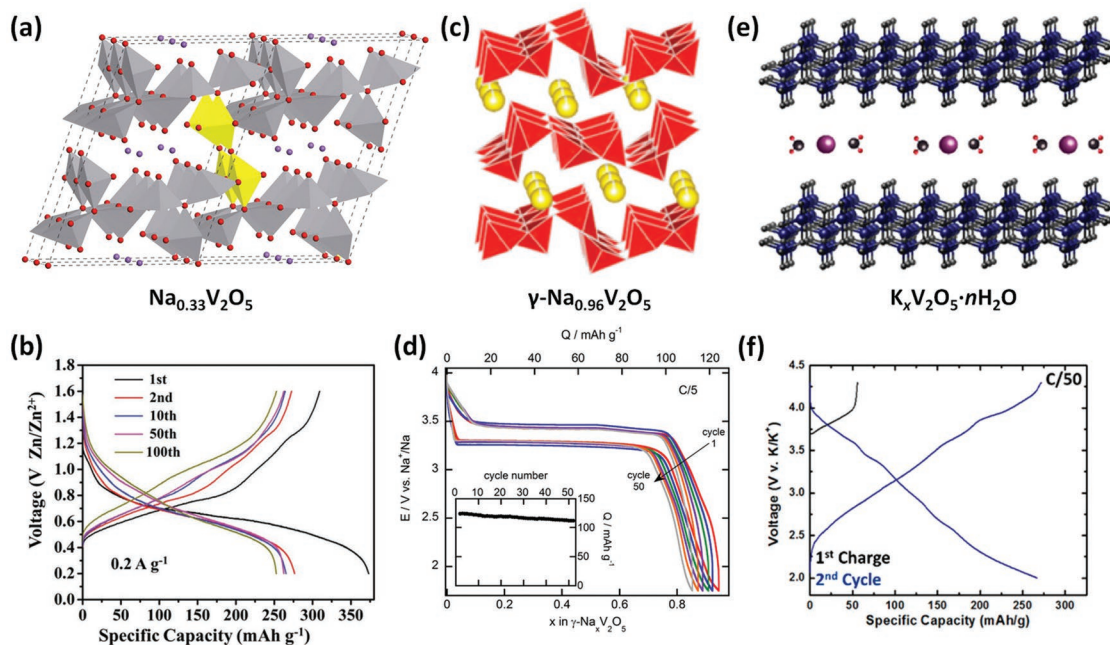


Figure 12. a) Crystal structure of $\text{Na}_{0.33}\text{V}_2\text{O}_5$. b) Charge/discharge profiles of $\text{Na}_{0.33}\text{V}_2\text{O}_5$ nanowires for ZIB cathode. Reproduced with permission.^[155] Copyright 2018, Wiley-VCH. c) Crystal structure of $\gamma\text{-Na}_{0.96}\text{V}_2\text{O}_5$. d) Charge/discharge profiles of $\gamma\text{-Na}_{0.96}\text{V}_2\text{O}_5$ for SIB cathode, and the inset is the cycling performance. Reproduced with permission.^[156] Copyright 2018, American Chemical Society. e) Crystal structure of $\text{K}_x\text{V}_2\text{O}_5 \cdot n\text{H}_2\text{O}$. f) Charge/discharge profiles of $\text{K}_x\text{V}_2\text{O}_5 \cdot n\text{H}_2\text{O}$ for PIB cathode. Reproduced with permission.^[157] Copyright 2018, American Chemical Society.

low current rates of C/50 and C/15, respectively. When cycled for 50 cycles, a capacity retention of 74% was demonstrated. It is believed that the preintercalated K-ions in the bilayered structure can play a similar role like Na-ions in $\text{Na}_{0.33}\text{V}_2\text{O}_5$ to enhance the structure stability.

4.1.4. Na_xVO_2

Na_xVO_2 is a member of the well-known lamellar AMO_2 family, and thus its Na deintercalation/intercalation properties have attracted some research interests recently, even though it seems not to be a good candidate for applications due to its oxygen sensitivity and thermodynamic instability in air. The electrochemical Na^+ deintercalation process of NaVO_2 was first investigated by Delmas's group.^[192] Reversible deintercalation/intercalation of 0.5 Na^+ per unit formula was demonstrated at a voltage range of 1.4–2.5 V, corresponding to a capacity of 126.4 mAh g^{-1} . When the upper limit of voltage increased to 3.0 V, the reversibility was found to loss, suggesting the structural collapse resulting from the Na^+ deintercalation. Concurrently, Rozier's group reported the Na storage properties of O3- NaVO_2 and P2- $\text{Na}_{0.7}\text{VO}_2$.^[158] Both phases were found to reversibly react with 0.5 Na^+ in 1.2–2.4 V with multiple voltage plateaus. Through in situ XRD measurements, the reversible structure evolution of P2- $\text{Na}_{0.7}\text{VO}_2$ was manifested, and four single-phase domains were identified. The lattice parameters were demonstrated to vary as a function of the Na content during charge/discharge, without drastic structural change. Soon after, a more detailed phase diagram of the P2- Na_xVO_2 during electrochemical Na^+ intercalation/deintercalation was reported by Delmas's group.^[193] Similarly,

four main single-phase domains were demonstrated in the x range from 0.5 to 0.9.

4.2. Alkali Earth Metal Vanadates

Unlike the alkali metal vanadates, alkali earth metal vanadates seem to be ignored for a long period of time in the investigation of electrode materials for energy storage. However, several recent studies on alkali earth metal vanadates reveal exciting electrochemical properties, indicating that this field is worthy of attention. Xia et al.^[159] demonstrated that layered $\text{Ca}_{0.25}\text{V}_2\text{O}_5 \cdot n\text{H}_2\text{O}$ is a good candidate for aqueous ZIB cathode. A high capacity of 340 mAh g^{-1} at 0.2 C and capacity retention of 96% after 3000 cycles at 80 C were achieved. When compared with the reported $\text{Zn}_{0.25}\text{V}_2\text{O}_5 \cdot n\text{H}_2\text{O}$ at earlier stage (which will be introduced in the following section of transition metal vanadates), $\text{Ca}_{0.25}\text{V}_2\text{O}_5 \cdot n\text{H}_2\text{O}$ was found to show higher electrical conductivity (185 S m^{-1} compared to 46 S m^{-1}) and larger layer spacing (10.6 Å compared to 10.2 Å) due to the larger CaO_7 polyhedra than the ZnO_6 octahedra in the layers. Besides, the lower molecular weight can result in higher gravimetric capacity. Soon after that, Ming et al.^[194] further identified a $\text{Mg}_{0.34}\text{V}_2\text{O}_5 \cdot n\text{H}_2\text{O}$ for aqueous ZIBs, which shows a similar bilayered structure with that of $\text{Ca}_{0.25}\text{V}_2\text{O}_5 \cdot n\text{H}_2\text{O}$ and $\text{Zn}_{0.25}\text{V}_2\text{O}_5 \cdot n\text{H}_2\text{O}$. This investigation is motivated by the fact that Mg has a lower molecular weight than Zn and Ca, and thus a higher capacity (352 mAh g^{-1} at 100 mA g^{-1}) can be obtained. Interestingly, it was found that $\text{Mg}_{0.34}\text{V}_2\text{O}_5 \cdot n\text{H}_2\text{O}$ shows a much larger interlayer spacing (13.4 Å) than that of $\text{Ca}_{0.25}\text{V}_2\text{O}_5 \cdot n\text{H}_2\text{O}$ and $\text{Zn}_{0.25}\text{V}_2\text{O}_5 \cdot n\text{H}_2\text{O}$.

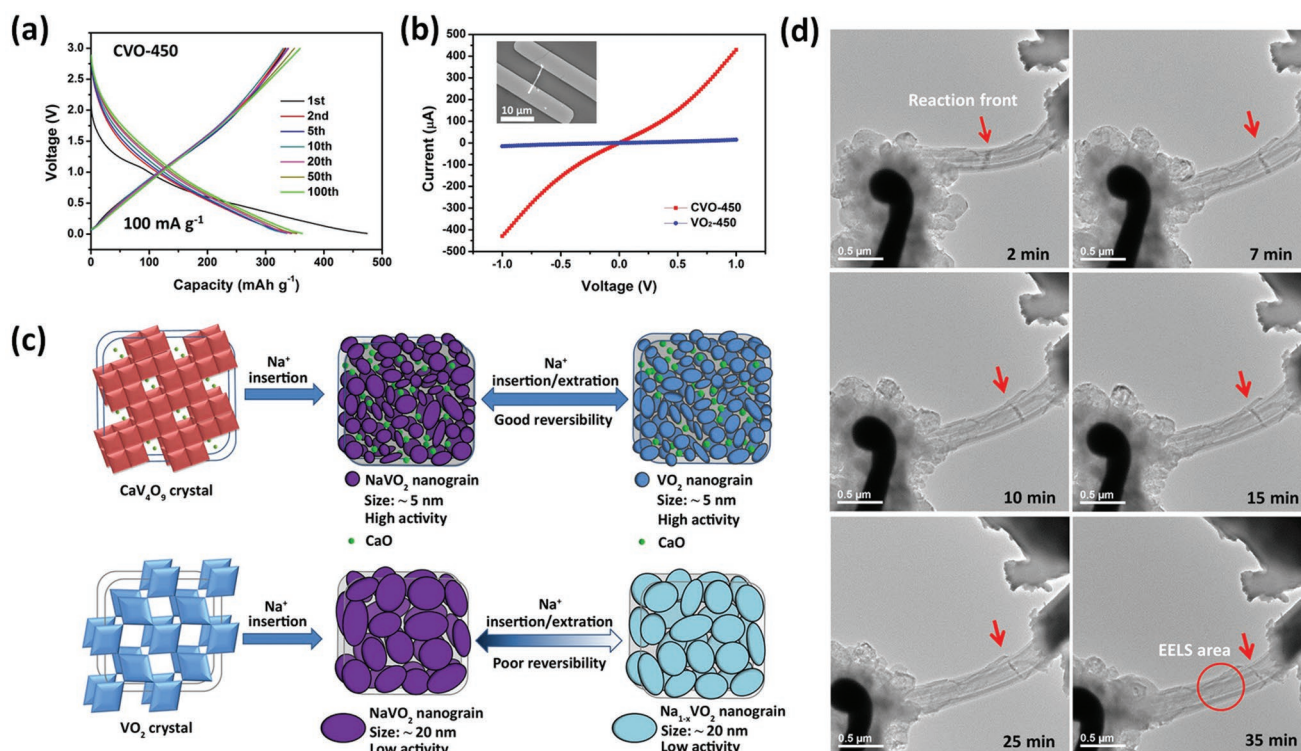


Figure 13. a) Charge/discharge profiles of CaV_4O_9 nanowires in the voltage range of 0.01–3.0 V versus Na^+/Na . b) I – V curves of CaV_4O_9 nanowire and VO_2 nanowire. Inset is the SEM image of the CaV_4O_9 single nanowire device. c) Schematic illustrations of the sodium storage mechanism of CaV_4O_9 and VO_2 . d) In situ TEM measurements of CaV_4O_9 nanowires. Reproduced with permission.^[150] Copyright 2017, Springer Nature.

Very recently, Xu et al.^[151] developed a bilayered $\text{Mg}_{0.3}\text{V}_2\text{O}_5 \cdot 1.1\text{H}_2\text{O}$ nanowires with interlayer spacing of 11.9 Å and investigated the Mg^{2+} storage performance. Remarkably, with $\text{Mg}(\text{TFSI})_2$ in acetonitrile as electrolyte and ACC as counter electrode, an ultralong cycling stability for 10 000 cycles with capacity retention over 80% was demonstrated. Based on the comparison with the control samples $\text{V}_2\text{O}_5 \cdot \text{H}_2\text{O}$ and $\text{Mg}_{0.3}\text{V}_2\text{O}_5$, it is believed that the excellent cycling stability of $\text{Mg}_{0.3}\text{V}_2\text{O}_5 \cdot 1.1\text{H}_2\text{O}$ is attributed to the synergistic effect of the inherent Mg^{2+} ions and crystal water. Soon after, a different bilayered $\text{Mg}_{0.25}\text{V}_2\text{O}_5 \cdot \text{H}_2\text{O}$ with an interlayer spacing of 10.76 Å and a parallelogram-shaped plate morphology was reported by Xu and coauthors for Ca^{2+} storage.^[160] Notably, an ultrastable structure feature of $\text{Mg}_{0.25}\text{V}_2\text{O}_5 \cdot \text{H}_2\text{O}$ was demonstrated during Ca^{2+} ions intercalation/deintercalation, with a tiny interlayer spacing variation of only ≈ 0.09 Å, which results in an excellent cycling stability for 500 cycles with retention of 86.9%. Based on experimental characterizations and ab initio calculation, it is proved that Mg^{2+} ions are more stable in the interlayers, while Ca^{2+} ions are more diffusible in the structure.

Considering the bilayered structures with large layer spacing, the good structure stability pillared by alkali earth metal ions, and charge screen effect from the crystal waters between the layers, $\text{Mg}_x\text{V}_2\text{O}_5 \cdot n\text{H}_2\text{O}$ and $\text{Ca}_x\text{V}_2\text{O}_5 \cdot n\text{H}_2\text{O}$ are very promising candidates for the emerging multivalent metal-ion batteries. The above investigations about their application in aqueous ZIBs, MIBs and CIBs is an excellent beginning. Further works about these phases for multivalent metal-ion

batteries are expected in the future. Besides, deeper insights into the effects of different kind of alkali earth metal ions or different amounts of ions and crystal water on the structure features and electrochemical properties are desired.

Apart from acting as pillars in the layered structure to improve the performance of a cathode, the Ca^{2+} ions (or other alkali earth metal ions) can also bring a different positive effect in the conversion-reaction based anode materials. Recently, Xu et al.^[150] identified the outstanding electrochemical properties of alkali earth metal vanadates as SIB anodes. The prepared CaV_4O_9 nanowires was found to display superior Na^+ storage performance compared to the control sample VO_2 nanowires, including an applicable reversible capacity over 300 mAh g^{-1} (Figure 13a), a good rate capability and an excellent long-term cycling stability over 1600 cycles. Through single nanowire device (Figure 13b), the CaV_4O_9 nanowire was demonstrated to possess a high electric conductivity over 100 S cm^{-1} . Based on in situ/ex situ characterizations, it was found that the initial Na^+ insertion resulted in an irreversible conversion from CaV_4O_9 to NaVO_2 and CaO nanograins, and in the subsequent processes, NaVO_2 was proposed to reversibly convert to VO_2 (Figure 13c). Notably, unlike the typical conversion reaction observed in other transition metal oxides (such as Fe/Co/Ni/Cu-based oxides), the whole conversion process from CaV_4O_9 to NaVO_2 and then to VO_2 only accompanied by a small volume change less than 10%, evidenced by theoretical calculation and in situ TEM measurement (Figure 13d). This feature substantially ensures the structure stability in the electrochemical charge/discharge

processes. Besides, based on the ab initio calculation and ex situ TEM characterization, a self-preserving effect from the generated CaO was revealed, which effectively inhibits the agglomeration and prevents the grain-growth of the generated active nanograins during charge/discharge, and preserve the electrodes in a high reversibility. Inspired by the excellent properties of CaV_4O_9 , the authors further prepared nanosheet-assembled compact CaV_4O_9 microflowlers with an increased tap density of 0.74 g cm^{-3} .^[195] Benefiting from the improved tap density of the compact microflower structure and the intrinsic small volume change of CaV_4O_9 , a high areal capacity of $\approx 1.0 \text{ mAh cm}^{-2}$ with stable cycling performance was obtained at a high mass loading for Na^+ storage. These results indicate that CaV_4O_9 is a promising anode material for SIBs in practical applications.

Considering that alkaline earth metal elements are very abundant and cost-effective, the exciting results stated above indicate that the alkaline earth metal vanadates have great potential for both high-performance cathodes and anodes in emerging energy storage. Even though the above achievements have been reported, more attentions should be paid to this material system in the future.

4.3. Transition Metal Vanadates

Transition metal vanadates have a big family with large number of members with different compositions, structures and properties. Most of the common transition metals (Ag, Cu, Co, Mn, Fe, Ni, Zn, etc.) can composite with vanadium oxides and form specific vanadates (Figure 9). Among them, $\text{Ag}_2\text{V}_4\text{O}_{11}$ is a typical example, which has been commercialized as a primary lithium battery cathode as early as 30 years ago.^[196] Both the physicochemical properties (crystal structure, conductivity, thermodynamic stability, etc.) and electrochemical characteristics (voltage, capacity, electrochemical stability, etc.) of the vanadates are highly affected by the species of incorporated transition metal elements. In the past years, most of the investigations about transition metal vanadates mainly focused on the Li storage properties following the research line of $\text{Ag}_2\text{V}_4\text{O}_{11}$, some of which shows interesting Li storage properties, such as $\text{Cu}_{2.33}\text{V}_4\text{O}_{11}$ as lithium battery cathode,^[197] $\text{Co}_3\text{V}_2\text{O}_8$ ^[198] and $\text{Zn}_2(\text{OH})_3\text{VO}_3$ ^[199] as LIB anodes. In recent years, some other new transition metal vanadates were discovered and were found to exhibit interesting electrochemical properties for emerging energy storage.

Wei et al.^[200] recently reported a novel layered $\text{Fe}_5\text{V}_{15}\text{O}_{39}(\text{OH})_9 \cdot 9\text{H}_2\text{O}$ nanosheets for LIB cathode, which was found to exhibit a high reversible capacity (350 mAh g^{-1} at 0.1 A g^{-1}) and ultrahigh-rate capability (90 mAh g^{-1} at 20 A g^{-1}). The superior performance inspired them to further study this material in aqueous ZIB, and the results were also satisfactory. A high capacity (385 mAh g^{-1} at 0.1 A g^{-1}) and good cycling stability (retained 80% after 300 cycles at 5 A g^{-1}) were achieved when used as ZIB cathode.^[201]

$\text{Mo}_{2.5+y}\text{VO}_{9+\delta}$ with a 3D microporous framework were found to display a superior Mg^{2+} storage property in MIBs.^[161] A high initial capacity of 397 mAh g^{-1} (corresponding to 3.49 Mg^{2+} intercalation) was obtained at C/70, retaining $\approx 235 \text{ mAh g}^{-1}$ after 15 cycles. Besides, the average discharge voltage is $\approx 2.1 \text{ V}$, which is higher than that of traditional Chevrel cathodes. It is

believed that the combination of Mo and V ions in the cathode is beneficial to the charge redistribution to maintain electro-neutrality during intercalation of Mg^{2+} ions.

Nazar's group reported a $\text{Zn}_{0.25}\text{V}_2\text{O}_5 \cdot n\text{H}_2\text{O}$ nanobelts for aqueous rechargeable ZIBs (Figure 14a,b).^[22] This compound is a bilayered structure with a large layer spacing over 10.0 \AA , and the indigenous Zn ions and water molecule act as pillars in the interlayers to stabilize the layered structure (Figure 14d). The favorable structural features and the nanobelt morphology result in a superior electrochemical performance. The presented aqueous zinc battery displays a high capacity of 282 mAh g^{-1} (corresponding to 1.1 Zn^{2+} intercalation) (Figure 14e), a high energy density of $\approx 250 \text{ Wh kg}^{-1}$ (based on the mass of cathode), and a good cycling stability for 1000 cycles with capacity retention over 80% (Figure 14f). After that, another two zinc vanadates for aqueous ZIBs were reported, those are $\text{Zn}_3\text{V}_2\text{O}_7(\text{OH})_2 \cdot 2\text{H}_2\text{O}$ nanowires^[162] and $\text{Zn}_2\text{V}_2\text{O}_7$ nanowires,^[163] respectively. $\text{Zn}_3\text{V}_2\text{O}_7(\text{OH})_2 \cdot 2\text{H}_2\text{O}$ nanowires was found to display reversible capacity of 213 mAh g^{-1} at 50 mA g^{-1} and cycling stability up to 300 cycles at 200 mA g^{-1} . $\text{Zn}_2\text{V}_2\text{O}_7$ nanowires exhibited reversible capacity of $\approx 250 \text{ mAh g}^{-1}$ at 50 mA g^{-1} and $\approx 150 \text{ mAh g}^{-1}$ at 4000 mA g^{-1} . Good cycling stability for 1000 cycles at 4000 mA g^{-1} was obtained. The Zn storage mechanism for these phases was all demonstrated to be intercalation/deintercalation reaction. Considering the low cost of zinc, vanadium and aqueous electrolyte, combined with the superior reported electrochemical performance, the aqueous Zn//Zn–V–O batteries are very promising for large-scale energy storage.

4.4. Other Vanadates

Apart from the alkali metal vanadates, alkali earth metal vanadates and transition metal vanadates, some others not belonging to these three categories were also successively reported recently, such as ammonium vanadates^[202] and AlV_3O_9 ,^[203] which further indicate the plentiful family members of the vanadates. As an example, $\text{NH}_4\text{V}_4\text{O}_{10}$ has recently been reported as a high-capacity cathode for both MIBs^[204] and CIBs,^[164] respectively. Even though limited works about these phases for emerging electrochemical energy storage, they provide more opportunities in the future.

In this section, we have summarized and discussed the structures, properties and electrochemical performances of various vanadates in emerging electrochemical energy storage. It could be noticed that there is a large number of members in this family, which is originated from the features of vanadium-based oxides with facile distortion of V–O polyhedrons and the multivalent variation of vanadium. Among them, several phases have displayed promising electrochemical properties for beyond LIBs, such as CaV_4O_9 for SIB anode, $\text{Zn}_{0.25}\text{V}_2\text{O}_5 \cdot x\text{H}_2\text{O}$ and $\text{Ca}_{0.25}\text{V}_2\text{O}_5 \cdot n\text{H}_2\text{O}$ for ZIB cathodes. Compared to the vanadium oxides, vanadates generally exhibit improved electrochemical performance especially in cycling and rate, due to the optimizing effects (such as pillar effect or self-preserving effect) from the additional metal ions in the structure. Besides, the diversity of different vanadates with various properties provides a lot of choices for the development of emerging battery

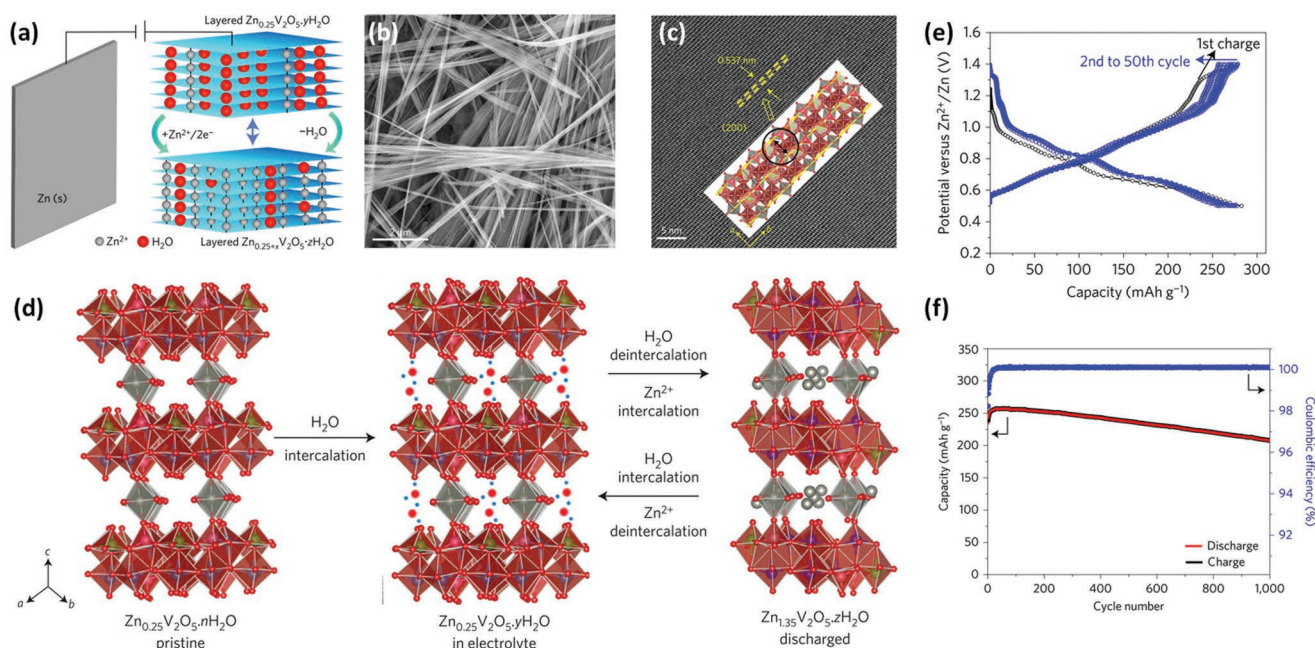


Figure 14. a) Schematic of the zinc battery based on $\text{Zn}_{0.25}\text{V}_2\text{O}_5 \cdot n\text{H}_2\text{O}$ as cathode. b) SEM image of $\text{Zn}_{0.25}\text{V}_2\text{O}_5 \cdot n\text{H}_2\text{O}$ nanobelts. c) HRTEM image of $\text{Zn}_{0.25}\text{V}_2\text{O}_5 \cdot n\text{H}_2\text{O}$ nanobelts showing the (200) planes. d) Illustration of the reaction process of Zn^{2+} ions and water molecule during electrochemical discharge process. e) Galvanostatic discharge and charge profiles of the $\text{Zn}_{0.25}\text{V}_2\text{O}_5 \cdot n\text{H}_2\text{O}$ nanobelts. f) Cycling performance and corresponding coulombic efficiency of $\text{Zn}_{0.25}\text{V}_2\text{O}_5 \cdot n\text{H}_2\text{O}$ nanobelts. Reproduced with permission.^[22] Copyright 2016, Springer Nature.

systems. We believe that more unexploited electrode materials will be identified and interesting/exciting results will be discovered with the further investigation of vanadates group.

5. Vanadium Phosphates

Vanadium phosphates, including $\text{Li}_3\text{V}_2(\text{PO}_4)_3$ (LVP), $\text{Na}_3\text{V}_2(\text{PO}_4)_3$ (NVP), vanadium fluorophosphates, vanadium pyrophosphates, and others, are a class of promising electrodes for energy storage, due to their advantages of high output voltage, stable framework and fast ion diffusion coefficient.^[49,205,206] For example, NVP has been extensively studied for SIBs recently. It is noteworthy that NVP has a unique Na superionic conductor (NASICON) structure, which possesses an open framework containing large interstitial channels with high ionic mobility.^[205] Vanadium phosphates consisting of $[\text{PO}_4]$ tetrahedrons and $[\text{VO}_6]$ octahedrons generally exhibit robust crystal structures with good structural stability during the ions insertion/extraction. Meanwhile, the excellent chemical stability of $(\text{PO}_4)^{3-}$ groups endows these electrode materials with better thermal safety compared with other vanadium-based materials.^[207] Besides, the inductive effect produced by $(\text{PO}_4)^{3-}$ groups results in a generally high output voltage of vanadium phosphates than vanadium oxides or vanadates.^[49]

However, like other phosphate electrodes, vanadium phosphates generally suffer from inferior electronic conductivity because the $[\text{VO}_6]$ octahedrons are separated by phosphate groups. Therefore, improving the electrical conductivity becomes a very important research topic scientifically for vanadium phosphates. To enhance the practical capacity

and rate capability in energy storages, extensive efforts from carbon coating, metal-ion doping, and nanocomposite design (Figure 15) have been carried out for vanadium phosphates. The different strategies for enhanced electrochemical performances of representative vanadium phosphates in emerging metal-ion batteries are listed in Table 3. More details will be reviewed carefully in the following sections.

5.1. $\text{Li}_3\text{V}_2(\text{PO}_4)_3$

Lithium vanadium phosphate, $\text{Li}_3\text{V}_2(\text{PO}_4)_3$ (LVP), has been extensively studied as a cathode for LIBs recently, which exhibits a high average potential of ≈ 4.0 V (V vs Li^+/Li), a considerable theoretical specific capacity of 197 mAh g^{-1} (3 Li^+ insertion/extraction) and a fast lithium-ion diffusion coefficient of 10^{-9} to $10^{-10} \text{ cm}^2 \text{ s}^{-1}$.^[49,222–224] Since the superior structure features and electrochemical properties, LVP also attracted interests for Na storage. The as-prepared 3D graphene framework wrapped LVP composite reported by Xiong et al.^[208] exhibits a high energy density of 501.3 Wh kg^{-1} when used as SIB cathode. It was found that Na ions replace partial Li ions of LVP during the first cycle, and the topotactic reaction (reversible insertion/extraction of Na^+ ions) occurs during the subsequent cycles.

5.2. $\text{Na}_3\text{V}_2(\text{PO}_4)_3$

$\text{Na}_3\text{V}_2(\text{PO}_4)_3$ (NVP) has been widely studied for SIBs due to its stable 3D NASICON structure, applicable operation potential (3.40 V vs Na^+/Na) and moderate capacity (117 mAh g^{-1}) when

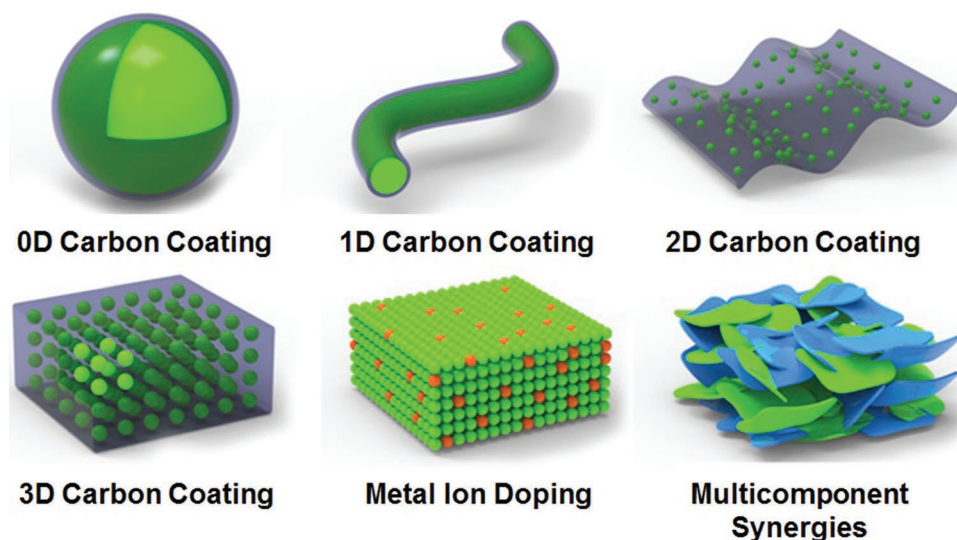


Figure 15. Schematic illustration of the strategies for enhanced electrochemical performance of vanadium phosphates.

used as an SIB cathode.^[205] In addition, the redox couple of V^{3+}/V^{2+} indicate that NVP can be also used as an anode for SIBs. It is generally known that the thermodynamically stable phase of NVP is rhombohedral.^[225] Recently, a monoclinic NVP has also been reported, which was obtained at a low temperature.^[226] In rhombohedral NVP framework, the Na^+ ions have two different sites (**Figure 16a**); one occupies in the six-coordinate Na–O sites (Na1), and the other in the eight-coordinate Na–O sites (Na2). The representative ion occupations based on the calculated $[Na_3V_2(PO_4)_3]_2$ unit model are shown in **Figure 16b–d**. Three main migration mechanisms are considered within this

3D NASICON structure involving conventional vacancy hopping between neighboring Na positions (**Figure 16e–g**).^[227]

As a cathode, NVP delivers a theoretical capacity of 117 mAh g^{-1} , which corresponds to $\approx 2.0 \text{ Na}^+$ extraction from NVP to form $NaV_2(PO_4)_3$; while as the anode, $>1.0 \text{ Na}^+$ can be inserted in the voltage window of 1.0–3.0 V to form $Na_4V_2(PO_4)_3$. Jian et al. further studied the insertion behavior at a lower voltage window.^[228] When discharged to 0.01 V, the fifth Na^+ ion will be inserted into the framework to form $Na_5V_2(PO_4)_3$, which presents a smooth plateau at around 0.31 V versus Na^+/Na . In a large voltage range of 0.01–3.8 V, three plateaus can be clearly

Table 3. The typical vanadium phosphates nanomaterials, strategies and electrochemical performance for emerging metal-ion batteries.

Materials	Systems	Strategies	Highest capacity [mAh g^{-1}]	Discharge plateaus [V]	Cycling stability (current rate, specific capacity, cycle numbers, capacity retention)	Refs.
$Li_3V_2(PO_4)_3$	SIBs	2D carbon coating	100	3.78, 3.19 and 3.16	500 mA g^{-1} , 80 mAh g^{-1} , 500 cycles, 65%	[208]
$Na_3V_2(PO_4)_3$	SIBs	0D carbon coating	104.3	≈ 3.36	5 C, 95 mAh g^{-1} , 700 cycles, 96%	[209]
	SIBs	1D carbon coating	114	≈ 3.33	20 C, 90 mAh g^{-1} , 10 000 cycles, 100%	[210]
	SIBs	2D carbon coating	117	≈ 3.4	50 C, 90 mAh g^{-1} , 15 000 cycles, 70%	[211]
	SIBs	3D carbon coating	115	≈ 3.4	30 C, 105 mAh g^{-1} , 20 000 cycles, 54%	[62]
	SIBs	Metal doping	101	3.6 and 3.3	1 C, 101 mAh g^{-1} , 1000 cycles, 89%	[212]
	SIBs	Composite with Ni_2P	110	≈ 3.4	16 C, 84 mAh g^{-1} , 1500 cycles, 90%	[213]
	ZIBs	2D carbon coating	97	1.1	0.5 C, 97 mAh g^{-1} , 100 cycles, 74%	[214]
$VOPO_4$	SIBs	Ultrathin nanosheet fabrication	136	≈ 3.5	5 C, 73 mAh g^{-1} , 500 cycles, 73%	[64]
	MIBs	Interlayer expansion	310	≈ 0.9	100 mA g^{-1} , 280 mAh g^{-1} , 500 cycles, 68%	[215]
$Na_3V_2(PO_4)_2F_3$	SIBs	2D carbon coating	110	3.98 and 3.51	10 C, 110 mAh g^{-1} , 1000 cycles, 75%	[216]
$NaVPO_4F$	SIBs	1D carbon coating	111	3.43	2 C, 105 mAh g^{-1} , 1000 cycles, 96.5%	[217]
$Na_3(VO)_2(PO_4)_2F$	SIBs	3D carbon coating	127.2	4.0 and 3.6	30 C, 90 mAh g^{-1} , 2000 cycles, 83%	[218]
$Na_7V_4(P_2O_7)_4(PO_4)$	SIBs	2D carbon coating	91	3.88	C/2, 91 mAh g^{-1} , 1000 cycles, 78.3%	[219]
$K_3V_2(PO_4)_3$	SIBs	1D carbon coating	119	Without voltage plateau	1000 mA g^{-1} , 68 mAh g^{-1} , 2000 cycles, 96%	[220]
	PIBs	3D carbon coating	57	≈ 3.6	20 mA g^{-1} , 54 mAh g^{-1} , 100 cycles, 96%	[221]

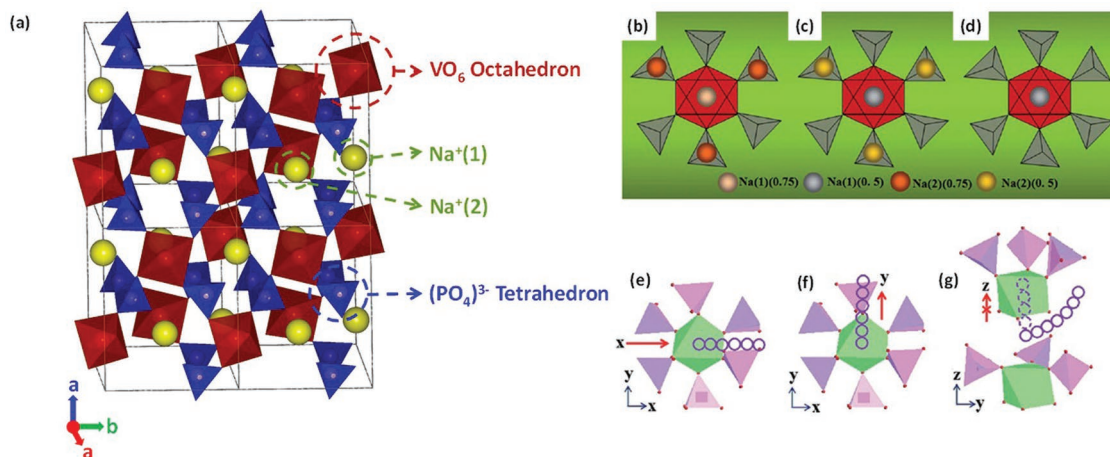


Figure 16. a) Schematic diagrams of NVP. Scheme representing ion occupations based on the calculated $[\text{Na}_3\text{V}_2(\text{PO}_4)_3]_2$ unit model: b) the primary state with 0.75 occupation for all Na sites; c) one Na ion extracted configuration with 0.5 occupation for the sites, and d) two Na ions extracted configuration with 0.5 occupation for the left Na(1) sites. Possible Na ion migration paths in $\text{Na}_3\text{V}_2(\text{PO}_4)_3$ along e) x, f) y, and g) curved z directions. Reproduced with permission.^[227] Copyright 2014, Royal Society of Chemistry.

observed, which correspond to the phase changes between $\text{Na}_3\text{V}_2(\text{PO}_4)_3$ and $\text{NaV}_2(\text{PO}_4)_3$ at 3.40 V, between $\text{Na}_3\text{V}_2(\text{PO}_4)_3$ and $\text{Na}_4\text{V}_2(\text{PO}_4)_3$ at 1.65 V, and between $\text{Na}_4\text{V}_2(\text{PO}_4)_3$ and $\text{Na}_5\text{V}_2(\text{PO}_4)_3$ at 0.31 V, respectively (Figure 17a). Three reversible redox couples of 3.35/3.49, 1.61/1.70, and 0.22/0.40 V are observed in the corresponding CV curves (Figure 17b).^[205] Such a Na^+ insertion/extraction characteristic of NVP enables that a symmetric Na-ion full battery with output voltage of ≈ 1.8 V or ≈ 3.0 V can be realized by using NVP as both anode and cathode.^[229,230]

Although NVP as an SIB electrode has many advantages, it still suffers from intrinsic low electric conductivity like LVP, which limits the practical rate capability and cycling performance.^[233–237] The NVP nanocrystal coated by carbon layer to form different NVP@C composites, such as 0D, 1D, 2D and 3D carbon coating structure (Figure 18), are particularly favorable because of both reduced diffusion length for Na^+ insertion/extraction and enhanced electronic conductivity.^[209,238,239] For example, Ren et al.^[61] constructed a novel

NVP/C nanofiber network through a facile self-sacrificed templated method (Figure 18b). The as-synthesized material displays superior cycling stability (retained 95.9% after 1000 cycles at 10 C) and outstanding high-rate performance (94 mAh g^{-1} at 100 C). Jiang et al.^[210] constructed bundled NVP nanofibers with carbon scaffold structure, which maintained at least 96.1% of the initial capacity after 1000 cycles when operated at 1, 2, and 5 C between 2.6 and 3.8 V versus Na^+/Na , and 99.9% of the initial capacity was available even after 10 000 cycles at 20 C. Xu et al.^[211] presented a novel 2D layer-by-layer NVP@rGO nanocomposite, which delivers an outstanding rate performance with capacity of 118 mAh g^{-1} (0.5 C), 91 mAh g^{-1} (50 C) and 41 mAh g^{-1} (200 C), respectively. Rui et al.^[231] proposed a meso/macroporous NVP-based hybrid cathode, which consists of carbon-coated NVP nanocrystals and wrapped reduced graphene oxide nanosheets (Figure 18c). Even at 80 and 100 C, the reversible capacities of 91 and 86 mAh g^{-1} are obtained, corresponding to 77% and 73% capacity utilization within 45 and

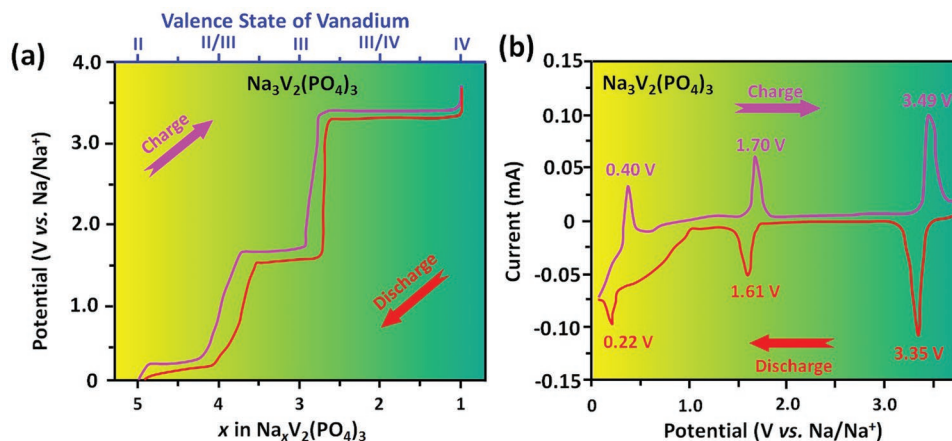


Figure 17. Electrochemical voltage–composition a) and CV b) curves in the voltage range of 0.01–3.8 V versus Na^+/Na of NVP. Reproduced with permission.^[205] Copyright 2017, Wiley-VCH.

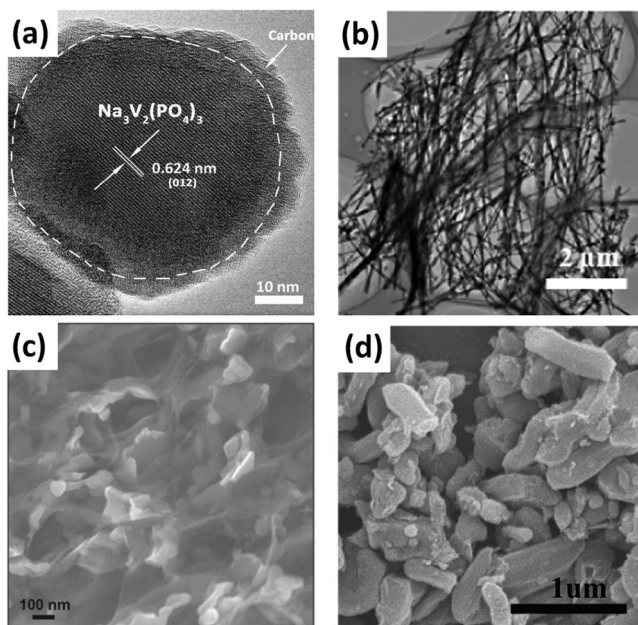


Figure 18. a) HRTEM image of 0D NVP@C nanocomposite. Reproduced with permission.^[209] Copyright 2014, Royal Society of Chemistry. b) TEM image of 1D NVP@C nanofiber network. Reproduced with permission.^[61] Copyright 2016, Elsevier. c) SEM image of 2D NVP@C@rGO nanocomposite. Reproduced with permission.^[231] Copyright 2015, Wiley-VCH. d) SEM image of the 3D NVP@C nanocomposite. Reproduced with permission.^[232] Copyright 2015, Wiley-VCH.

36 s, respectively. Cao group^[62] designed a hierarchical carbon framework wrapped $\text{Na}_3\text{V}_2(\text{PO}_4)_3$, in which the carbon framework consists of carbon coating layers and interconnected carbon nanofibers. Remarkable sodium storage performance with both ultrahigh rate capability (38 mAh g^{-1} at 500 C) and ultralong cycle life (20 000 cycles at 30 C with 54% retention) were achieved.

Besides carbon-based conducting additives, metal oxides and phosphides were also used to form composites to enhance the electrochemical performance, such as NVP- $\text{Ni}_2\text{P}/\text{C}$.^[213] Moreover, several works about various ions doped NVP for SIBs were reported, such as Mg, Mn, Fe, and Ni.^[212,240–243] Goodenough and co-workers^[212] reported an investigation of Mn, Fe and Ni doped NASICON structured $\text{Na}_3\text{MV}(\text{PO}_4)_3$ ($M = \text{Mn, Fe, or Ni}$) as SIB cathodes. The $\text{Na}_4\text{MnV}(\text{PO}_4)_3$ was trigonal structure constructed by Mn/ VO_6 octahedral and PO_4 tetrahedral by corner sharing. It exhibits two charge/discharge plateaus at 3.6 and 3.3 V, corresponding to the redox behaviors of $\text{Mn}^{3+}/\text{Mn}^{2+}$ and $\text{V}^{4+}/\text{V}^{3+}$, respectively. A reversible capacity of around 101 mA h g^{-1} at 1 C was achieved, and after 1000 cycles, 90 mAh g^{-1} was retained, corresponding to a capacity retention of $\approx 89\%$. $\text{Na}_3\text{FeV}(\text{PO}_4)_3$ has a little difference in structure compared to that of $\text{Na}_4\text{MnV}(\text{PO}_4)_3$. The distortion of the FeO_6 octahedron cooperatively distorts the crystal structure to monoclinic. $\text{Na}_3\text{FeV}(\text{PO}_4)_3$ exhibits a similar reversible capacity and cycling stability to $\text{Na}_4\text{MnV}(\text{PO}_4)_3$. However, the relatively lower charge/discharge plateaus at 3.3 and 2.5 V were observed, which corresponding to the redox behavior of $\text{V}^{4+}/\text{V}^{3+}$ and $\text{Fe}^{3+}/\text{Fe}^{2+}$. For $\text{Na}_4\text{NiV}(\text{PO}_4)_3$, the pure phase with NASICON structure was found hard to be obtained.

Due to the promising NASICON structure, NVP attracted extensive interests not only for SIBs, but also for hybrid LIBs,^[244–246] emerging ZIBs^[214] and AIBs.^[247] Li et al.^[214] applied NVP as the cathode for aqueous ZIBs. A reversible capacity of 97 mAh g^{-1} at 0.5 C with a relatively high discharge voltage plateau of 1.1 V was obtained, which retained 74% after 100 cycles. Besides, the charge/discharge rate can be up to 10 C.

In brief, as a typical NASICON compound, NVP is basically the most stable host material for Na^+ storage. Over 10 000 cycles have been achieved by several reports.^[62,210,211,231] This advantage, together with the fast Na^+ diffusion coefficient, applicable voltage, moderate capacity and abundant resource, enable it a highly promising candidate for SIBs in practical applications, especially for large-scale energy storage where long cycle life and low cost are more important than energy density. Increasing the electronic conductivity using a facile and cost-effective way is very important. In the future, an important target may be how to make a balance between performance (high rate and long life) and synthesis strategy (high yields and low cost).

5.3. VOPO₄

VOPO_4 has seven polymorphs with different structures, including α_1 ($P4/n$), α_{11} ($P4/n$), β ($Pnma$), δ ($P4_2/mbc$), ϵ (Cc), ω ($P4_2/mmc$), and γ ($Pbam$).^[248,249] Among all the polymorphs of VOPO_4 , $\alpha_1\text{-VOPO}_4$ is a special one due to its layered crystal structure. The layers are stacked along c direction. In each VOPO_4 plane, PO_4 tetrahedra and distorted VO_5 polyhedra are alternatively arranged by a corner-sharing oxygen.^[65] The synergic advantages of layered structure and potential high voltage (due to the inductive effect from PO_4 group) attract interests about $\alpha_1\text{-VOPO}_4$ in SIBs. He et al.^[65] successfully prepared layered VOPO_4 by a chemical delithiation process from tetragonal $\alpha_1\text{-LiVOPO}_4$ (Figure 19a). The obtained VOPO_4 sample exhibited a discharge plateau around 3.5 V versus Na^+/Na (Figure 19b), and a capacity of $\approx 110 \text{ mAh g}^{-1}$ (0.67 Na^+) in 1.5–4.3 V without any conductive coating. After a preliminary optimization using rGO nanosheets, a higher reversible capacity of $\approx 150 \text{ mAh g}^{-1}$ (0.90 Na^+) was demonstrated.

The other important method to prepare layered VOPO_4 is through a dehydration of $\alpha\text{-VOPO}_4 \cdot 2\text{H}_2\text{O}$. Since the weak hydrogen bonds between water molecules and oxygen atoms in $\alpha\text{-VOPO}_4 \cdot 2\text{H}_2\text{O}$, it is feasible to exfoliate VOPO_4 ultrathin nanosheets from the $\text{VOPO}_4 \cdot 2\text{H}_2\text{O}$ (Figure 19c,d).^[63,64,66,250] Yu research group reported ultrathin VOPO_4 nanosheets for high-rate and long-life alkali-ion storage.^[64,66,250] The exfoliated VOPO_4 nanosheets exhibit high reversible capacities of 154 and 136 mAh g^{-1} for Li^+ and Na^+ storage at 0.1 C, and 100 and 70 mAh g^{-1} at 5 C, respectively. Kinetics analysis revealed the intercalation pseudocapacitive behavior for both Li^+ and Na^+ storage.^[64] Additionally, the as-prepared VOPO_4 nanosheets can also act as a promising cathode for full SIBs matching with $\text{Na}_2\text{Ti}_3\text{O}_7$ anode. The full cell exhibited a high output voltage of $\approx 2.9 \text{ V}$ (Figure 19e) and a high energy density of 220 Wh kg^{-1} (based on the mass of both the cathode and anode materials). Good rate capability (Figure 19f) and superior

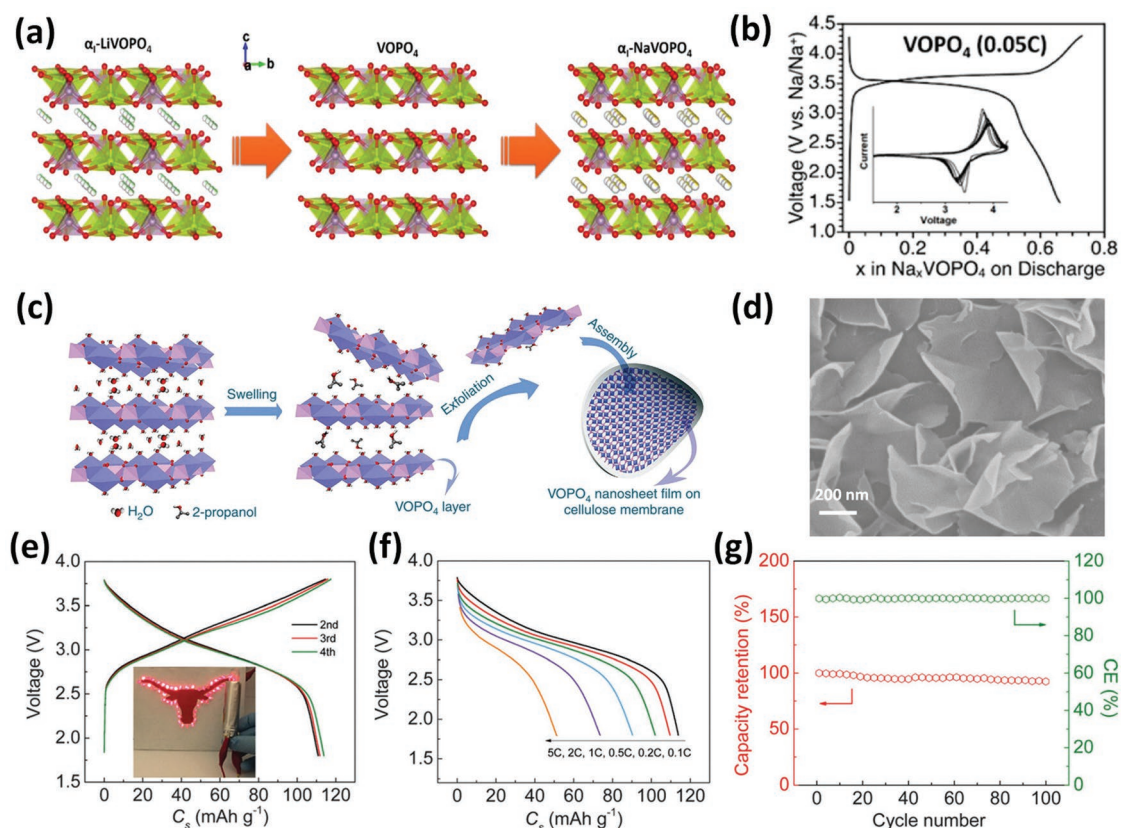


Figure 19. a) Illustration of the structure evolution of α -LiVOPO₄, α -VOPO₄, and α -NaVOPO₄. b) Discharge/charge curves of VOPO₄ in the voltage range of 1.5–4.3 V (vs Na⁺/Na); inset is the corresponding CV curves. Reproduced with permission.^[65] Copyright 2016, American Chemical Society. c) Illustration of the exfoliation process from α -VOPO₄·2H₂O to VOPO₄ nanosheets. d) SEM image of the prepared VOPO₄ ultrathin nanosheets using exfoliation method. Reproduced with permission.^[63] Copyright 2013, Nature Publishing Group. e) Typical charge/discharge profiles of Na₂Ti₃O₇//VOPO₄ full cells, and the inset shows the red LEDs powered by the full cells under rolled state. f) The discharge profiles of the Na₂Ti₃O₇//VOPO₄ full cells at different rates. g) Cycling performance with coulombic efficiency of the Na₂Ti₃O₇//VOPO₄ full cell at 1 C. Reproduced with permission.^[66] Copyright 2016, Royal Society of Chemistry.

cycling performance (Figure 19g) of the full cell for 100 cycles with a capacity retention of 92.4% was achieved.^[66]

Very recently, layered VOPO₄ was further studied for rechargeable MIBs. But it was found that pristine VOPO₄ showed poor Mg²⁺ storage performance, and the special modifications are necessary. Zhou et al.^[215] effectively expanded the interlayer spacing of VOPO₄·2H₂O from 0.74 to 1.42 nm by phenylamine molecules preintercalation. The enlarged layer spacing results in the fast diffusion kinetics of MgCl⁺ ions with low polarization. Ascribed to that, a high reversible capacity of 310 mAh g⁻¹ and good cycling stability for 500 cycles was realized. Ji et al.^[251] found that introducing water both in VOPO₄ structure and in the electrolytes is the other way to activate the Mg²⁺ storage performance of the VOPO₄ cathode, since water can effectively lubricate the diffusion of Mg²⁺ ions and release the capacity limited by diffusion kinetics.

Note that NaVOPO₄^[252–254] and KVOPO₄^[255,256] have also been investigated as cathode materials for SIBs and PIBs, respectively. Similar to VOPO₄, NaVOPO₄ was reported to exhibit an average potential of 3.6 V when used as an SIB cathode.^[252] For KVOPO₄, it was reported that it can deliver a high voltage over 4.0 V for PIBs.^[255] But since the limited

reports, the syntheses, electrochemical properties and reaction behaviors of these phases need to be further studied.

5.4. Vanadium Fluorophosphates

Vanadium fluorophosphates, owing to their high voltage platform, high energy density and excellent thermal stability, are considered to be potential high-energy electrode materials for next-generation LIBs and beyond.^[257,258] The typical vanadium fluorophosphates include LiVPO₄F, NaVPO₄F, KVPO₄F, Na₃V₂(PO₄)₂F₃, Na₃(VO)₂(PO₄)₂F, and Na₃V₂O_{2x}(PO₄)₂F_{3–2x}. These kinds of electrode materials exhibit high output voltages, which is attributed to the strong inductive effect from the (PO₄)^{3–} polyanion and the highly electronegative F[–] anion.^[259] Besides, the additional fluorine atoms in the skeleton structures are beneficial to develop novel polyanion systems due to the stable V–F bond.^[259,260] Like other phosphate cathodes, fluorophosphates generally suffer from low electronic conductivity.^[261] Besides, synthesis of pure phase of several vanadium fluorophosphates is also a big challenge. Up to now, many efforts have been made to overcome these obstacles.^[34,262]

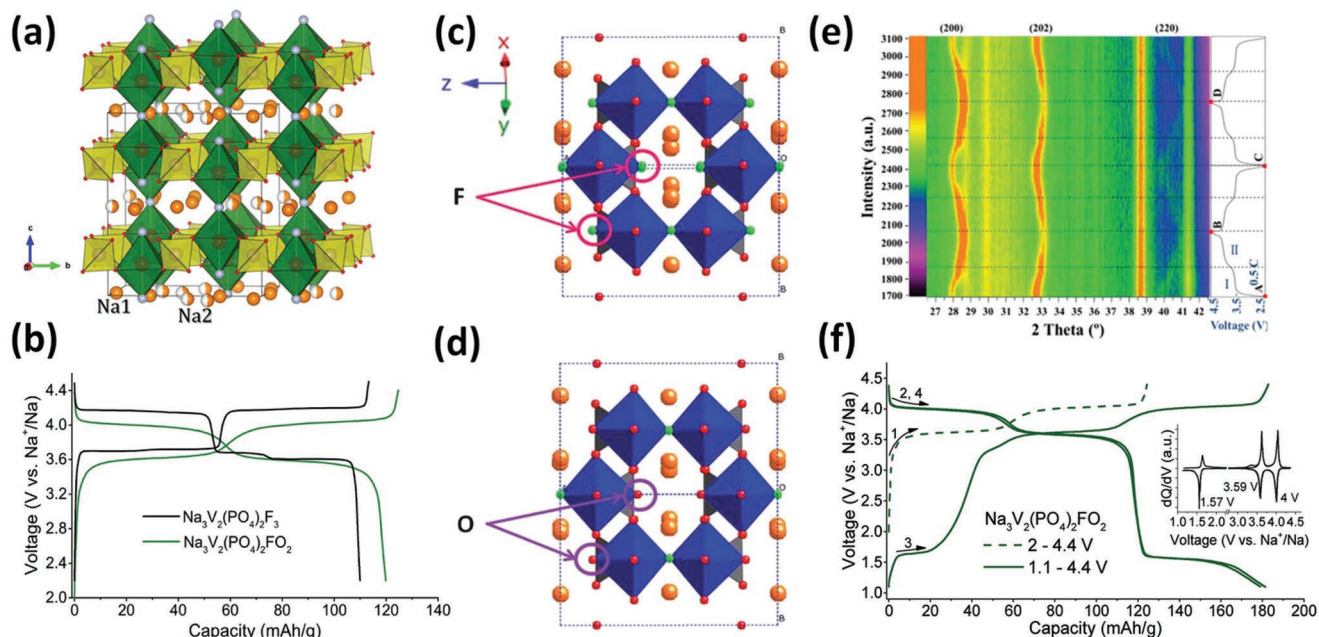


Figure 20. a) Crystal structure of $\text{Na}_3\text{V}_2(\text{PO}_4)_2\text{F}_3$ showing an open framework. Reproduced with permission.^[272] Copyright 2014, American Chemical Society. b) Comparison of the charge/discharge curves between $\text{Na}_3\text{V}_2(\text{PO}_4)_2\text{F}_3$ and $\text{Na}_3(\text{VO})_2(\text{PO}_4)_2\text{F}$ during Na^+ intercalation/deintercalation. Reproduced with permission.^[273] Copyright 2017, Wiley-VCH. c) Comparison of the crystal structure between $\text{Na}_3\text{V}_2(\text{PO}_4)_2\text{F}_3$ (c) and $\text{Na}_3(\text{VO})_2(\text{PO}_4)_2\text{F}$ (d). Reproduced with permission.^[269] Copyright 2012, Royal Society of Chemistry. e) In situ XRD patterns of $\text{Na}_3(\text{VO})_2(\text{PO}_4)_2\text{F}$ during the Na^+ intercalation/deintercalation between 2.5 and 4.5 V. Reproduced with permission.^[218] Copyright 2017, Elsevier. f) Charge/discharge profiles of $\text{Na}_3(\text{VO})_2(\text{PO}_4)_2\text{F}$ in the voltage range of 1–4.4 V, showing an additional voltage plateau at ≈ 1.6 V. Reproduced with permission.^[273] Copyright 2017, Wiley-VCH.

5.4.1. AVPO_4F ($A = \text{Na}$ and K)

NaVPO_4F (NVPF) with a tetragonal structure was firstly reported by Barker et al.^[263] to be a new cathode for SIBs. A high average discharge voltage of ≈ 3.7 V and a reversible capacity of 82 mAh g^{-1} were displayed. But the capacity was found to decrease to less than 50% only after 30 cycles. To improve the electrochemical performance, several strategies such as Cr doping,^[264] carbon coating^[265,266] and graphene modification^[267] have been reported. The graphene modified NVPF reported by Ruan et al.^[267] exhibits distinct increased capacity of 120.9 mAh g^{-1} at 0.02 C with capacity retention of 97.7% after 50 cycles. Recently, Jin et al.^[217] successfully prepared self-standing NVPF/C nanofibers using an electrospinning method followed by heat treatment for SIB cathode. The NVPF nanoparticles with the size of ≈ 6 nm were found to be embedded in porous carbon matrix. A high capacity of 126.3 mAh g^{-1} at 1 C with distinct voltage plateaus at $\approx 3.58/3.43$ V (vs Na^+/Na) was achieved. Besides, ultralong cyclability for 1000 cycles with retention of 96.5% at 2 C was demonstrated.

KVPO_4F (KVPF) was recently reported as a high-voltage cathode material for PIBs.^[255,268] It was found that KVPF exhibits a high working voltage of ≈ 4.02 V versus K^+/K , with a discharge capacity of $\approx 70 \text{ mAh g}^{-1}$ in the voltage range of 2.0–4.8 V. When the upper voltage limit was extended to 5.0 V, a discharge capacity of 92 mAh g^{-1} was achieved. Based on the operando XRD measurements, the lattice volume change during cycles was demonstrated to be only 5.8% for KVPF, suggesting the outstanding structure stability during K^+

insertion/extraction.^[255] These results indicate that KVPF is a promising high-voltage cathode for PIBs.

5.4.2. $\text{Na}_3\text{V}_2\text{O}_{2x}(\text{PO}_4)_2\text{F}_{3-2x}$

$\text{Na}_3\text{V}_2\text{O}_{2x}(\text{PO}_4)_2\text{F}_{3-2x}$ is the general formula of an important family of sodium-vanadium fluorophosphates with 3D open framework structure (Figure 20a).^[269–272] Two extreme phases with $x = 0$ and $x = 1$ are $\text{Na}_3\text{V}_2(\text{PO}_4)_2\text{F}_3$ and $\text{Na}_3(\text{VO})_2(\text{PO}_4)_2\text{F}$, respectively, which have attracted extensive interests recently for SIB cathodes due to their high operating voltages (Figure 20b). The vanadium oxidation states of the two end-member compounds are +3 and +4, respectively, while the intermediate compounds are $\text{V}^{3+}/\text{V}^{4+}$ mixed-valence phases. Rojo group^[269] prepared a series of $\text{Na}_3\text{V}_2\text{O}_{2x}(\text{PO}_4)_2\text{F}_{3-2x}$ samples via a hydrothermal method by varying the type and content of carbon in the synthesis. They concluded that the vanadium oxidation state and thus fluorine and oxygen content (x value) varied along with the amount of remaining carbon in the material. In $\text{Na}_3\text{V}_2\text{O}_{2x}(\text{PO}_4)_2\text{F}_{3-2x}$ structure, oxygen substitutes for fluorine in the vanadium-centered biotetrahedra and render vanadium of a higher average oxidation state. Figure 20c,d shows the comparison of structure between the two extreme phases $\text{Na}_3\text{V}_2(\text{PO}_4)_2\text{F}_3$ and $\text{Na}_3(\text{VO})_2(\text{PO}_4)_2\text{F}$. The two phases present the same framework, while one of the fluorine atoms in $\text{Na}_3\text{V}_2(\text{PO}_4)_2\text{F}_3$ is replaced by an oxygen in $\text{Na}_3(\text{VO})_2(\text{PO}_4)_2\text{F}$. The increased oxygen content renders a slightly lower operating voltage (about 100 mV) for the end phase where $x = 1$ (Figure 20b).^[273]

The investigations primarily concentrated on the two end-member phases of this family, $\text{Na}_3\text{V}_2(\text{PO}_4)_2\text{F}_3$ and $\text{Na}_3(\text{VO})_2(\text{PO}_4)_2\text{F}$. $\text{Na}_3\text{V}_2(\text{PO}_4)_2\text{F}_3$ has a tetragonal crystal structure with the space group of $\text{P}4_2/\text{mnm}$,^[274] which exhibits two plateaus with average voltages of about 3.7 and 4.2 V (redox couple of $\text{V}^{3+}/\text{V}^{4+}$) (Figure 20b). The high potential of $\text{V}^{3+}/\text{V}^{4+}$ in this material is believed to originate from the strong inductive effects of anion groups. Due to the high output voltage, $\text{Na}_3\text{V}_2(\text{PO}_4)_2\text{F}_3$ possesses a high theoretical energy density of $\approx 507 \text{ Wh kg}^{-1}$, which is higher than that of $\text{Na}_3\text{V}_2(\text{PO}_4)_3$ ($\approx 400 \text{ Wh kg}^{-1}$), and comparable to that of commercialized LIBs cathodes LiFePO_4 ($\approx 580 \text{ Wh kg}^{-1}$) and LiMn_2O_4 ($\approx 480 \text{ Wh kg}^{-1}$).^[275] Moreover, the high voltage cathode delivers excellent structure stability for SIBs.^[276] Therefore, $\text{Na}_3\text{V}_2(\text{PO}_4)_2\text{F}_3$ has recently attracted great interests about its detailed intrinsic properties and reaction mechanisms. Ji research group^[277] investigated electrochemical properties of $\text{Na}_3\text{V}_2(\text{PO}_4)_2\text{F}_3$ and revealed the Na^+ ion migration mechanisms by the first principles calculations. Grey group^[278] revealed the rapid Na^+ mobility during Na^+ extraction process using NMR spectroscopy combined with XRD. Bianchini et al. revealed the detailed phase diagram during Na extraction^[275] and structural distortion^[272] using high angular and intensity resolution synchrotron radiation diffraction. Broux et al.^[279] investigated the influence of the oxygen substitution for fluorine on the structural and transport properties of $\text{Na}_3\text{V}_2(\text{PO}_4)_2\text{F}_3$ as a function of temperature. Yu group^[216] investigated the intrinsic ionic and electronic conductivities, as well as the chemical diffusion coefficient of Na^+ of $\text{Na}_3\text{V}_2(\text{PO}_4)_2\text{F}_3$. They confirmed that the electronic conductivity in $\text{Na}_3\text{V}_2(\text{PO}_4)_2\text{F}_3$ was much smaller than the ionic one. Based on that, they developed optimized design with 0D $\text{Na}_3\text{V}_2(\text{PO}_4)_2\text{F}_3$ nanoparticles (30–50 nm) connected to the 3D graphene network, ensuring the good electric contact between nanoparticles and graphene network, and resulting in the superior energy and power densities as an SIB cathode. A high energy density of 348 Wh kg^{-1} and excellent cycling stability for 1000 cycles at a fast rate of 10 C (6 min per charge and discharge) was obtained.

$\text{Na}_3(\text{VO})_2(\text{PO}_4)_2\text{F}$ (NVOPF) is based on $\text{V}^{4+}/\text{V}^{5+}$ redox couple during the electrochemical process. Since the less F-anions in the structure, it exhibits a slightly lower operating voltage than $\text{Na}_3\text{V}_2(\text{PO}_4)_2\text{F}_3$ as mentioned above. However, a lower F content means a weaker inductive effect, which could result in a faster Na^+ diffusion and a lower polarization.^[280,281] Therefore, recently more works have focused on NVOPF. Improving the electronic conductivity of NVOPF is very important for the electrochemical performance. Goodenough group^[282] prepared NVOPF/rGO sandwich structure as the SIB cathode by a facile one-step solvothermal method, and a high reversible capacity (120 mAh g^{-1} at C/20) and good cycling stability (200 cycles with retention of 91.4% at C/10) were achieved. Peng et al.^[283] synthesized RuO₂-coated NVOPF nanowires with the diameter of $\approx 50 \text{ nm}$, and a high reversible capacity of 120 mAh g^{-1} at 1 C and 95 mAh g^{-1} at 20 C after 1000 cycles were demonstrated when used as an SIB cathode. Yin et al.^[218] obtained 3D graphene skeleton encapsulated NVOPF nanoparticles through a spray-drying method. When used as an SIB cathode, a high capacity of 127.2 mAh g^{-1} was obtained, and outstanding high-rate capability (70.3 mAh g^{-1} at 100 C) and excellent ultralong

cycling stability (2000 cycles at 30 C with 83.4% retention) were achieved. Besides, a two-step single solid solution reaction mechanism was revealed by in situ XRD measurements (Figure 20e). Guo group^[281] recently reported a carbon-free NVOPF nano-tetraprisms, which also exhibited excellent high rate and long life performance when used as an SIB cathode. Besides, the superior low temperature performance was also demonstrated with a capacity retention of 76.4% as the temperature decreased from 25 to $-25 \text{ }^\circ\text{C}$. Notably, Hu group^[284] reported a rapid room-temperature strategy for large-scale synthesis (150 g per batch) of NVOPF microspheres very recently, which is very significant for speeding up the commercialization of NVOPF cathode for SIBs.

Due to the high potentials of ≈ 3.7 and $\approx 4.2 \text{ V}$ with 2 Na^+ deintercalation, $\text{Na}_3\text{V}_2\text{O}_{2x}(\text{PO}_4)_2\text{F}_{3-2x}$ has the ability to deliver a high energy density of $\approx 500 \text{ Wh kg}^{-1}$. Recently, it was reported that the energy density of $\text{Na}_3\text{V}_2\text{O}_{2x}(\text{PO}_4)_2\text{F}_{3-2x}$ can be further improved. Ceder group^[273] demonstrated that an additional Na^+ insertion can be realized for $\text{Na}_3(\text{VO})_2(\text{PO}_4)_2\text{F}$ at $\approx 1.6 \text{ V}$ (Figure 20f) to reach $\text{Na}_4(\text{VO})_2(\text{PO}_4)_2\text{F}$, which increases the theoretical specific energy to 600 Wh kg^{-1} . Goodenough group^[285] used first-principle calculations to predict that the third Na in $\text{Na}_3(\text{VO})_2(\text{PO}_4)_2\text{F}$ can possibly extract when substituting O with Cl to form $\text{Na}_3(\text{VCl})_2(\text{PO}_4)_2\text{F}$. And the energy density of the new compound increases to 758 Wh kg^{-1} with three active Na^+ . Tarascon group^[286] demonstrated that the activity of the third sodium in $\text{Na}_3\text{V}_2(\text{PO}_4)_2\text{F}_3$ can be triggered by electrochemically charging to 4.8 V (vs Na^+/Na) to form a disordered $\text{Na}_x\text{V}_2(\text{PO}_4)_2\text{F}_3$, which can reversibly uptake 3 Na^+ afterward between 1.0 and 4.8 V (vs Na^+/Na). This provides a 20% increase in energy density. These results together with the above-mentioned progresses indicate that $\text{Na}_3\text{V}_2\text{O}_{2x}(\text{PO}_4)_2\text{F}_{3-2x}$ is a very promising family for high-energy SIB cathodes.

5.5. Vanadium Pyrophosphate

The family of pyrophosphates hold potential for discovery of next generation cathode materials with high voltage.^[287] The structure of these phases is built on robust P_2O_7 groups, which is created by two PO_4 tetrahedral units linked with bridging oxygen. LiVP_2O_7 is a typical vanadium pyrophosphate, which has a theoretical capacity of 117 mAh g^{-1} with a high potential of 4.2 V (vs Li^+/Li) when Li^+ is extracted to form VP_2O_7 .^[288–290] NaVP_2O_7 has a theoretical capacity of 108 mAh g^{-1} in SIBs. However, the experimental study by Kee et al.^[291] found that the initial specific capacity was only 38.4 mAh g^{-1} at 1/20 C (1 C = 108 mA g^{-1}) in 2.5–4.0 V. Through DFT calculations and electrochemical characterizations, the authors proposed that the limited electrochemical activity of this compound is not only attributed to sluggish Na^+ ion migration kinetics, but also intrinsically high resistance, which limits the phase transition kinetics between NaVP_2O_7 and $\text{Na}_{1-x}\text{VP}_2\text{O}_7$. Barpanda et al.^[292] reported a new $\text{Na}_2(\text{VO})\text{P}_2\text{O}_7$ for SIB cathode, and a high redox potential of $\approx 3.8 \text{ V}$ ($\text{V}^{5+}/\text{V}^{4+}$) with a reversible capacity of $\approx 80 \text{ mAh g}^{-1}$ was achieved. Recently, another new promising vanadium pyrophosphate, $\text{Na}_7\text{V}_3(\text{P}_2\text{O}_7)_4$, was reported by Kang group^[293] and Deng group,^[294,295] respectively. This phase was found to possess a high voltage over 4.0 V (based on $\text{V}^{3+}/\text{V}^{4+}$)

with reversible capacity of $\approx 80 \text{ mAh g}^{-1}$ when used as an SIB cathode, and superior cycling stability over 500 cycles was demonstrated. The good cycling performance was attributed to the small volume change ($\approx 1\%$) and open crystal framework.

5.6. Vanadium-Based Mixed Polyanion Materials

Mixed polyanion materials further expand the research scope of polyanion materials and provide new opportunities for the high-energy batteries.^[296] Vanadium-based mixed polyanion materials, mainly including $\text{Li}_9\text{V}_3(\text{P}_2\text{O}_7)_3(\text{PO}_4)_2$ ^[297–300] and $\text{Na}_7\text{V}_4(\text{P}_2\text{O}_7)_4(\text{PO}_4)$,^[219,301–305] have been investigated. $\text{Na}_7\text{V}_4(\text{P}_2\text{O}_7)_4(\text{PO}_4)$ was firstly reported by Lim et al.^[219] in 2014 as an SIB cathode. This material shows a 3D framework with well-defined ionic channels for Na^+ insertion/extraction. The structure can be regarded as the repetition of a basic unit, $(\text{VP}_2\text{O}_7)_4\text{PO}_4$, in which a central tetrahedron $[\text{PO}_4]$ shares corners with four $[\text{VO}_6]$ octahedra, and every two adjacent $[\text{VO}_6]$ octahedra are linked by a $[\text{P}_2\text{O}_7]$ group by sharing the corners. As a cathode material for SIBs, $\text{Na}_7\text{V}_4(\text{P}_2\text{O}_7)_4(\text{PO}_4)$ was demonstrated to exhibit a high single voltage plateau at 3.88 V versus Na^+/Na . After optimized by rGO integration, the sample showed an initial capacity of 91 mAh g^{-1} at C/2, and retained 78.3% after 1000 cycles. The authors pointed out that the observed single plateau and long cycle life was due to the existence of a shallow intermediate phase during charge/discharge processes, which can reduce the reaction barriers and result in a better kinetics during the battery operations.

5.7. Others

Apart from the above-mentioned typical vanadium phosphates, recently some works about the other types of phases have also been reported, including $\text{Na}_4\text{VO}(\text{PO}_4)_2$,^[306,307] $\text{Na}_3\text{V}(\text{PO}_3)_3\text{N}$,^[308,309] $\text{K}_3\text{V}_2(\text{PO}_4)_3$,^[220,221] etc. These newly reported materials exhibit exciting properties and provide us new choices and opportunities in the way for better batteries. $\text{Na}_4\text{VO}(\text{PO}_4)_2$ was demonstrated to be a potential high power cathode for SIBs.^[307] The high power ability was ascribed to its open framework structure with large amounts of Na ions, which may provide numerous possible Na^+ diffusion pathways. Electrochemical analyses revealed that one Na^+ ions can be extracted through a biphasic reaction mechanism, with an average voltage of $\approx 3.5 \text{ V}$ versus Na^+/Na . $\text{Na}_3\text{V}(\text{PO}_3)_3\text{N}$ was demonstrated to be a new 4V-class cathode with zero-strain property for SIBs.^[308] The volume change of this material was found to be only $\approx 0.24\%$, suggesting the virtually zero strain, which results in the excellent cycling stability with a capacity retention of $\approx 67\%$ after 3000 cycles.

In this section, the structures, electrochemical performances, optimization strategies and charge storage mechanisms of different vanadium phosphates have been summarized and discussed. This family is highly promising for high-energy and long-life SIBs and PIBs, due to the high voltage, stable framework and high thermal stability. Especially for $\text{Na}_3\text{V}_2(\text{PO}_4)_3$ and $\text{Na}_3(\text{VO})_2(\text{PO}_4)_2\text{F}$, after taking full consideration of the high voltage, applicable specific capacity, excellent structure reversibility, good thermal stability and the recent advances with facile

synthesis and excellent performance, we believe that these phases are highly potential to realize commercialization in near future. Even though the low electronic conductivity is a non-negligible drawback, it can be well addressed by carbon coating or other modification strategies based on recent investigations. For the commercialization, making a balance between superior performance (high rate and long life) and facile production (high yields and low cost) is very important. Besides, some new vanadium phosphate phases with outstanding electrochemical performance have been identified recently, which inspired that this family is deserved to be further explored.

6. Oxygen-Free Vanadium-Based Compounds

Oxygen-free vanadium-based nanomaterials, including vanadium sulfides, vanadium nitrides, vanadium carbides and vanadium selenides, have attracted interests for energy-related applications in recent years due to their unique and fascinating electrochemical properties. For example, VS_2 , VN , and V_2C all have metallic properties with high electronic conductivity. Besides, VS_2 , VSe_2 and V_2C possesses typical layered structures with large interlayer spacing, which enables the reversible intercalation/deintercalation of cations with decreased diffusion barrier compared with vanadium oxides, due to the decreased electrostatic interactions. The high electronic conductivity and decreased ion diffusion barrier determine that they are good candidates for metal-ion batteries, especially for the emerging metal-ion batteries with larger ions (Na^+ or K^+) or multivalent ions (Zn^{2+} , Mg^{2+} , etc.) as charge carriers.

6.1. Vanadium Sulfides

Vanadium sulfides mainly include VS_2 and VS_4 . VS_2 is a typical layered transition-metal dichalcogenides (TMDs), in which the layers are stacked together by weak van der Waals interactions.^[310] Like other TMDs, the structure feature of VS_2 endows it a great potential as a graphene analogue and thus attracted enormous interests not only in energy storage,^[311] but also in other fields such as sensors,^[312] electrocatalysis,^[313] and field emission.^[314] Different from VS_2 , VS_4 is a chain-like structure with S_2^{2-} dimer.^[315] The different structure features of these two vanadium sulfides also result in the totally different physicochemical and electrochemical properties.

6.1.1. VS_2

VS_2 was firstly reported as early as 40 years ago, but the systematic research works of this material mainly center on recent years, due to the lack of facile synthesis methods before. As mentioned above, VS_2 is a typical layered TMD with an interlayer spacing of 5.76 \AA , which was stacked by 2D sandwiched S–V–S layers (Figure 21a). Different from most of TMDs, like MoS_2 and WS_2 which are semiconducting, VS_2 is metallic with high electronic conductivity.^[316,317] The layered structure feature and the high conductivity of VS_2 attracted considerable interests about its application in emerging energy storage.

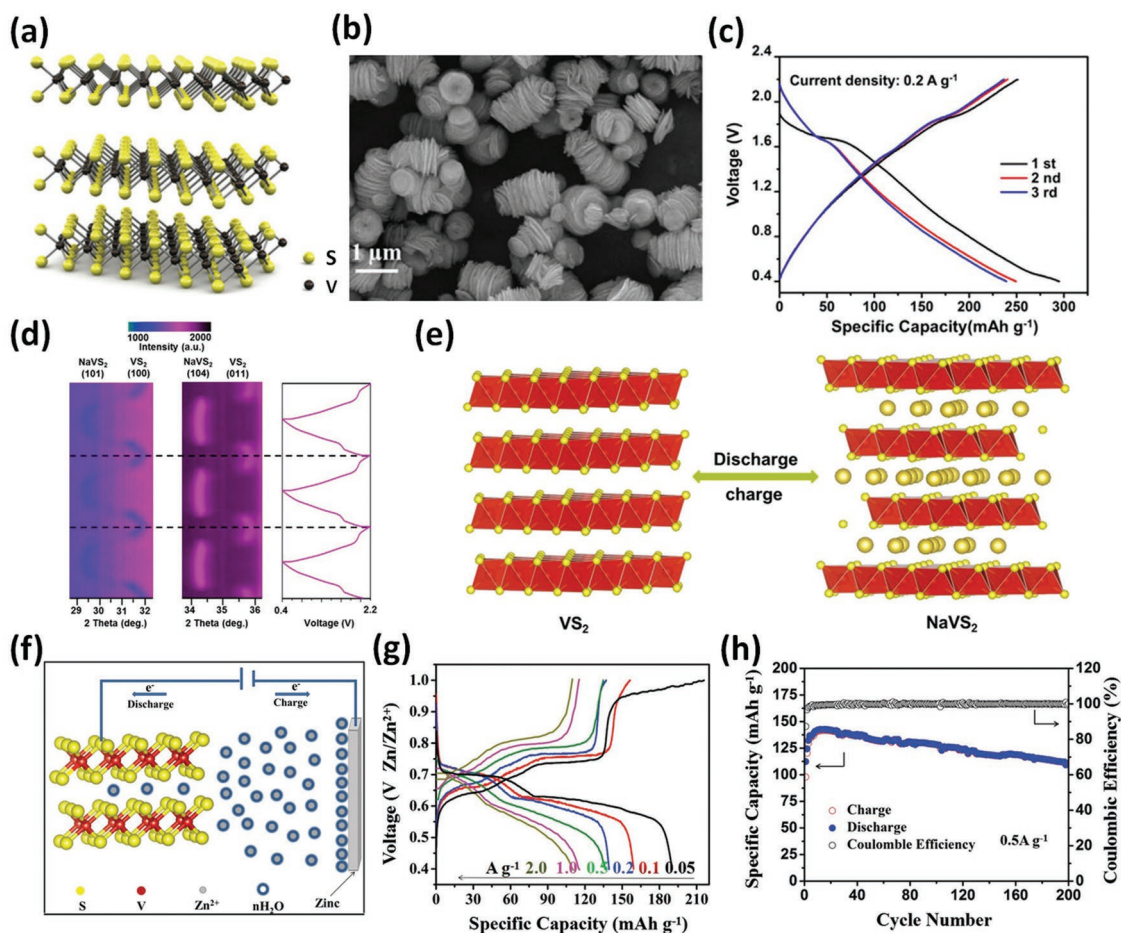


Figure 21. Crystal structure and electrochemical properties of VS_2 . a) Crystal structure of VS_2 . Reproduced with permission.^[316] Copyright 2012, Nature Publishing Group. b) SEM image of layer-by-layer VS_2 -stacked nanosheets. c) Charge/discharge profiles of VS_2 nanosheets for Na storage in 0.4–2.2 V (vs Na^+/Na). d) In situ XRD characterization of VS_2 nanosheets for Na storage in 0.4–2.2 V (vs Na^+/Na). e) Illustration of the crystal phase transformation between VS_2 and NaVS_2 during Na intercalation/deintercalation. Reproduced with permission.^[77] Copyright 2017, Elsevier. f) Illustration of the Zn// VS_2 aqueous rechargeable Zn-ion battery. g) Charge/discharge profiles of the Zn// VS_2 aqueous battery at different current densities in 0.4–1.0 V. h) Cycling performance of the Zn// VS_2 aqueous battery at 0.5 A g^{-1} . Reproduced with permission.^[76] Copyright 2017, Wiley-VCH.

Recently, Sun et al. performed a systematic work about the Na^+ storage property and mechanism of VS_2 nanosheets.^[77] The prepared layer-by-layer VS_2 -stacked nanosheets (Figure 21b) exhibit a reversible discharge capacity of 250 mAh g^{-1} at 0.2 A g^{-1} in a voltage range of 0.4–2.2 V (vs Na^+/Na) (Figure 21c). Long-term cycling performance for 600 cycles at 5 A g^{-1} with no capacity fading was demonstrated. Based on in situ XRD and ex situ TEM measurements, a highly reversible intercalation/deintercalation mechanism accompanied by a two-phase reaction from VS_2 to NaVS_2 was revealed (Figure 21d,e). Besides, the authors found that the cut-off voltage was very important for the reaction mechanism and electrochemical performance. When the voltage range was from 0.01 to 2.2 V, a high initial capacity but a fast capacity fading was observed, due to the conversion reaction mechanism with the generation of Na_2S in 0.01 V.

Zhou et al. further carried out a systematic work about VS_2 for Li/Na/K storage.^[78] They successfully synthesized hierarchical VS_2 nanosheet assemblies by a facile hydrothermal method. The thickness of individual nanosheets was characterized to be only a few atomic layers. The as-prepared VS_2 nanosheets

were used for Li^+ , Na^+ , and K^+ storage, respectively. Note that different from the above mentioned works, the electrochemical measurements for the hierarchical VS_2 nanosheet assemblies were performed in a voltage window between 0.01 and 3.0 V. Impressively, much higher reversible specific capacities of $>1000 \text{ mAh g}^{-1}$ for Li^+ storage, $\approx 700 \text{ mAh g}^{-1}$ for Na^+ storage and $\approx 400 \text{ mAh g}^{-1}$ for K^+ storage were achieved. Besides, good cycling stability not only for Li^+ storage (500 cycles), but also for Na^+ (200 cycles) and K^+ storage (100 cycles) were also demonstrated. The authors believed that the obtained outstanding performance was caused not only by the intrinsic properties of VS_2 , but also by the hierarchical ultrathin nanosheets structure.

VS_2 was also regarded as a promising host material for multivalent-ion batteries since the large interlayer spacing and decreased electrostatic interactions with metal ions compared to vanadium oxides. The application of VS_2 in ZIBs (Figure 21f) was investigated by He et al. recently.^[76] It was found that the VS_2 nanosheets exhibited a high capacity of 190.3 mAh g^{-1} at a current density of 0.05 A g^{-1} in a voltage range of 0.4–1.0 V (vs Zn^{2+}/Zn) (Figure 21g), corresponding to 0.23 Zn^{2+}

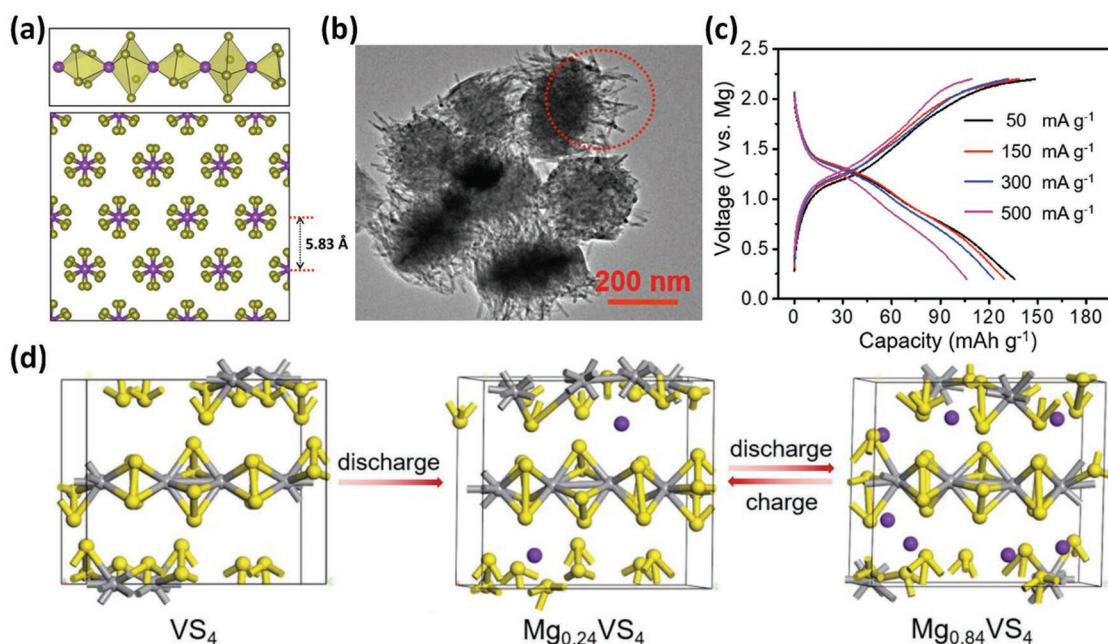


Figure 22. a) Schematic illustration of the chain-like structure of VS_4 . Reproduced with permission.^[315] Copyright 2013, American Chemical Society. b) SEM image of the sea-urchin-like VS_4 nanodendrites. c) Charge/discharge profiles of VS_4 nanodendrites for MIBs at different current densities. d) The illustration of the Mg^{2+} storage process of VS_4 . Reproduced with permission.^[322] Copyright 2018, Wiley-VCH.

intercalation per formula. Two discharge voltage plateaus at 0.72 and 0.63 V were observed, indicating a two-step Zn^{2+} intercalation process. Cycling stability for 200 cycles was demonstrated (Figure 21h). By ex situ/in situ measurements, the highly reversible Zn^{2+} intercalation mechanism was revealed. Wu et al.^[318] recently reported the application of VS_2 as cathode for rechargeable AIBs. The graphene decorated VS_2 exhibited a high initial discharge capacity of 186 mAh g^{-1} at 100 mA g^{-1} . However, the fast capacity fading was observed even though there is no obvious structure degradation based on in situ XRD results. The intrinsic reason for the fast capacity fading requires a further clarification.

It should be noted that the research works about VS_2 in energy storage are still infant at present, but the above publications have indicated that VS_2 is a versatile material for emerging metal-ion batteries. Considering the 2D layered structure features with large interlayer spacing, metallic property and exfoliative characteristic, VS_2 nanostructures deserves more attention in energy storage in the future. As the advance in synthesis methods, more interesting works are expected to come out.

6.1.2. VS_4

VS_4 is another important vanadium sulfide which has a special chain-like structure (Figure 22a). The interests about VS_4 in energy storage starts from the work by Rout et al. in 2013.^[315] They found that VS_4/rGO hybrids exhibited a high reversible Li^+ storage capacity of 1066 mAh g^{-1} with a distinct voltage plateau at $\approx 2.0 \text{ V}$ when cycled in the voltage range of 0.01–3.0 V. Inspired by the impressive Li^+ storage performance, Sun et al. further investigated the Na^+ storage properties of

VS_4 .^[319] The prepared VS_4 grown on rGO delivered an initial reversible capacity of 362 mAh g^{-1} at 100 mA g^{-1} , which remained at 240.8 mAh g^{-1} after 50 cycles. Through ex situ TEM and XRD results, the authors proposed that Na_2S and metallic V were generated at the end of discharge, suggesting a similar Na^+ storage mechanism to that for Li^+ storage. But the achieved Na^+ storage capacity is much lower than that in the case of Li^+ storage. To improve the electrochemical performance of VS_4 , Zhou et al. synthesized VS_4 nanoparticles rooted by amorphous carbon-coated multiwalled carbon nanotubes (MWCNTs@a-C).^[320] In such a prepared composite, the buried and unburied part of MWCNTs can increase the charge-transfer properties inside and outside, respectively, which results in a greatly enhanced electrochemical performance for Na^+ storage. As an SIB anode, a high reversible capacity of 641 mAh g^{-1} was obtained at 0.1 A g^{-1} , but the capacity started to decrease quickly only after 25 cycles. Wang et al.^[321] further optimized the performance of VS_4 as SIB anode both in electrode and electrolyte. They found that using ester-based electrolyte resulted in much stable cycling performance than that using ether-based electrolyte. The stable cycling performance for 300 cycles (retained $\approx 98\%$ at 0.5 A g^{-1}) with capacity of $\approx 400 \text{ mAh g}^{-1}$ was obtained after optimization. They found that the residual Na-containing intermediate phases in desodiation process in ether-based electrolyte account for the capacity fading.

Very recently, the application of VS_4 as cathode for MIBs was also reported.^[322] The sea-urchin-like VS_4 nanodendrites (Figure 22b) were prepared through a solution-phase process, which exhibits reversible Mg^{2+} storage capacity of 137 mAh g^{-1} at 50 mA g^{-1} and 106 mAh g^{-1} at 500 mA g^{-1} (Figure 22c). Besides, long-term cycling stability for 800 cycles at 500 mA g^{-1} was also demonstrated. It is believed that chain-like structure

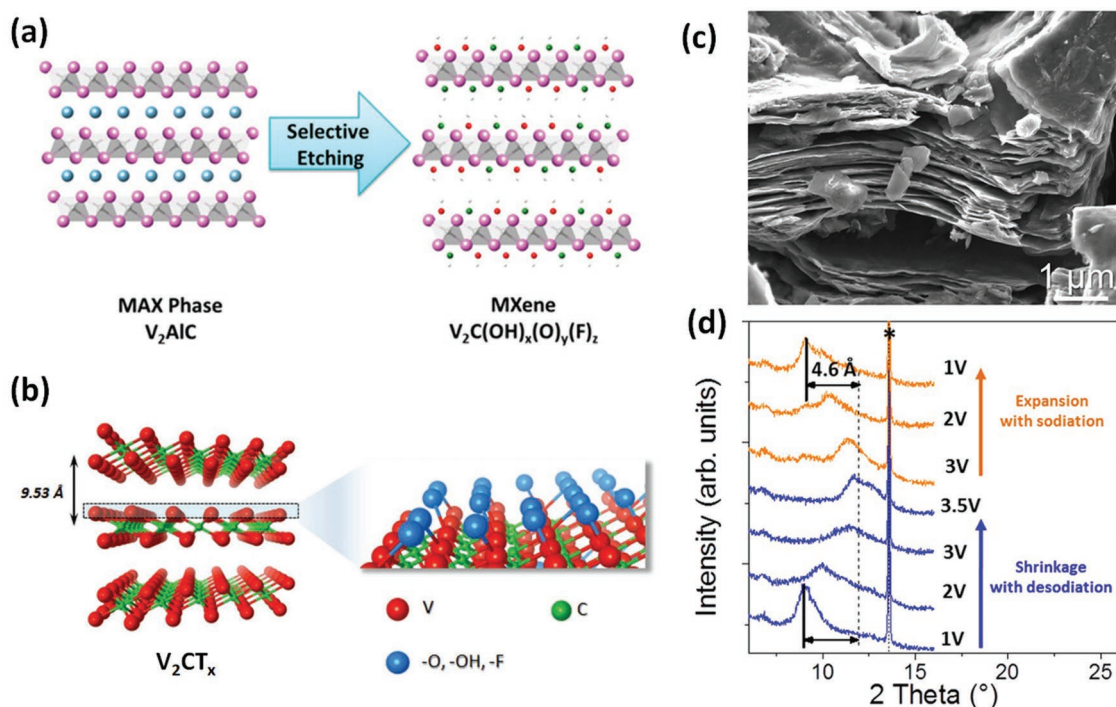


Figure 23. a) Schematic illustration of the synthesis of V_2CT_x . Reproduced with permission.^[70] Copyright 2015, American Chemical Society. b) Schematic illustration of the crystal structure of V_2CT_x and the surface configurations. Reproduced with permission.^[71] Copyright 2017, Wiley-VCH. c) SEM image of the obtained V_2CT_x . Reproduced with permission.^[69] Copyright 2013, American Chemical Society. d) Ex situ XRD results of V_2CT_x during desodiation/sodiation process. The peak marked by (*) represents unreacted V_2AlC . Reproduced with permission.^[70] Copyright 2015, American Chemical Society.

of VS_4 with chains bonded by weak van der Waals forces is beneficial for the diffusion of Mg^{2+} ions. Besides, the S_2^{2-} dimers could provide abundant active sites for Mg^{2+} insertion. Based on the ex situ XRD and Raman spectra, it was found that the chain-like structure of VS_4 was well preserved with morphology unchanged during Mg^{2+} insertion/extraction. Ex situ XPS together with DFT calculations revealed that the Mg^{2+} insertion resulted in partial reduction of S_2^{2-} to S^{2-} and partial oxidation of V^{4+} to V^{5+} , forming $Mg_{0.84}VS_4$ at the final discharge state. In the charge process, the Mg^{2+} extraction results in the formation of $Mg_{0.24}VS_4$ in the charge state (Figure 22d). This work further indicates the application potential of VS_4 for multivalent metal-ion batteries.

6.2. Vanadium Nitride

Vanadium nitride (VN) is a rock salt structure similar to NaCl. An important characteristic of VN is its metallic electronic conductivity ($\approx 10^6 \text{ S m}^{-1}$),^[74,323] which together with the variety of oxidation states of V render it a promising candidate in electrochemical energy storage and conversion, including supercapacitors,^[72,74,75,324–331] batteries^[73,332–334] and electrocatalysis.^[335–337]

The electrochemical properties of VN as battery anodes attracted interests because of its high electronic conductivity. Besides, the element V in VN has a high valence (+3 for vanadium) compared with other metal nitrides (such as Cu_3N , Ge_3N_4 , Fe_3N , etc.), suggesting a higher theoretical specific capacity (1236 mAh g^{-1} for VN). Wang et al. prepared

hybrid 2D-0D graphene-VN quantum dots electrode for superior Na^+ storage.^[73] In such a structure, the 2D graphene backbone can accommodate the volume changes of 0D VN nanodots, prevent their aggregation during cycling and allow for fast ion/electron diffusion through the electrode. When used as SIB anodes, a reversible capacity of 237 mAh g^{-1} at 0.2 C and 149 mAh g^{-1} at 5 C were achieved, and stable cycling for 800 cycles at 1 C was also demonstrated.

Except being used in metal-ion batteries, Sun et al.^[323] and Zhong et al.^[338] recently demonstrated the application of VN as a chemical anchor of polysulfides for high-performance Li-S batteries.

6.3. Vanadium Carbide

2D early transition metal carbides and carbonitrides, which are called MXenes, were recently discovered and extensively studied as a new family of 2D materials by Gogotsi and co-workers.^[79,339,340] Vanadium carbide (V_2C) is a typical member of this family and attracted considerable interests about its synthesis, characterization and application in energy storage.

Like other MXenes, 2D V_2C was usually obtained by selectively etching the atomic layers of Al from V_2AlC phase using the HF solution (Figure 23a). In such an etching process, the etched Al layer will be replaced by the OH, O, and/or F. The replacement results in the transformation from strong metallic bonds between the Al-C layers to weaker hydrogen bonds, thus allowing for the facile preparation of 2D few

layered V_2C with the aid of sonication. By using this synthesis approach, the obtained MXene layer surface are generally not bare but terminated by OH, O and/or F atoms (Figure 23b). To differentiate from that with bare surfaces, the surface functionalized MXenes were usually labeled as $M_{n+1}X_nT_x$.^[79,339] The surface termination was found to have a significant impact on the electronic structure and energy storage capability of V_2C .^[341]

2D V_2CT_x was firstly synthesized by Naguib et al.^[69] in 2013 using the above-mentioned method (Figure 23c), but the yield was found to be around 60%, and unreacted V_2AlC was detected. The Na^+ storage properties and mechanism of V_2CT_x were investigated recently.^[70,71] A high capacitance of $\approx 100\text{ F g}^{-1}$ at 0.2 mV s^{-1} and $\approx 50\text{ F g}^{-1}$ at 50 mV s^{-1} was achieved for Na^+ storage (at a voltage range of 1.0–3.5 V vs Na^+/Na). The reversible Na^+ intercalation/deintercalation was evidenced by ex situ XRD results, with a 2.3 \AA expansion/shrinkage of the interlayer spacing (Figure 23d). Based on 2D V_2CT_x as the positive electrode, a hybrid Na -ion capacitor was constructed coupled with hard carbon, and a capacity of $\approx 50\text{ mAh g}^{-1}$ (based on the total weight of both positive and negative electrodes) was achieved at C/3 with an average voltage of $\approx 1.5\text{ V}$ and a maximum voltage of 3.5 V .^[70] To further understand the Na^+ storage mechanism of V_2CT_x , Bak et al. applied several advanced spectroscopy analyses, including hard X-ray absorption near edge spectroscopy, soft X-ray absorption spectroscopy, etc. to study the charge storage mechanism during Na^+ intercalation/deintercalation between 0.1 and 3.0 V (vs Na^+/Na).^[71] Their results suggested that the V site was the redox reaction center which was responsible for the electrochemical charge storage. Based on the V *K*-edge energy shift from XANES spectra, the average charge transfer number of vanadium is about 0.2 electron per V atom, which corresponds to a theoretical capacity of about 94 mAh g^{-1} , consistent well with the experimental results.

Note that the present synthesized V_2CT_x generally mixed with residual mother phase V_2AlC , while the V_2AlC phase is electrochemically inactive, which together with the functionalized layer surface will limit the experimental capacity from the theoretical one. Therefore, it is expected that there is still much room for the performance optimization and the capacity of this material can be further improved with the advance of the synthesis route.

In this section, several typical oxygen-free vanadium-based nanomaterials including VS_2 , VS_4 , VN , and V_2C were discussed about their application in emerging metal-ion batteries. The intrinsic advantages of this group, such as high electronic conductivity and low electrostatic reaction with metal ions, endow them great potential as high-performance electrodes for next-generation metal-ion batteries. However, since the synthesis of these compounds suffers more challenges, the investigations about these materials in energy storage are still infant. Further studies to get deeper insights about the charge storage mechanism or intrinsic electrochemical properties of these materials are required to confirm their future potential. Besides, attentions should be paid on the oxygen sensitivity of these materials in air and the effect of oxygen erosion on the electrochemical performance. Most importantly, the efficient synthesis strategies with both high impurity and high yields are highly required to push the development of these materials toward the practical applications.

7. Conclusions and Outlooks

The emerging electrochemical energy storage devices will definitely play vital roles in the future energy landscape of the world. The innovation of electrode materials is determinant for the development of emerging electrochemical energy storage devices. Vanadium-based electrode materials have a big family with a large number of members with various compositions, structures and properties, which provides huge possibilities for exploring and identifying new electrode materials for emerging energy storage. This review provides a comprehensive overview about the recent advances of vanadium-based nanomaterials in emerging metal-ion batteries, categorized by vanadium oxides, vanadates, vanadium phosphates and oxygen-free vanadium-based compounds. Among them, vanadium oxides and vanadates with moderate electrochemical potential and open structure attract extensive interests for multivalent metal-ion batteries, such as MIBs and ZIBs. Besides, vanadates group is fascinating which is like a treasure box; all kinds of interesting phases for potential applications in SIBs, PIBs, MIBs, ZIBs, and CIBs have been reported. Vanadium phosphates generally display high voltage for Na^+ and K^+ ions storage, indicating the potential to be promising cathodes for high-energy-density SIBs and PIBs. Oxygen-free vanadium-based compounds display unique features compared with vanadium oxides and vanadates, which also attract considerable interests for emerging SIBs, PIBs, ZIBs, and AIBs. Through this review, we can conclude that vanadium-based nanomaterials show great promise in next-generation metal-ion batteries beyond Li and deserve the further investigations. Here we would like to give our viewpoints about the possible future development directions of vanadium-based nanomaterials for emerging energy storage:

- 1) The emerging aqueous ZIBs have the advantages of high energy/power density, low cost and high safety, showing high promise for large-scale energy storage. Vanadium oxides and vanadates generally have a moderate electrochemical potential, which is very suitable for aqueous electrolyte battery system. Notably, we have witnessed the great interests and exciting results about vanadium-based nanomaterials for aqueous ZIBs very recently. Therefore, we believe it is an important application direction of vanadium-based nanomaterials for aqueous ZIBs in the future. The dissolution problem of vanadium-based electrodes in aqueous electrolytes is a non-negligible issue. Resolving the dissolution problem through electrolyte optimization and electrode modification, and clarifying the detailed dissolution mechanism are important targets in next step. Besides, the unambiguous characterization of the Zn^{2+} storage mechanism, including the structure evolution of vanadium-based nanomaterials, the effect of water (water cointercalation and the charge screen effect of water), and the relationships between electrode/electrolyte and electrochemical performance, are highly desired to push the development of vanadium-based electrodes for application in aqueous ZIBs.
- 2) Vanadium phosphates family has generated several promising high-voltage cathodes for SIBs which exhibit high potential to realize commercialization in near future, such as $Na_3V_2(PO_4)_3$ and $Na_3(VO)_2(PO_4)_2F$. Their superior

comprehensive properties, including high voltage, applicable specific capacity, excellent structure reversibility, good thermal stability and high ion diffusion coefficient, are comparable to or even better than the present commercialized LIB cathodes. The recently reported results also demonstrated that these cathode materials can exhibit ultrahigh rate capability and ultrastable cyclability after conductive modification. To realize the commercialization, making a balance between superior performance and facile production is very important. Since the low valence state of vanadium in these phases, an inert atmosphere is necessary for the high-temperature calcination during the fabrication of $\text{Na}_3\text{V}_2(\text{PO}_4)_3$ and $\text{Na}_3(\text{VO})_2(\text{PO}_4)_2\text{F}$, which may be an obstacle for their mass production. Therefore, in the next step, developing facile fabrication methods with high yields, low cost and effective conductive modification are very important for the practical applications of these promising cathodes. This target needs the joint efforts from industry and scientific community.

- 3) The emerging nonaqueous multivalent metal-ion batteries, such as Mg-ion batteries, Ca-ion batteries, and Al-ion batteries, are important research directions for electrochemical energy storage fields in the future. Exploring suitable intercalation cathodes is a great challenge for these battery systems, since the sluggish diffusion kinetics of the multivalent ions in the solid phase which is caused by the strong electrostatic interaction. The diversity in structure, composition and properties of vanadium-based electrodes make it highly possible to discover suitable candidates for multivalent metal-ion batteries. For example, the bilayered vanadium oxides have been demonstrated to possess superior Mg^{2+} intercalation/deintercalation properties, due to the large layer spacing over 10.0 Å and the charge shielding effect of crystal water in the interlayers. The oxygen-free chain-like VS_4 have been reported to exhibit excellent Mg^{2+} storage properties, which can be mainly ascribe to the decreased electrostatic interaction between Mg^{2+} and S_2^{2-} compared with Mg^{2+} and O^{2-} . These examples are inspiring. But limited by the lacking of mature electrolyte, the related researches about vanadium-based electrodes for nonaqueous multivalent metal-ion batteries are still insufficient at present. The further investigations are expected to produce more encouraging results.
- 4) Whether using nanostructured materials for battery electrodes or not is still a controversy. On the one hand, nanostructured materials will effectively improve the cycling and rate performance of the electrodes, due to the increased electrode/electrolyte contact area, shortened ion diffusion distance, and better strain release, while on the other hand, nanostructured materials generally possess a low tap density, which will result in a thicker electrode at the same mass loading, and thus a decreased volumetric capacity and energy density. The root of this contradiction originated from the present battery architecture. Our present batteries are 2D devices, in which the cathode, anode, separator and current collector are all 2D. This feature determines that it is always a tradeoff between energy density and power density, since a thick electrode is required for high energy while a thin electrode is desired for high power. Such a contradiction of present batteries also limits the practical application of nanostructured materials. However, in the long run, we believe

that nanostructured materials are the ultimate developing direction for battery electrodes, especially in the emerging energy storage system where large-sized or multivalent ions are used as the charge carriers. To overcome the low tap density issue of nanostructured electrode materials, a thorough innovation of the battery architecture from 2D electrodes to 3D electrodes may be the future direction. Since an additional dimension is utilized for loading active materials, 3D electrodes are potential to increase the active mass loading without increase the charge transport pathway, thus essentially resolve the issue caused by low tap density of nanomaterials, and also resolve the contradiction between energy density and power density in present battery architecture.

- 5) Exploring unexploited vanadium-based electrodes is still necessary and important, even though a large number of vanadium-based materials have been investigated for electrochemical energy storage. The recently reported new vanadium-based electrodes are encouraging, such as CaV_4O_9 for Na-ion battery anode, bilayered $\text{Zn}_{0.25}\text{V}_2\text{O}_5 \cdot n\text{H}_2\text{O}$ for aqueous Zn-ion battery cathode, $\text{Mg}_{0.3}\text{V}_2\text{O}_5 \cdot n\text{H}_2\text{O}$ for Mg-ion battery cathode, etc. Unexploited field means new hope. The above examples inspired that we should keep going on the way for exploring and discovering new vanadium-based electrode materials for next-generation electrochemical energy storage devices.

Acknowledgements

This work was supported by the National Natural Science Fund for Distinguished Young Scholars (51425204), the National Natural Science Foundation of China (51832004, 21905218, and 51602239), the National Key Research and Development Program of China (2016YFA0202603 and 2016YFA0202601), the Programme of Introducing Talents of Discipline to Universities (B17034), and the Yellow Crane Talent (Science and Technology) Program of Wuhan City, State Key Laboratory of Advanced Technology for Materials Synthesis and Processing (WUT:2019-KF-2,2019-KF-5).

Conflict of Interest

The authors declare no conflict of interest.

Keywords

charge storage mechanism, electrochemical performance, emerging metal-ion batteries, optimization strategies, vanadium-based nanomaterials

Received: June 2, 2019
Revised: November 28, 2019
Published online: January 8, 2020

- [1] S. Chu, A. Majumdar, *Nature* **2012**, *488*, 294.
- [2] S. Chu, Y. Cui, N. Liu, *Nat. Mater.* **2017**, *16*, 16.
- [3] Z. Yang, J. Zhang, M. C. W. Kintner-Meyer, X. Lu, D. Choi, J. P. Lemmon, J. Liu, *Chem. Rev.* **2011**, *111*, 3577.
- [4] D. Bruce, K. Haresh, T. Jean-Marie, *Science* **2011**, *334*, 928.
- [5] M. Armand, J. M. Tarascon, *Nature* **2008**, *451*, 652.
- [6] M. C. Lin, M. Gong, B. Lu, Y. Wu, D. Y. Wang, M. Guan, M. Angell, C. Chen, J. Yang, B. J. Hwang, H. Dai, *Nature* **2015**, *520*, 324.

- [7] T. Lin, I. W. Chen, F. Liu, C. Yang, H. Bi, F. Xu, F. Huang, *Science* **2015**, 350, 1508.
- [8] M. R. Lukatskaya, O. Mashtalir, C. E. Ren, Y. D. Agnese, P. Rozier, P. L. Taberna, M. Naguib, P. Simon, M. W. Barsoum, Y. Gogotsi, *Science* **2013**, 341, 1502.
- [9] X. Yang, C. Cheng, Y. Wang, L. Qiu, D. Li, *Science* **2013**, 341, 534.
- [10] P. Saha, M. K. Datta, O. I. Velikokhatnyi, A. Manivannan, D. Alman, P. N. Kumta, *Prog. Mater. Sci.* **2014**, 66, 1.
- [11] P. Simon, Y. Gogotsi, B. Dunn, *Science* **2014**, 343, 1210.
- [12] K. Kang, Y. S. Meng, J. Bréger, C. P. Grey, G. Ceder, *Science* **2006**, 311, 977.
- [13] A. Kraysberg, Y. Ein-Eli, *Adv. Energy Mater.* **2012**, 2, 922.
- [14] V. Palomares, P. Serras, I. Villaluenga, K. B. Hueso, J. Carretero-gonzález, T. Rojo, *Energy Environ. Sci.* **2012**, 5, 5884.
- [15] N. Yabuuchi, K. Kubota, M. Dahbi, S. Komaba, *Chem. Rev.* **2014**, 114, 11636.
- [16] D. Kundu, E. Talaie, V. Duffort, L. F. Nazar, *Angew. Chem., Int. Ed.* **2015**, 54, 3431.
- [17] Z. Jian, Z. Xing, C. Bommier, Z. Li, X. Ji, *Adv. Energy Mater.* **2016**, 6, 1501874.
- [18] Z. Jian, W. Luo, X. Ji, *J. Am. Chem. Soc.* **2015**, 137, 11566.
- [19] W. Luo, J. Wan, B. Ozdemir, W. Bao, Y. Chen, J. Dai, H. Lin, Y. Xu, F. Gu, V. Barone, *Nano Lett.* **2015**, 15, 7671.
- [20] H. Pan, Y. S. Hu, L. Chen, *Energy Environ. Sci.* **2013**, 6, 2338.
- [21] H. D. Yoo, Y. Liang, H. Dong, J. Lin, H. Wang, Y. Liu, L. Ma, T. Wu, Y. Li, Q. Ru, *Nat. Commun.* **2017**, 8, 339.
- [22] D. Kundu, B. D. Adams, V. Duffort, S. H. Vajargah, L. F. Nazar, *Nat. Energy* **2016**, 1, 16119.
- [23] H. Pan, Y. Shao, P. Yan, Y. Cheng, K. S. Han, Z. Nie, C. Wang, J. Yang, X. Li, P. Bhattacharya, *Nat. Energy* **2016**, 1, 16039.
- [24] G. A. Elia, K. Marquardt, K. Hoepfner, S. Fantini, R. Lin, E. Knipping, W. Peters, J. F. Drillet, S. Passerini, R. Hahn, *Adv. Mater.* **2016**, 28, 7564.
- [25] J. Muldoon, C. B. Bucur, T. Gregory, *Chem. Rev.* **2014**, 114, 11683.
- [26] Y. Wang, R. Chen, T. Chen, H. Lv, G. Zhu, L. Ma, C. Wang, Z. Jin, J. Liu, *Energy Storage Mater.* **2016**, 4, 103.
- [27] P. Canepa, G. S. Gautam, D. C. Hannah, R. Malik, L. Miao, K. G. Gallagher, K. A. Persson, G. Ceder, *Chem. Rev.* **2017**, 117, 4287.
- [28] A. Ponrouch, C. Frontera, F. Bardé, M. R. Palacín, *Nat. Mater.* **2016**, 15, 169.
- [29] D. Wang, X. Gao, Y. Chen, L. Jin, C. Kuss, P. G. Bruce, *Nat. Mater.* **2018**, 17, 16.
- [30] M. Wang, C. Jjiang, S. Zhang, X. Song, Y. Tang, H. M. Cheng, *Nat. Chem.* **2018**, 10, 667.
- [31] J. B. Goodenough, Y. Kim, *Chem. Mater.* **2010**, 22, 587.
- [32] H. Sun, L. Mei, J. Liang, Z. Zhao, C. Lee, H. Fei, M. Ding, J. Lau, M. Li, C. Wang, *Science* **2017**, 356, 599.
- [33] V. Augustyn, J. Come, M. A. Lowe, J. W. Kim, P. L. Taberna, S. H. Tolbert, H. D. Abruña, P. Simon, B. Dunn, *Nat. Mater.* **2013**, 12, 518.
- [34] Y. Wang, G. Cao, *Adv. Mater.* **2008**, 20, 2251.
- [35] L. Mai, X. Tian, X. Xu, L. Chang, L. Xu, *Chem. Rev.* **2014**, 114, 11828.
- [36] Y. Sun, N. Liu, Y. Cui, *Nat. Energy* **2016**, 1, 16071.
- [37] L. Zhou, Z. Zhuang, H. Zhao, M. Lin, D. Zhao, L. Mai, *Adv. Mater.* **2017**, 29, 1602914.
- [38] L. Yu, H. Hu, H. B. Wu, X. W. Lou, *Adv. Mater.* **2017**, 29, 1604563.
- [39] Q. Wei, F. Xiong, S. Tan, L. Huang, E. H. Lan, B. Dunn, L. Mai, *Adv. Mater.* **2017**, 29, 1602300.
- [40] P. G. Bruce, B. Scrosati, J. M. Tarascon, *Angew. Chem., Int. Ed.* **2008**, 47, 2930.
- [41] M. S. Whittingham, *J. Electrochem. Soc.* **1976**, 123, 315.
- [42] M. S. Whittingham, *Chem. Rev.* **2004**, 104, 4271.
- [43] N. A. Chernova, M. Roppolo, A. C. Dillon, M. S. Whittingham, *J. Mater. Chem.* **2009**, 19, 2526.
- [44] T. Chirayil, P. Y. Zavalij, M. S. Whittingham, *Chem. Mater.* **1998**, 10, 2629.
- [45] M. S. Whittingham, Y. Song, S. Lutta, P. Y. Zavalij, N. A. Chernova, *J. Mater. Chem.* **2005**, 15, 3362.
- [46] C. Wu, Y. Xie, *Energy Environ. Sci.* **2010**, 3, 1191.
- [47] F. Cheng, J. Chen, *J. Mater. Chem.* **2011**, 21, 9841.
- [48] Y. Yan, B. Li, W. Guo, H. Pang, H. Xue, *J. Power Sources* **2016**, 329, 148.
- [49] C. Liu, R. Massé, X. Nan, G. Cao, *Energy Storage Mater.* **2016**, 4, 15.
- [50] A. Moretti, S. Passerini, *Adv. Energy Mater.* **2016**, 6, 1600868.
- [51] M. Liu, B. Su, Y. Tang, X. Jiang, A. Yu, *Adv. Energy Mater.* **2017**, 7, 1700885.
- [52] P. Liu, K. Zhu, Y. Gao, H. Luo, L. Lu, *Adv. Energy Mater.* **2017**, 7, 1700547.
- [53] Y. Yuan, L. Hong, *Adv. Energy Mater.* **2017**, 7, 1601625.
- [54] M. L. Evans, B. D. Neff, *J. Power Sources* **2014**, 267, 831.
- [55] C. Wu, F. Feng, Y. Xie, *Chem. Soc. Rev.* **2013**, 42, 5157.
- [56] J. Yao, Y. Lia, R. C. Massé, E. Uchaker, G. Cao, *Energy Storage Mater.* **2018**, 11, 205.
- [57] Q. Wang, J. Xu, W. Zhang, M. Mao, Z. Wei, C. Cui, L. Wang, Y. Zhu, J. Ma, *J. Mater. Chem. A* **2018**, 6, 8815.
- [58] Y. Zhao, C. Han, J. Yang, J. Su, X. Xu, S. Li, L. Xu, R. Fang, H. Jiang, X. Zou, *Nano Lett.* **2015**, 15, 2180.
- [59] H. Liu, Y. Wang, L. Li, K. Wang, E. Hosono, H. Zhou, *J. Mater. Chem.* **2009**, 19, 7885.
- [60] X. Xu, Y. Z. Luo, L. Q. Mai, Y. L. Zhao, Q. Y. An, L. Xu, F. Hu, L. Zhang, Q. J. Zhang, *NPG Asia Mater.* **2012**, 4, e20.
- [61] W. Ren, Z. Zheng, C. Xu, C. Niu, Q. Wei, Q. An, K. Zhao, M. Yan, M. Qin, L. Mai, *Nano Energy* **2016**, 25, 145.
- [62] Y. Fang, L. Xiao, X. Ai, Y. Cao, H. Yang, *Adv. Mater.* **2015**, 27, 5895.
- [63] C. Wu, X. Lu, L. Peng, K. Xu, X. Peng, J. Huang, G. Yu, Y. Xie, *Nat. Commun.* **2013**, 4, 2431.
- [64] Y. Zhu, L. Peng, D. Chen, G. Yu, *Nano Lett.* **2016**, 16, 742.
- [65] G. He, W. H. Kan, A. Manthiram, *Chem. Mater.* **2016**, 28, 682.
- [66] H. Li, L. Peng, Y. Zhu, D. Chen, X. Zhang, G. Yu, *Energy Environ. Sci.* **2016**, 9, 3399.
- [67] A. K. Padhi, J. B. Goodenough, K. S. Nanjundaswamy, *J. Electrochem. Soc.* **1997**, 144, 1188.
- [68] K. S. Nanjundaswamy, A. K. Padhi, J. B. Goodenough, S. Okada, H. Ohtsuka, H. Arai, J. Yamaki, *Solid State Ionics* **1996**, 92, 1.
- [69] M. Naguib, J. Halim, J. Lu, K. M. Cook, L. Hultman, Y. Gogotsi, M. W. Barsoum, *J. Am. Chem. Soc.* **2013**, 135, 15966.
- [70] Y. Dall'Agnese, P. L. Taberna, Y. Gogotsi, P. Simon, *J. Phys. Chem. Lett.* **2015**, 6, 2305.
- [71] S. Bak, R. Qiao, W. Yang, S. Lee, X. Yu, B. Anasori, H. Lee, Y. Gogotsi, X. Q. Yang, *Adv. Energy Mater.* **2017**, 7, 1700959.
- [72] W. Bi, Z. Hu, X. Li, C. Wu, J. Wu, Y. Wu, Y. Xie, *Nano Res.* **2015**, 8, 193.
- [73] L. Wang, J. Sun, R. Song, S. Yang, H. Song, *Adv. Energy Mater.* **2016**, 6, 1502067.
- [74] X. Lu, M. Yu, T. Zhai, G. Wang, S. Xie, T. Liu, C. Liang, Y. Tong, Y. Li, *Nano Lett.* **2013**, 13, 2628.
- [75] Y. Wu, F. Ran, *J. Power Sources* **2017**, 344, 1.
- [76] P. He, M. Yan, G. Zhang, R. Sun, L. Chen, Q. An, L. Mai, *Adv. Energy Mater.* **2017**, 7, 1601920.
- [77] R. Sun, Q. Wei, J. Sheng, C. Shi, Q. An, S. Liu, L. Mai, *Nano Energy* **2017**, 35, 396.
- [78] J. Zhou, L. Wang, M. Yang, J. Wu, F. Chen, W. Huang, N. Han, H. Ye, F. Zhao, Y. Li, *Adv. Mater.* **2017**, 29, 1702061.
- [79] B. Anasori, M. R. Lukatskaya, Y. Gogotsi, *Nat. Rev. Mater.* **2017**, 2, 16098.
- [80] X. Huang, X. Rui, H. H. Hng, Q. Yan, *Part. Part. Syst. Charact.* **2015**, 32, 276.
- [81] H. T. Tan, X. Rui, W. Sun, Q. Yan, T. M. Lim, *Nanoscale* **2015**, 7, 14595.

- [82] D. W. Su, S. X. Dou, G. X. Wang, *J. Mater. Chem. A* **2014**, *2*, 11185.
- [83] N. Sa, H. Wang, D. L. Proffitt, A. L. Lipson, B. Key, M. Liu, Z. Feng, T. T. Fister, Y. Ren, C.-J. Sun, J. T. Vaughney, P. A. Fenter, K. A. Persson, A. K. Burrell, *J. Power Sources* **2016**, *323*, 44.
- [84] N. Jayaprakash, S. K. Das, L. A. Archer, *Chem. Commun.* **2011**, *47*, 12610.
- [85] N. Zhang, Y. Dong, M. Jia, X. Bian, Y. Wang, M. Qiu, J. Xu, Y. Liu, L. Jiao, F. Cheng, *ACS Energy Lett.* **2018**, *3*, 1366.
- [86] Q. Wei, J. Liu, W. Feng, J. Sheng, X. Tian, L. He, Q. An, L. Mai, *J. Mater. Chem. A* **2015**, *3*, 8070.
- [87] D. Imamura, M. Miyayama, M. Hibino, T. Kudo, *J. Electrochem. Soc.* **2003**, *150*, A753.
- [88] M. Yan, P. He, Y. Chen, S. Wang, Q. Wei, K. Zhao, X. Xu, Q. An, Y. Shuang, Y. Shao, *Adv. Mater.* **2018**, *30*, 1703725.
- [89] M. S. Balogun, Y. Luo, F. Lyu, F. Wang, H. Yang, H. Li, C. Liang, M. Huang, Y. Huang, Y. Tong, *ACS Appl. Mater. Interfaces* **2016**, *8*, 9733.
- [90] T. Luo, Y. Liu, H. Su, R. Xiao, L. Huang, Q. Xiang, Y. Zhou, C. Chen, *Electrochim. Acta* **2018**, *260*, 805.
- [91] W. Wang, B. Jiang, W. Xiong, H. Sun, Z. Lin, L. Hu, J. Tu, J. Hou, H. Zhu, S. Jiao, *Sci. Rep.* **2013**, *3*, 3383.
- [92] J. Ding, Z. Du, L. Gu, B. Li, L. Wang, S. Wang, Y. Gong, S. Yang, *Adv. Mater.* **2018**, *30*, 1800762.
- [93] D. Wang, Q. Wei, J. Sheng, P. Hu, M. Yan, R. Sun, X. Xu, Q. An, L. Mai, *Phys. Chem. Chem. Phys.* **2016**, *18*, 12074.
- [94] H. Tang, N. Xu, C. Pei, F. Xiong, S. Tan, W. Luo, Q. An, L. Mai, *ACS Appl. Mater. Interfaces* **2017**, *9*, 28667.
- [95] P. He, Y. Quan, X. Xu, M. Yan, W. Yang, Q. An, L. He, L. Mai, *Small* **2017**, *13*, 1702551.
- [96] H. Fei, Y. Lin, M. Wei, *J. Colloid Interface Sci.* **2014**, *425*, 1.
- [97] X. Xia, D. Chao, Y. Zhang, J. Zhan, Y. Zhong, X. Wang, Y. Wang, Z. X. Shen, J. Tu, H. J. Fan, *Small* **2016**, *12*, 3048.
- [98] Y. Yue, H. Liang, *Adv. Energy Mater.* **2017**, *7*, 1602545.
- [99] D. McNulty, D. N. Buckley, C. O'Dwyer, *J. Power Sources* **2014**, *267*, 831.
- [100] G. Ali, J. H. Lee, S. H. Oh, B. W. Cho, K. W. Nam, K. Y. Chung, *ACS Appl. Mater. Interfaces* **2016**, *8*, 6032.
- [101] V. Raju, J. Rains, C. Gates, W. Luo, X. Wang, W. F. Stickle, G. D. Stucky, X. Ji, *Nano Lett.* **2014**, *14*, 4119.
- [102] E. Uchaker, Y. Z. Zheng, S. Li, S. L. Candelaria, S. Hu, G. Z. Cao, *J. Mater. Chem. A* **2014**, *2*, 18208.
- [103] M. Safrany Renard, N. Emery, R. Baddour-Hadjean, J.-P. Pereira-Ramos, *Electrochim. Acta* **2017**, *252*, 4.
- [104] S. Liu, Z. Tong, J. Zhao, X. Liu, J. Wang, X. Ma, C. Chi, Y. Yang, X. Liu, Y. Li, *Phys. Chem. Chem. Phys.* **2016**, *18*, 25645.
- [105] J. P. Pereira-Ramos, R. Messina, J. Perichon, *J. Electroanal. Chem. Interfacial Electrochem.* **1987**, *218*, 241.
- [106] D. Aurbach, Z. Lu, A. Schechter, Y. Gofer, H. Gizbar, R. Turgeman, Y. Cohen, M. Moshkovich, E. Levi, *Nature* **2000**, *407*, 724.
- [107] G. G. Amatucci, F. Badway, A. Singhal, B. Beaudoin, G. Skandan, T. Bowmer, I. Plitz, N. Pereira, T. Chapman, R. Jaworski, *J. Electrochem. Soc.* **2001**, *148*, A940.
- [108] L. Jiao, H. Yuan, Y. Si, Y. Wang, J. Cao, X. Gao, M. Zhao, X. Zhou, Y. Wang, *J. Power Sources* **2006**, *156*, 673.
- [109] G. Gershinshy, H. D. Yoo, Y. Gofer, D. Aurbach, *Langmuir* **2013**, *29*, 10964.
- [110] X. Du, G. Huang, Y. Qin, L. Wang, *RSC Adv.* **2015**, *5*, 76352.
- [111] C. Drosos, C. Jia, S. Mathew, R. G. Palgrave, B. Moss, A. Kafizas, D. Vernardou, *J. Power Sources* **2018**, *384*, 355.
- [112] S. Gu, H. Wang, C. Wu, Y. Bai, H. Li, F. Wu, *Energy Storage Mater.* **2017**, *6*, 9.
- [113] L. D. Reed, E. Menke, *J. Electrochem. Soc.* **2013**, *160*, A915.
- [114] M. Chiku, H. Takeda, S. Matsumura, E. Higuchi, H. Inoue, *ACS Appl. Mater. Interfaces* **2015**, *7*, 24385.
- [115] P. Hu, M. Yan, T. Zhu, X. Wang, X. Wei, J. Li, L. Zhou, Z. Li, L. Chen, L. Mai, *ACS Appl. Mater. Interfaces* **2017**, *9*, 42717.
- [116] L. W. Wangoh, Y. Huang, R. L. Jezorek, A. B. Kehoe, G. W. Watson, F. Omenya, N. F. Quackenbush, N. A. Chernova, M. S. Whittingham, L. F. Piper, *ACS Appl. Mater. Interfaces* **2016**, *8*, 11532.
- [117] H. Liu, Y. Wang, H. Li, W. Yang, H. Zhou, *ChemPhysChem* **2010**, *11*, 3273.
- [118] P. E. Tang, J. S. Sakamoto, E. Baudrin, B. Dunn, *J. Non-Cryst. Solids* **2004**, *350*, 67.
- [119] Q. Wei, Z. Jiang, S. Tan, Q. Li, L. Huang, M. Yan, L. Zhou, Q. An, L. Mai, *ACS Appl. Mater. Interfaces* **2015**, *7*, 18211.
- [120] A. Moretti, F. Maroni, I. Osada, F. Nobili, S. Passerini, *ChemElectroChem* **2015**, *2*, 529.
- [121] X. Xiang, K. Zhang, J. Chen, *Adv. Mater.* **2015**, *27*, 5343.
- [122] S. Tepavcevic, H. Xiong, V. R. Stamenkovic, X. Zuo, M. Balasubramanian, V. B. Prakapenka, C. S. Johnson, T. Rajh, *ACS Nano* **2012**, *6*, 530.
- [123] Q. An, Y. Li, H. D. Yoo, S. Chen, Q. Ru, L. Mai, Y. Yao, *Nano Energy* **2015**, *18*, 265.
- [124] S. Tepavcevic, Y. Liu, D. Zhou, B. Lai, J. Maser, X. Zuo, H. Chan, P. Král, C. S. Johnson, V. Stamenkovic, *ACS Nano* **2015**, *9*, 8194.
- [125] M. Yan, P. He, Y. Chen, S. Wang, Q. Wei, K. Zhao, X. Xu, Q. An, Y. Shuang, Y. Shao, K. T. Mueller, L. Mai, J. Liu, J. Yang, *Adv. Mater.* **2018**, *30*, 1703725.
- [126] D. Lv, T. Xu, P. Saha, M. K. Datta, M. L. Gordin, A. Manivannan, P. N. Kumta, D. Wang, *J. Electrochem. Soc.* **2013**, *160*, A351.
- [127] P. Senguttuvan, S.-D. Han, S. Kim, A. L. Lipson, S. Tepavcevic, T. T. Fister, I. D. Bloom, A. K. Burrell, C. S. Johnson, *Adv. Energy Mater.* **2016**, *6*, 1600826.
- [128] Y. Yang, Y. Tang, G. Fang, L. Shan, J. Guo, W. Zhang, C. Wang, L. Wang, J. Zhou, S. Liang, *Energy Environ. Sci.* **2018**, *11*, 3157.
- [129] M. Clites, E. Pomerantseva, *Energy Storage Mater.* **2018**, *11*, 30.
- [130] X. Yao, Y. Zhao, F. A. Castro, L. Mai, *ACS Energy Lett.* **2019**, *4*, 771.
- [131] N. Park, K. S. Ryu, Y. J. Park, M. G. Kang, D. Kim, S. Kang, K. M. Kim, S. Chang, *J. Power Sources* **2002**, *103*, 273.
- [132] O. Y. Posudievsky, O. A. Kozarenko, V. S. Dyadyun, S. W. Jorgensen, J. A. Spearot, V. G. Koshechko, V. D. Pokhodenko, *J. Power Sources* **2011**, *196*, 3331.
- [133] M. D. Wei, H. Sugihara, I. Honma, M. Ichihara, H. S. Zhou, *Adv. Mater.* **2005**, *17*, 2964.
- [134] G. Armstrong, J. Canales, A. R. Armstrong, P. G. Bruce, *J. Power Sources* **2008**, *178*, 723.
- [135] W. Wang, B. Jiang, L. Hu, Z. Lin, J. Hou, S. Jiao, *J. Power Sources* **2014**, *250*, 181.
- [136] D. Chao, C. Zhu, X. Xia, J. Liu, X. Zhang, J. Wang, P. Liang, J. Lin, H. Zhang, Z. X. Shen, H. J. Fan, *Nano Lett.* **2015**, *15*, 565.
- [137] C. Pei, F. Xiong, J. Sheng, Y. Yin, S. Tan, D. Wang, C. Han, Q. An, L. Mai, *ACS Appl. Mater. Interfaces* **2017**, *9*, 17060.
- [138] L. Chen, Y. Ruan, G. Zhang, Q. Wei, Y. Jiang, T. Xiong, P. He, W. Yang, M. Yan, Q. An, L. Mai, *Chem. Mater.* **2019**, *31*, 699.
- [139] C. Zhang, H. Song, C. Zhang, C. Liu, Y. Liu, G. Cao, *J. Phys. Chem. C* **2015**, *119*, 11391.
- [140] Q. Pang, C. Sun, Y. Yu, K. Zhao, Z. Zhang, P. M. Voyle, G. Chen, Y. Wei, X. Wang, *Adv. Energy Mater.* **2018**, *8*, 1800144.
- [141] Y. L. Ding, Y. Wen, C. Wu, P. A. van Aken, J. Maier, Y. Yu, *Nano Lett.* **2015**, *15*, 1388.
- [142] M. Z. A. Munshi, *J. Electrochem. Soc.* **1989**, *136*, 1847.
- [143] M. Z. A. Munshi, W. H. Smyrl, *Solid State Ionics* **1991**, *45*, 183.
- [144] M. Yu, Y. Zeng, Y. Han, X. Cheng, W. Zhao, C. Liang, Y. Tong, H. Tang, X. Lu, *Adv. Funct. Mater.* **2015**, *25*, 3534.
- [145] W. Gou, X. Kong, Y. Wang, Y. Ai, S. Liang, A. Pan, G. Cao, *Chem. Eng. J.* **2019**, *374*, 545.
- [146] A. Tranchant, R. Messina, J. Perichon, *J. Electroanal. Chem. Interfacial Electrochem.* **1980**, *113*, 225.
- [147] H. Li, P. Balaya, J. Maier, *J. Electrochem. Soc.* **2004**, *151*, A1878.
- [148] Y. Cai, G. Fang, J. Zhou, S. Liu, Z. Luo, A. Pan, G. Cao, S. Liang, *Nano Res.* **2018**, *11*, 449.

- [149] S. Tan, Y. Jiang, Q. Wei, Q. Huang, Y. Dai, F. Xiong, Q. Li, Q. An, X. Xu, Z. Zhu, X. Bai, L. Mai, *Adv. Mater.* **2018**, *30*, 1707122.
- [150] X. Xu, C. Niu, M. Duan, X. Wang, L. Huang, J. Wang, L. Pu, W. Ren, C. Shi, J. Meng, B. Song, L. Mai, *Nat. Commun.* **2017**, *8*, 460.
- [151] Y. Xu, X. Deng, Q. Li, G. Zhang, F. Xiong, S. Tan, Q. Wei, J. Lu, J. Li, Q. An, L. Mai, *Chem* **2019**, *5*, 1194.
- [152] M. H. Alfaruqi, V. Mathew, J. Song, S. Kim, S. Islam, D. T. Pham, J. Jo, S. Kim, J. P. Baboo, Z. Xiu, *Chem. Mater.* **2017**, *29*, 1684.
- [153] Y. Dong, S. Li, K. Zhao, C. Han, W. Chen, B. Wang, L. Wang, B. Xu, Q. Wei, L. Zhang, X. Xu, L. Mai, *Energy Environ. Sci.* **2015**, *8*, 1267.
- [154] P. Hu, T. Zhu, X. Wang, X. Wei, M. Yan, J. Li, W. Luo, W. Yang, W. Zhang, L. Zhou, *Nano Lett.* **2018**, *18*, 1758.
- [155] P. He, G. Zhang, X. Liao, M. Yan, X. Xu, Q. An, J. Liu, L. Mai, *Adv. Energy Mater.* **2018**, *8*, 1702463.
- [156] N. Emery, R. Baddour-Hadjean, D. Batyrbekuly, B. Laik, Z. Bakenov, J.-P. Pereira-Ramos, *Chem. Mater.* **2018**, *30*, 5305.
- [157] M. Clites, J. L. Hart, M. L. Taheri, E. Pomerantseva, *ACS Energy Lett.* **2018**, *3*, 562.
- [158] D. Hamani, M. Ati, J. M. Tarascon, P. Rozier, *Electrochem. Commun.* **2011**, *13*, 938.
- [159] C. Xia, J. Guo, P. Li, X. Zhang, H. N. Alshareef, *Angew. Chem. Int. Ed.* **2018**, *57*, 3943.
- [160] X. Xu, M. Duan, Y. Yue, Q. Li, X. Zhang, L. Wu, P. Wu, B. Song, L. Mai, *ACS Energy Lett.* **2019**, *4*, 1328.
- [161] W. Kaveevivitchai, A. J. Jacobson, *Chem. Mater.* **2016**, *28*, 4593.
- [162] C. Xia, J. Guo, Y. Lei, H. Liang, C. Zhao, H. N. Alshareef, *Adv. Mater.* **2018**, *30*, 1705580.
- [163] B. Sambandam, V. Soundharrajan, S. Kim, M. H. Alfaruqi, J. Jo, S. Kim, V. Mathew, Y. K. Sun, J. Kim, *J. Mater. Chem. A* **2018**, *6*, 3850.
- [164] T. N. Vo, H. Kim, J. Hur, W. Choi, I. T. Kim, *J. Mater. Chem. A* **2018**, *6*, 22645.
- [165] A. Pan, J. Liu, J. G. Zhang, G. Cao, W. Xu, Z. Nie, X. Jie, D. Choi, B. W. Arey, C. Wang, *J. Mater. Chem.* **2010**, *21*, 1153.
- [166] H. Song, M. Luo, A. Wang, *ACS Appl. Mater. Interfaces* **2017**, *9*, 2875.
- [167] A. Caballero, J. Morales, O. Vargas, *J. Power Sources* **2010**, *195*, 4318.
- [168] F. Wan, Z. Niu, *Angew. Chem., Int. Ed.* **2019**, *58*, 2.
- [169] H. Kim, J. Hong, K. Park, H. Kim, S. Kim, K. Kang, *Chem. Rev.* **2014**, *114*, 11788.
- [170] H. Wang, S. Liu, Y. Ren, W. Wang, A. Tang, *Energy Environ. Sci.* **2012**, *5*, 6173.
- [171] Y. Tang, D. Sun, H. Wang, X. Huang, H. Zhang, S. Liu, Y. Liu, *RSC Adv.* **2014**, *4*, 8328.
- [172] H. Wang, W. Wang, Y. Ren, K. Huang, S. Liu, *J. Power Sources* **2012**, *199*, 263.
- [173] S. Liang, C. Tao, A. Pan, D. Liu, Q. Zhu, G. Cao, *ACS Appl. Mater. Interfaces* **2013**, *5*, 11913.
- [174] S. Liang, J. Zhou, G. Fang, J. Liu, Y. Tang, X. Li, A. Pan, *ACS Appl. Mater. Interfaces* **2013**, *5*, 8704.
- [175] H. He, G. Jin, H. Wang, X. Huang, Z. Chen, D. Sun, Y. Tang, *J. Mater. Chem. A* **2014**, *2*, 3563.
- [176] S. Yuan, Y.-B. Liu, D. Xu, D.-L. Ma, S. Wang, X.-H. Yang, Z.-Y. Cao, X.-B. Zhang, *Adv. Sci.* **2015**, *2*, 1400018.
- [177] E. Uchaker, H. Jin, P. Yi, G. Cao, *Chem. Mater.* **2015**, *27*, 7082.
- [178] C. Deng, S. Zhang, Z. Dong, Y. Shang, *Nano Energy* **2014**, *4*, 49.
- [179] Y. Cai, F. Liu, Z. Luo, G. Fang, J. Zhou, A. Pan, S. Liang, *Energy Storage Mater.* **2018**, *13*, 168.
- [180] F. Wan, L. Zhang, X. Dai, X. Wang, Z. Niu, J. Chen, *Nat. Commun.* **2018**, *9*, 1656.
- [181] V. Soundharrajan, B. Sambandam, S. Kim, M. H. Alfaruqi, D. Y. Putro, J. Jo, V. Mathew, Y. K. Sun, J. Kim, *Nano Lett.* **2018**, *18*, 2402.
- [182] Y. Xu, X. Han, L. Zheng, W. Yan, Y. Xie, *J. Mater. Chem.* **2011**, *21*, 14466.
- [183] Y. Cai, J. Zhou, G. Fang, G. Cai, A. Pan, S. Liang, *J. Power Sources* **2016**, *328*, 241.
- [184] Y. Lu, J. Wu, J. Liu, L. Ming, S. Tang, P. Lu, L. Yang, H. Yang, Y. Qian, *ACS Appl. Mater. Interfaces* **2015**, *7*, 17433.
- [185] Q. Tan, Q. Zhu, A. Pan, Y. Wang, Y. Tang, X. Tan, S. Liang, G. Cao, *CrystEngComm* **2015**, *17*, 4774.
- [186] X. Wang, S. Zheng, S. Wang, Y. Zhang, H. Du, *Nano Energy* **2016**, *22*, 179.
- [187] H. Liu, H. Zhou, L. Chen, Z. Tang, W. Yang, *J. Power Sources* **2011**, *196*, 814.
- [188] E. Khoo, J. M. Wang, J. Ma, P. S. Lee, *J. Mater. Chem.* **2010**, *20*, 8368.
- [189] D. Sun, G. Jin, H. Wang, P. Liu, Y. Ren, Y. Jiang, Y. Tang, X. Huang, *J. Mater. Chem. A* **2014**, *2*, 12999.
- [190] M. Zhao, W. Zhang, F. Qu, F. Wang, X. Song, *Electrochim. Acta* **2014**, *138*, 187.
- [191] D. Muller-Bouvet, R. Baddour-Hadjean, M. Tanabe, L. T. N. Huynh, M. L. P. Le, J. P. Pereira-Ramos, *Electrochim. Acta* **2015**, *176*, 586.
- [192] C. Didier, M. Guignard, C. Denage, O. Szajwaj, S. Ito, I. Saadoun, J. Darriet, C. Delmas, *Electrochem. Solid-State Lett.* **2011**, *14*, A75.
- [193] M. Guignard, C. Didier, J. Darriet, P. Bordet, E. Elkaïm, C. Delmas, *Nat. Mater.* **2013**, *12*, 74.
- [194] F. Ming, H. Liang, Y. Lei, S. Kandambeth, M. Eddaoudi, H. N. Alshareef, *ACS Energy Lett.* **2018**, *3*, 2602.
- [195] X. Xu, P. Wu, Q. Li, W. Yang, X. Zhang, X. Wang, J. Meng, C. Niu, L. Mai, *Nano Energy* **2018**, *50*, 606.
- [196] K. J. Takeuchi, A. C. Marschilok, S. M. Davis, R. A. Leising, E. S. Takeuchi, *Coord. Chem. Rev.* **2001**, *219–221*, 283.
- [197] M. Morcrette, P. Rozier, L. Dupont, E. Mugnier, L. Sannier, J. Galy, J. M. Tarascon, *Nat. Mater.* **2003**, *2*, 755.
- [198] G. Yang, H. Cui, G. Yang, C. Wang, *ACS Nano* **2014**, *8*, 4474.
- [199] G. Yang, M. Wu, C. Wang, *ACS Appl. Mater. Interfaces* **2016**, *8*, 23746.
- [200] Q. Wei, Q. Wang, Q. Li, Q. An, Y. Zhao, Z. Peng, Y. Jiang, S. Tan, M. Yan, L. Mai, *Nano Energy* **2018**, *47*, 294.
- [201] Z. Peng, Q. Wei, S. Tan, P. He, W. Luo, Q. An, L. Mai, *Chem. Commun.* **2018**, *54*, 4041.
- [202] H. Wang, Y. Ren, W. Wang, X. Huang, K. Huang, Y. Wang, S. Liu, *J. Power Sources* **2012**, *199*, 315.
- [203] G. Yang, H. Song, G. Yang, M. Wu, C. Wang, *Nano Energy* **2015**, *15*, 281.
- [204] E. A. Esparcia, M. S. Chae, J. D. Ocon, S. T. Hong, *Chem. Mater.* **2018**, *30*, 3690.
- [205] Z. Jian, Y. S. Hu, X. Ji, W. Chen, *Adv. Mater.* **2017**, *29*, 1601925.
- [206] C. Masquelier, L. Croguennec, *Chem. Rev.* **2013**, *113*, 6552.
- [207] L. Wang, J. Bai, P. Gao, X. Wang, J. P. Looney, F. Wang, *Chem. Mater.* **2015**, *27*, 5712.
- [208] F. Xiong, S. Tan, Q. Wei, G. Zhang, J. Sheng, Q. An, L. Mai, *Nano Energy* **2017**, *32*, 347.
- [209] W. Duan, Z. Zhu, H. Li, Z. Hu, K. Zhang, F. Cheng, J. Chen, *J. Mater. Chem. A* **2014**, *2*, 8668.
- [210] X. Jiang, L. Yang, B. Ding, B. Qu, G. Ji, J. Y. Lee, *J. Mater. Chem. A* **2016**, *4*, 14669.
- [211] Y. Xu, Q. Wei, C. Xu, Q. Li, Q. An, P. Zhang, J. Sheng, L. Zhou, L. Mai, *Adv. Energy Mater.* **2016**, *6*, 1600389.
- [212] W. Zhou, L. Xue, X. Lü, H. Gao, Y. Li, S. Xin, G. Fu, Z. Cui, Y. Zhu, J. B. Goodenough, *Nano Lett.* **2016**, *16*, 7836.
- [213] J. Song, S. Park, V. Mathew, J. Gim, S. Kim, J. Jo, S. Kim, M. H. Alfaruqi, J. P. Baboo, I. H. Kim, *ACS Appl. Mater. Interfaces* **2016**, *8*, 35235.
- [214] G. Li, Z. Yang, Y. Jiang, C. Jin, W. Huang, X. Ding, Y. Huang, *Nano Energy* **2016**, *25*, 211.
- [215] L. Zhou, Q. Liu, Z. Zhang, K. Zhang, F. Xiong, S. Tan, Q. An, Y.-M. Kang, Z. Zhou, L. Mai, *Adv. Mater.* **2018**, *30*, 1801984.
- [216] C. Zhu, C. Wu, C. C. Chen, P. Kopold, P. A. V. Aken, J. Maier, Y. Yu, *Chem. Mater.* **2017**, *29*, 5207.

- [217] T. Jin, Y. Liu, Y. Li, K. Cao, X. Wang, L. Jiao, *Adv. Energy Mater.* **2017**, 7, 1700087.
- [218] Y. Yin, F. Xiong, C. Pei, Y. Xu, Q. An, S. Tan, Z. Zhuang, J. Sheng, Q. Li, L. Mai, *Nano Energy* **2017**, 41, 452.
- [219] S. Y. Lim, H. Kim, J. Chung, J. H. Lee, B. G. Kim, J.-J. Choi, K. Y. Chung, W. Cho, S.-J. Kim, W. A. Goddard, Y. Jung, J. W. Choi, *Proc. Natl. Acad. Sci. USA* **2014**, 111, 599.
- [220] X. Wang, C. Niu, J. Meng, P. Hu, X. Xu, X. Wei, L. Zhou, K. Zhao, W. Luo, M. Yan, *Adv. Energy Mater.* **2015**, 5, 1500716.
- [221] J. Han, G. N. Li, F. Liu, M. Wang, Y. Zhang, L. Hu, C. Dai, M. Xu, *Chem. Commun.* **2017**, 53, 1805.
- [222] N. Membreño, K. Park, J. B. Goodenough, K. J. Stevenson, *Chem. Mater.* **2015**, 27, 3332.
- [223] S. Liang, Q. Tan, W. Xiong, Y. Tang, X. Tan, L. Huang, A. Pan, G. Cao, *Sci. Rep.* **2016**, 6, 33682.
- [224] Y. Cheng, X. Ni, K. Feng, H. Zhang, X. Li, H. Zhang, *J. Power Sources* **2016**, 326, 203.
- [225] Z. Jian, L. Zhao, H. Pan, Y. S. Hu, H. Li, W. Chen, L. Chen, *Electrochem. Commun.* **2012**, 14, 86.
- [226] J. N. Chotard, G. Rousse, R. David, O. Mentré, M. Courty, C. Masquelier, *Chem. Mater.* **2015**, 27, 5982.
- [227] W. Song, X. Ji, Z. Wu, Y. Zhu, Y. Yang, J. Chen, M. Jing, F. Li, C. E. Banks, *J. Mater. Chem. A* **2014**, 2, 5358.
- [228] Z. Jian, Y. Sun, X. Ji, *Chem. Commun.* **2015**, 51, 6381.
- [229] S. Li, Y. Dong, L. Xu, X. Xu, L. He, L. Mai, *Adv. Mater.* **2014**, 26, 3545.
- [230] X. Yao, Z. Zhu, Q. Li, X. Wang, X. Xu, J. Meng, W. Ren, X. Zhang, Y. Huang, L. Mai, *ACS Appl. Mater. Interfaces* **2018**, 10, 10022.
- [231] X. Rui, W. Sun, C. Wu, Y. Yu, Q. Yan, *Adv. Mater.* **2015**, 27, 6670.
- [232] Y. Jiang, Z. Yang, W. Li, L. Zeng, F. Pan, M. Wang, X. Wei, G. Hu, L. Gu, Y. Yu, *Adv. Energy Mater.* **2015**, 5, 1402104.
- [233] J. Kang, S. Baek, V. Mathew, J. Gim, J. Song, H. Park, E. Chae, A. K. Rai, J. Kim, *J. Mater. Chem.* **2012**, 22, 20857.
- [234] W. Ren, X. Yao, C. Niu, Z. Zheng, K. Zhao, Q. An, Q. Wei, M. Yan, L. Zhang, L. Mai, *Nano Energy* **2016**, 28, 216.
- [235] M. J. Aragón, J. Gutiérrez, R. Klee, P. Lavela, R. Alcántara, J. L. Tirado, *J. Electroanal. Chem.* **2017**, 784, 47.
- [236] S. Tao, P. Cui, W. Huang, Z. Yu, X. Wang, S. Wei, D. Liu, L. Song, W. Chu, *Carbon* **2016**, 96, 1028.
- [237] W. Song, X. Ji, Y. Yao, H. Zhu, Q. Chen, Q. Sun, C. E. Banks, *Phys. Chem. Chem. Phys.* **2014**, 16, 3055.
- [238] Y. H. Jung, C. H. Lim, D. K. Kim, *J. Mater. Chem. A* **2013**, 1, 11350.
- [239] S. Y. Lim, H. Kim, R. A. Shaloor, Y. Jung, J. W. Choi, *J. Electrochem. Soc.* **2012**, 159, A1393.
- [240] H. Li, X. Yu, Y. Bai, F. Wu, C. Wu, L. Y. Liu, X. Q. Yang, *J. Mater. Chem. A* **2015**, 3, 9578.
- [241] R. Klee, P. Lavela, M. J. Aragón, R. Alcántara, J. L. Tirado, *J. Power Sources* **2016**, 313, 73.
- [242] R. Klee, M. Wiatrowski, M. J. Aragón, P. Lavela, G. F. Ortiz, R. Alcántara, J. L. Tirado, *ACS Appl. Mater. Interfaces* **2017**, 9, 1471.
- [243] W. Shen, H. Li, Z. Guo, Z. Li, Q. Xu, H. Liu, Y. Wang, *RSC Adv.* **2016**, 6, 71581.
- [244] K. Du, H. Guo, G. Hu, Z. Peng, Y. Cao, *J. Power Sources* **2013**, 223, 284.
- [245] W. Song, X. Ji, C. Pan, Y. Zhu, Q. Chen, C. E. Banks, *Phys. Chem. Chem. Phys.* **2013**, 15, 14357.
- [246] Q. An, F. Xiong, Q. Wei, J. Sheng, L. He, D. Ma, Y. Yao, L. Mai, *Adv. Energy Mater.* **2015**, 5, 1401963.
- [247] F. Nacimiento, M. Cabello, R. Alcántara, P. Lavela, J. L. Tirado, *Electrochim. Acta* **2018**, 260, 798.
- [248] B. M. Azmi, T. Ishihara, H. Nishiguchi, Y. Takita, *J. Power Sources* **2003**, 119–121, 273.
- [249] Y. C. Lin, M. F. V. Hidalgo, I. H. Chu, N. A. Chernova, M. S. Whittingham, S. P. Ong, *J. Mater. Chem. A* **2017**, 5, 17421.
- [250] L. Peng, Y. Zhu, X. Peng, Z. Fang, W. Chu, Y. Wang, Y. Xie, Y. Li, J. J. Cha, G. Yu, *Nano Lett.* **2017**, 17, 6273.
- [251] X. Ji, J. Chen, F. Wang, W. Sun, Y. Ruan, L. Miao, J. Jiang, C. Wang, *Nano Lett.* **2018**, 18, 6441.
- [252] J. Song, M. Xu, L. Wang, J. B. Goodenough, *Chem. Commun.* **2013**, 49, 5280.
- [253] G. He, A. Huq, W. H. Kan, A. Manthiram, *Chem. Mater.* **2016**, 28, 1503.
- [254] Y. Fang, Q. Liu, L. Xiao, Y. Rong, Y. Liu, Z. Chen, X. Ai, Y. Cao, H. Yang, J. Xie, *Chem* **2018**, 4, 1167.
- [255] K. Chihara, A. Katogi, K. Kubota, S. Komaba, *Chem. Commun.* **2017**, 53, 5208.
- [256] J. Ding, Y.-C. Lin, J. Liu, J. Rana, H. Zhang, H. Zhou, I.-H. Chu, K. M. Wiaderek, F. Omenya, *Adv. Energy Mater.* **2018**, 8, 1800221.
- [257] N. Recham, J. N. Chotard, L. Dupont, K. Djellab, M. Armand, J. M. Tarascon, *J. Electrochem. Soc.* **2009**, 156, A993.
- [258] J. Barker, M. Y. Saidi, J. L. Swoyer, *J. Electrochem. Soc.* **2004**, 151, A1670.
- [259] K. Cui, S. Hu, Y. Li, *J. Power Sources* **2016**, 325, 465.
- [260] J. Barker, M. Y. Saidi, J. L. Swoyer, *J. Electrochem. Soc.* **2003**, 150, A1394.
- [261] P. Rangaswamy, V. R. Shetty, G. S. Suresh, K. M. Mahadevan, *J. Appl. Electrochem.* **2017**, 47, 1.
- [262] S. T. Myung, K. Amine, Y. K. Sun, *J. Mater. Chem.* **2010**, 20, 7074.
- [263] J. Barker, M. Y. Saidi, J. L. Swoyer, *Electrochem. Solid-State Lett.* **2003**, 6, A1.
- [264] H. Zhuo, X. Wang, A. Tang, Z. Liu, S. Gamboa, P. J. Sebastian, *J. Power Sources* **2006**, 160, 698.
- [265] Y. Lu, S. Zhang, Y. Li, L. Xue, G. Xu, X. Zhang, *J. Power Sources* **2014**, 247, 770.
- [266] M. Xu, C. J. Cheng, Q. Q. Sun, S. J. Bao, Y. B. Niu, H. He, Y. Li, J. Song, *RSC Adv.* **2015**, 5, 40065.
- [267] Y. L. Ruan, K. Wang, S. D. Song, X. Han, B. W. Cheng, *Electrochim. Acta* **2015**, 160, 330.
- [268] V. A. Nikitina, S. M. Kuzovchikov, S. S. Fedotov, N. R. Khasanova, A. M. Abakumov, E. V. Antipov, *Electrochim. Acta* **2017**, 258, 814.
- [269] P. Serras, V. Palomares, A. Goñi, I. G. D. Muro, P. Kubiak, L. Lezama, T. Rojo, *J. Mater. Chem.* **2012**, 22, 22301.
- [270] P. Serras, V. Palomares, J. Alonso, N. Sharma, J. M. L. D. Amo, P. Kubiak, M. L. Fdez-Gubieda, T. Rojo, *Chem. Mater.* **2013**, 25, 4917.
- [271] P. Serras, V. Palomares, A. Goñi, P. Kubiak, T. Rojo, *J. Power Sources* **2013**, 241, 56.
- [272] M. Bianchini, N. Brisset, F. Fauth, F. Weill, E. Elkaim, E. Suard, C. Masquelier, L. Croguennec, *Chem. Mater.* **2014**, 26, 4238.
- [273] M. Bianchini, P. Xiao, Y. Wang, G. Ceder, *Adv. Energy Mater.* **2017**, 7, 1700514.
- [274] J. M. L. Meins, M. P. Crosnier-Lopez, A. Hemon-Ribaud, G. Courbion, *J. Solid State Chem.* **1999**, 148, 260.
- [275] M. Bianchini, F. Fauth, N. Brisset, F. Weill, E. Suard, C. Masquelier, L. Croguennec, *Chem. Mater.* **2015**, 27, 3009.
- [276] R. A. Shaloor, D. H. Seo, H. Kim, Y. U. Park, J. Kim, S. W. Kim, H. Gwon, S. Lee, K. Kang, *J. Mater. Chem.* **2012**, 22, 20535.
- [277] W. Song, X. Cao, Z. Wu, J. Chen, Y. Zhu, H. Hou, Q. Lan, X. Ji, *Langmuir* **2014**, 30, 12438.
- [278] Z. Liu, Y. Y. Hu, M. T. Dunstan, H. Huo, X. Hao, H. Zou, G. Zhong, Y. Yang, C. P. Grey, *Chem. Mater.* **2014**, 26, 2513.
- [279] T. Broux, B. Fleutot, R. David, A. Brüll, P. Veber, F. Fauth, M. Courty, L. Croguennec, C. Masquelier, *Chem. Mater.* **2018**, 30, 358.
- [280] Y. Qi, L. Mu, J. Zhao, Y. S. Hu, H. Liu, S. Dai, *Angew. Chem., Int. Ed.* **2015**, 54, 9911.
- [281] J. Z. Guo, P. F. Wang, X. L. Wu, X. H. Zhang, Q. Yan, H. Chen, J. P. Zhang, Y. G. Guo, *Adv. Mater.* **2017**, 29, 1701968.
- [282] M. Xu, L. Wang, X. Zhao, J. Song, H. Xie, Y. Lu, J. B. Goodenough, *Phys. Chem. Chem. Phys.* **2013**, 15, 13032.
- [283] M. Peng, B. Li, H. Yan, D. Zhang, X. Wang, D. Xia, G. Guo, *Angew. Chem., Int. Ed.* **2015**, 54, 6452.

- [284] Y. Qi, Z. Tong, J. Zhao, L. Ma, T. Wu, H. Liu, C. Yang, J. Lu, Y.-S. Hu, *Joule* **2018**, 2, 2348.
- [285] M. Xu, P. Xiao, S. Stauffer, J. Song, G. Henkelman, J. B. Goodenough, *Chem. Mater.* **2014**, 26, 3089.
- [286] G. Yan, S. Mariyappan, G. Rousse, Q. Jacquet, M. Deschamps, R. David, B. Mirvaux, J. W. Freeland, J. M. Tarascon, *Nat. Commun.* **2019**, 10, 585.
- [287] P. Barpanda, S. I. Nishimura, A. Yamada, *Adv. Energy Mater.* **2012**, 2, 841.
- [288] N. Kalidas, K. Nallathamby, M. Minakshi, *ECS Trans.* **2013**, 50, 79.
- [289] J. Barker, R. K. B. Gover, P. Burns, A. Bryan, *Electrochim. Solid State Lett.* **2005**, 8, A446.
- [290] H. Yu, Z. Su, L. Wang, *Ceram. Int.* **2017**, 43, 17116.
- [291] Y. Kee, N. Dimov, A. Staikov, P. Barpanda, Y. C. Lu, K. Minami, S. Okada, *RSC Adv.* **2015**, 5, 64991.
- [292] P. Barpanda, G. Liu, M. Avdeev, A. Yamada, *ChemElectroChem* **2014**, 1, 1488.
- [293] J. Kim, I. Park, H. Kim, K. Y. Park, Y. U. Park, K. Kang, *Adv. Energy Mater.* **2016**, 6, 1502147.
- [294] C. Deng, S. Zhang, B. Zhao, *Energy Storage Mater.* **2016**, 4, 71.
- [295] L. Ke, T. Yu, B. Lin, B. Liu, S. Zhang, C. Deng, *Nanoscale* **2016**, 8, 19120.
- [296] Y. You, A. Manthiram, *Adv. Energy Mater.* **2018**, 8, 1701785.
- [297] Q. Kuang, J. Xu, Y. Zhao, X. Chen, L. Chen, *Electrochim. Acta* **2011**, 56, 2201.
- [298] J. Xu, Y. Zhao, Q. Kuang, Y. Dong, *Electrochim. Acta* **2011**, 56, 6562.
- [299] Z. Liang, Y. Zhao, *Electrochim. Acta* **2013**, 94, 374.
- [300] X. Lin, Y. Zhao, K. Quan, Z. Liang, D. Yan, X. Liu, Y. Dong, *Solid State Ionics* **2014**, 259, 46.
- [301] S. Zhang, C. Deng, Y. Meng, *J. Mater. Chem. A* **2014**, 2, 341.
- [302] C. Deng, S. Zhang, *ACS Appl. Mater. Interfaces* **2014**, 6, 9111.
- [303] C. Deng, S. Zhang, Y. Wu, *Nanoscale* **2015**, 7, 487.
- [304] Q. Li, B. Lin, S. Zhang, C. Deng, *J. Mater. Chem. A* **2016**, 4, 5719.
- [305] V. Kovrugin, J. N. Chotard, F. Fauth, A. Jamali, R. David, C. Masquelier, *J. Mater. Chem. A* **2017**, 5, 14365.
- [306] W. Deriouche, E. Anger, M. Freire, A. Maignan, N. Amdouni, V. Pralong, *Solid State Sci.* **2017**, 72, 124.
- [307] J. Kim, H. Kim, S. Lee, *Chem. Mater.* **2017**, 29, 3363.
- [308] J. Kim, G. Yoon, M. H. Lee, H. Kim, S. Lee, K. Kang, *Chem. Mater.* **2017**, 29, 7826.
- [309] M. Reynaud, A. Wizner, N. A. Katcho, L. C. Loaiza, M. Galceran, J. Carrasco, T. Rojo, M. Armand, M. Casas-Cabanas, *Electrochim. Commun.* **2017**, 84, 14.
- [310] M. Chhowalla, H. S. Shin, G. Eda, L. J. Li, K. P. Loh, H. Zhang, *Nat. Chem.* **2013**, 5, 263.
- [311] X. Xu, W. Liu, Y. Kim, J. Cho, *Nano Today* **2014**, 9, 604.
- [312] J. Feng, L. Peng, C. Wu, X. Sun, S. Hu, C. Lin, J. Dai, J. Yang, Y. Xie, *Adv. Mater.* **2012**, 24, 1969.
- [313] X. Chia, A. Ambrosi, P. Lazar, Z. Sofer, M. Pumera, *J. Mater. Chem. A* **2016**, 4, 14241.
- [314] C. Song, K. Yu, H. Yin, H. Fu, Z. Zhang, N. Zhang, Z. Zhu, *J. Mater. Chem. C* **2014**, 2, 4196.
- [315] C. S. Rout, B. H. Kim, X. Xu, J. Yang, H. Y. Jeong, D. Odkhuu, N. Park, J. Cho, H. S. Shin, *J. Am. Chem. Soc.* **2013**, 135, 8720.
- [316] Q. H. Wang, K. Kalantar-Zadeh, A. Kis, J. N. Coleman, M. S. Strano, *Nat. Nanotechnol.* **2012**, 7, 699.
- [317] J. Feng, X. Sun, C. Wu, L. Peng, C. Lin, S. Hu, J. Yang, Y. Xie, *J. Am. Chem. Soc.* **2011**, 133, 17832.
- [318] L. Wu, R. Sun, F. Xiong, C. Pei, K. Han, C. Peng, Y. Fan, W. Yang, Q. An, L. Mai, *Phys. Chem. Chem. Phys.* **2018**, 20, 22563.
- [319] R. Sun, Q. Wei, Q. Li, W. Luo, Q. An, J. Sheng, D. Wang, W. Chen, L. Mai, *ACS Appl. Mater. Interfaces* **2015**, 7, 20902.
- [320] Y. Zhou, J. Tian, H. Xu, J. Yang, Y. Qian, *Energy Storage Mater.* **2017**, 6, 149.
- [321] S. Wang, F. Gong, S. Yang, J. Liao, M. Wu, Z. Xu, C. Chen, X. Yang, F. Zhao, B. Wang, *Adv. Funct. Mater.* **2018**, 28, 1801806.
- [322] Y. Wang, Z. Liu, C. Wang, Y. Xu, R. Chen, L. Ma, H. Yi, G. Zhu, C. Tao, Z. Tie, *Adv. Mater.* **2018**, 30, 1802563.
- [323] Z. Sun, J. Zhang, L. Yin, G. Hu, R. Fang, H. M. Cheng, F. Li, *Nat. Commun.* **2017**, 8, 14627.
- [324] D. Choi, G. E. Blomgren, P. N. Kumta, *Adv. Mater.* **2006**, 18, 1178.
- [325] R. Lucio-Porto, S. Bouhitiyya, J. F. Pierson, A. Morel, F. Capon, P. Boulet, T. Brousse, *Electrochim. Acta* **2014**, 141, 203.
- [326] B. Gao, X. Li, X. Guo, X. Zhang, X. Peng, L. Wang, J. Fu, P. K. Chu, K. Huo, *Adv. Mater. Interfaces* **2015**, 2, 1500211.
- [327] Y. Xu, J. Wang, L. Shen, H. Dou, X. Zhang, *Electrochim. Acta* **2015**, 173, 680.
- [328] Y. Wang, M. Jiang, Y. Yang, F. Ran, *Electrochim. Acta* **2016**, 222, 1914.
- [329] P. J. Hanumantha, M. K. Datta, K. Kadakia, C. Okoli, P. Patel, P. N. Kumta, *Electrochim. Acta* **2016**, 207, 37.
- [330] O. Bondarchuk, A. Morel, D. Bélanger, E. Goikolea, T. Brousse, R. Mysyk, *J. Power Sources* **2016**, 324, 439.
- [331] Y. Yang, L. Zhao, K. Shen, Y. Liu, X. Zhao, Y. Wu, Y. Wang, F. Ran, *J. Power Sources* **2016**, 333, 61.
- [332] M. S. Balogun, W. Qiu, J. Jian, Y. Huang, Y. Luo, H. Yang, C. Liang, X. Lu, Y. Tong, *ACS Appl. Mater. Interfaces* **2015**, 7, 23205.
- [333] Q. Sun, Z. W. Fu, *Electrochim. Acta* **2008**, 54, 403.
- [334] X. Peng, W. Li, L. Wang, L. Hu, W. Jin, A. Gao, X. Zhang, K. Huo, P. K. Chu, *Electrochim. Acta* **2016**, 214, 201.
- [335] T. Huang, S. Mao, G. Zhou, Z. Wen, X. Huang, S. Ci, J. Chen, *Nanoscale* **2014**, 6, 9608.
- [336] K. Huang, K. Bi, C. Liang, S. Lin, R. Zhang, W. J. Wang, H. L. Tang, M. Lei, *Sci. Rep.* **2015**, 5, 11351.
- [337] X. Peng, L. Wang, L. Hu, Y. Li, B. Gao, H. Song, C. Huang, X. Zhang, J. Fu, K. Huo, P. K. Chu, *Nano Energy* **2017**, 34, 1.
- [338] Y. Zhong, D. Chao, S. Deng, J. Zhan, R. Y. Fang, Y. Xia, Y. Wang, X. Wang, X. Xia, J. Tu, *Adv. Funct. Mater.* **2018**, 28, 1706391.
- [339] M. Naguib, V. N. Mochalin, M. W. Barsoum, Y. Gogotsi, *Adv. Mater.* **2014**, 26, 992.
- [340] B. Mendoza-Sánchez, Y. Gogotsi, *Adv. Mater.* **2016**, 28, 6104.
- [341] J. Hu, B. Xu, C. Ouyang, S. A. Yang, Y. Yao, *J. Phys. Chem. C* **2014**, 118, 24274.